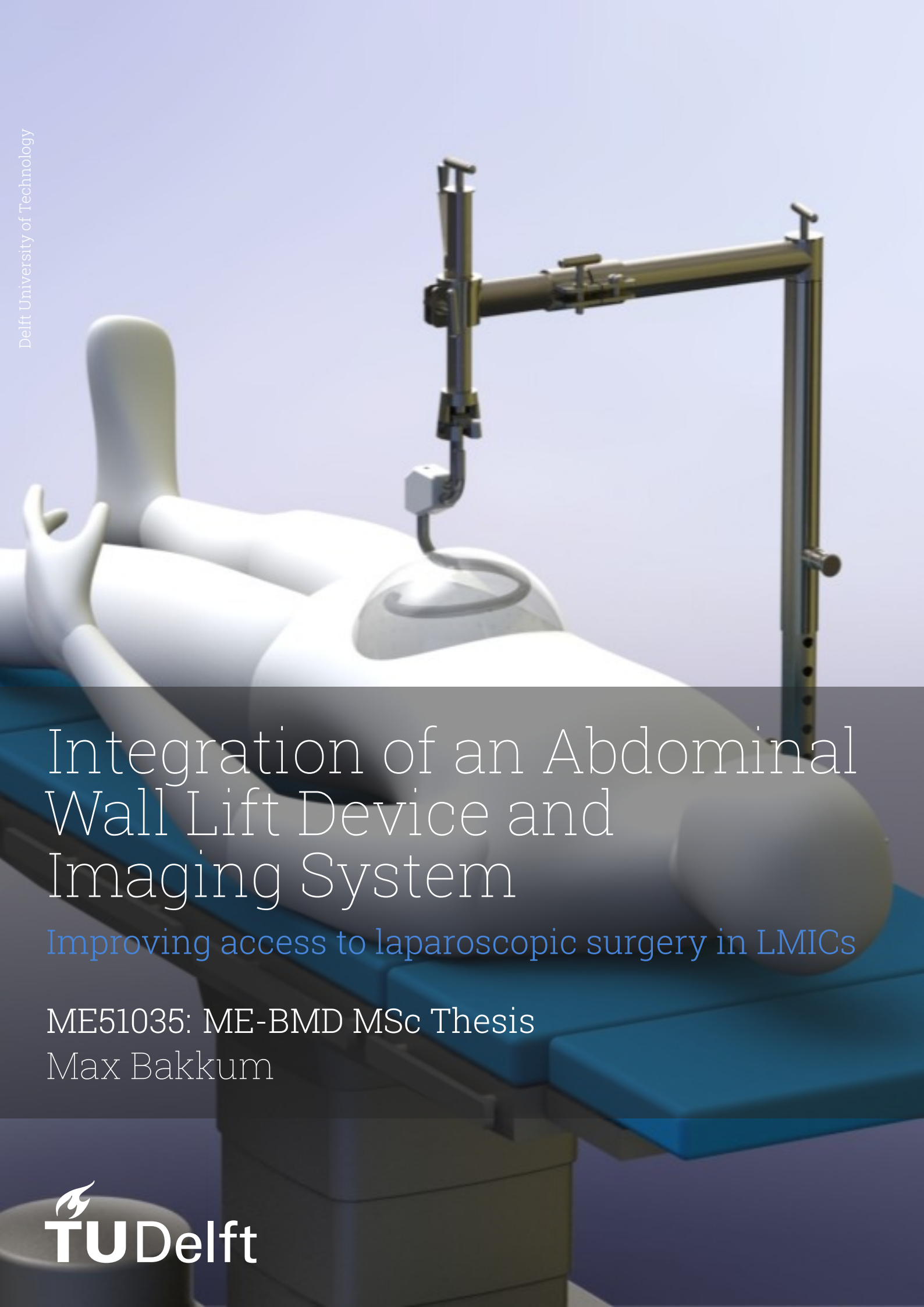

Delft University of Technology

Integration of an Abdominal Wall Lift Device and Imaging System

Improving access to laparoscopic surgery in LMICs

ME51035: ME-BMD MSc Thesis

Max Bakkum

TU Delft

Integration of an Abdominal Wall Lift Device and Imaging System

Improving access to laparoscopic surgery in LMICs

by

Max Bakkum

to obtain the degree of Master of Science
at the Delft University of Technology,
to be defended publicly on Monday, December 16, 2024, at 12:30 PM.

Student number:	4870301	
Project duration:	March 26, 2024 – December 16, 2024	
Faculty:	Faculty of Mechanical Engineering, Delft	
Department:	Department of BioMechanical Engineering	
Thesis committee:	Prof. dr. J. Dankelman,	TU Delft, main supervisor
	Dr. ir. R.M. Oosting,	TU Delft, daily supervisor

An electronic version of this thesis is available at `http://repository.tudelft.nl/`.

TU Delft

Abstract

Background: Laparoscopic surgery has improved patient outcomes and reduced healthcare costs in high-income countries but faces implementation barriers in low- and middle-income countries due to reliance on carbon dioxide insufflation, expensive equipment, and specialized personnel. Gas Insufflation-Less Laparoscopic Surgery (GILLS) provides an alternative by lifting the abdominal wall without carbon dioxide; however, expensive laparoscopes and assisting staff to operate those remain necessary. Hence, the need for a device that substitutes for the gas insufflation and laparoscope was identified.

Methods: This thesis aimed to integrate an abdominal wall lift (AWL) device and imaging system to enhance GILLS and Single-Incision Laparoscopic Surgery (SILS). Using a context-driven approach, the design focused on surgeon visibility, patient safety, cost-effectiveness, and user-friendliness. The device was developed using inexpensive, readily available components and conventional production techniques. The validation included seven verification tests and an expert user evaluation.

Results: The lifting device consists of a stainless steel tubular hook with LED lighting and a 5 MP camera module. It can be inserted in the abdomen through a small incision, lifts the abdominal wall, and creates a clear view inside the abdominopelvic cavity. An aluminum prototype had sufficient structural strength, was cost-effective, lightweight, and compatible with existing AWL systems, but it generated excessive heat, was not waterproof, and lacked a functional imaging system. Evaluation by a GILLS expert highlighted design strengths while emphasizing three areas for improvement: the frame's shape, the imaging system, and the sealing technique.

Conclusion: This study illustrated the potential of integrating an abdominal wall lift device and imaging system despite the substantial constraints of the current tubular design. The cost-effective alternative eliminates the reliance on carbon dioxide gas, expensive laparoscopes, general anesthesia, and untrained assisting staff. Therefore, development should continue to improve access to laparoscopic surgery worldwide.

Keywords: Gasless laparoscopy - Abdominal Wall Lift Device - Laparoscope - GILLS - LMIC

Acknowledgements

This MSc thesis concludes my seven years in Mechanical Engineering at Delft University of Technology, and I am profoundly grateful to the wonderful people who offered their support along this journey.

First, I would like to express my sincere gratitude to my daily supervisor, Roos Oosting, for her invaluable guidance from start to finish. I'm incredibly thankful for your efforts to make this project both rewarding and fun. I would also like to thank Jenny Dankelman for her insightful suggestions and critical questions.

A special appreciation goes to Sterre. I am deeply thankful for your constant support, motivation, and reminding me of the progress I made. I cherished the hours we studied together and will definitely miss them.

I would like to acknowledge Dr. Gnanaraj and Robbert for initiating this project and supporting me along the way. I would also like to thank the other surgeons who were open to discussing my ideas.

I am grateful to Thomas and Koen for their support with numerous practical matters. Your curiosity about my project was extremely rewarding, and our discussions were very pleasant.

I want to thank Damian, Jan, Reinier, and other faculty workshop members for their assistance in the production process. Additionally, I would like to thank Jan-Willem for setting up the box trainer experiment together and the participants for performing it.

My appreciation goes to Florian, Ted, Irene, and Thijs for the fun lunch and study sessions. I would also like to thank Bas, Jesse, Marjolein, and Noor for their support.

Lastly, I express my gratitude to my wonderful family for their support throughout my academic career and to my maandagavondcompetitie teammates for assisting me for a change.

My heartfelt thanks to all who supported me on this journey; your impact on this thesis's completion was sincerely appreciated.

Max Bakkum
Delft, December 2024

Contents

Part I

Problem Statement

”Of all the forms of inequality, injustice in health is the most shocking and inhumane.”

Martin Luther King, Jr.
Medical Committee for Human Rights conference

1

Introduction

1.1. The need for gas insufflation-less laparoscopic surgery

The implementation of laparoscopic surgery in low- and middle-income countries (LMICs) has been desultory and limited [1]. This lack of progress can be attributed to several factors, of which inadequate infrastructure and resources are considered the most critical barriers [2, 3, 4, 5]. Another significant barrier to the uptake of laparoscopic surgery is the cost. The price of laparoscopic surgery in a large West African hospital was $\$704$, compared to $\$150$ for traditional open surgery. Patients tend to weigh the costs higher than the benefits of the minimally invasive technique [6, 3, 7]. Furthermore, the cost of purchasing and maintaining the necessary equipment and supplies can be prohibitively high in many LMICs [8].

The benefits of laparoscopic surgery cannot be overstated. This minimally invasive technique has improved patient outcomes and reduced healthcare costs in high-income countries (HICs). Therefore, LMICs must be provided the necessary support to adopt this technique and enhance healthcare quality. Yet conventional laparoscopy with a carbon dioxide-insufflated pneumoperitoneum has several disadvantages, such as hypoventilation, hypercapnia, CO_2 embolus, pain from diaphragmatic stretching, and shoulder pain.

Gas Insufflation-Less Laparoscopic Surgery (GILLS)

Besides inadequate infrastructure, lack of resources, and a gap in knowledge and skills in LMICs, the global healthcare inequity is caused by slow development and adoption of context-appropriate surgical techniques and associated equipment [2, 10]. To face these challenges, an alternative form of conventional laparoscopy is adopted by surgeons in rural areas of Northeast India [11]. In Gas Insufflation-Less Laparoscopic Surgery (GILLS), Figure 1.1, the abdominal wall is physically raised by an abdominal-wall lift (AWL) device to create operative space [9]. This technique has various advantages over conventional laparoscopy, such as shorter hospital stays, less shoulder pain, less influence on cardiopulmonary function, and less postoperative nausea and vomiting [12, 13, 14, 15].

Without exception, all laparoscopic instruments originally designed for conventional laparoscopy are functional in GILLS. Even instruments for open surgery can be used with simple valveless trocars [16, 17]. GILLS can be performed under spinal anesthesia, eliminating the need for general anesthesia, an anesthetist, CO_2 gas, and specialized equipment [9].

GILLS has gained popularity in the last decade for emergency and elective abdominal surgery in low-resource settings due to its lower implementation costs [18, 11]. It is non-inferior and has no difference in peri-operative outcomes compared to conventional laparoscopy [19, 20]. Specialized training in GILLS could simplify the switch from open surgery to laparoscopy [21, 22, 23]. Thus, GILLS has great potential to be a cost-effective technology that accelerates the implementation of laparoscopy in low-resource settings [24].

Figure 1.1: Gas Insufflation-Less Laparoscopic Surgery (GILLS) [9].

Integration of an abdominal wall lift device and imaging system

The current AWL devices, however, require modifications to provide a uniform lift of the abdominal wall, allowing better visualization of the peritoneal cavity and achieving comparable views to conventional laparoscopy [24]. Due to a shortage of staff in LMICs, untrained assistants often operate the laparoscope [25, 26]. Training of laparoscopic assistants was identified to be a major obstacle [22]. Furthermore, the laparoscope is the most expensive piece of laparoscopic equipment [27].

To conclude, there are various barriers to the uptake of laparoscopic surgery in LMICs, and the conventional laparoscopic procedure, using CO_2 pneumoperitoneum, has several disadvantages. Development and adoption of context-appropriate surgical techniques and associated equipment are slow. GILLS addresses those barriers and disadvantages. Nonetheless, current AWL devices require improvement, and training assistants to operate laparoscopes is a barrier. Thus, the need for *integration of an abdominal wall lift device and imaging system* for GILLS was identified. This device could help the adoption of laparoscopic surgery in LMICs and ultimately improve treatment outcomes for countless patients.

This project

This MSc thesis is part of an initiative to increase global access to medical equipment through context-driven design [28]. The TU Delft Biomedical Engineering for Global Health Lab, led by Prof. Dr. Jenny Dankelman and Dr. ig. Roos Oosting, researches the current usage and barriers to medical equipment in hospitals globally, develops innovations to increase availability, and provides education within and outside Delft University of Technology [29].

Robbert den Butter initiated the project after consulting Dr. J. Gnanaraj, an expert on GILLS. The Indian surgeon identified the need for improved lifting devices and imaging equipment in low-resource settings for gasless laparoscopic tubal ligation procedures. This MSc thesis continues the research done by Den Butter [30].

In this thesis, the design process of an AWL device with an integrated imaging system will be described, and the results will be discussed. The specific problem definition will be provided in Chapter 2. First, the following sections present a brief introduction to laparoscopic surgery and AWL devices.

1.2. Laparoscopic Surgery

Laparoscopy is a minimally invasive surgery (MIS) technique performed in the abdominopelvic region using small incisions and few stitches [31, 32], which offers several advantages over open surgical procedures, such as decreased postoperative pain, faster recovery times, fewer operative and postoperative major complications, less scarring, and a shorter hospital stay [33, 34, 35]. Section A.1 describes laparoscopic surgery in more detail, explaining the preparation steps and common procedures.

Laparoscopic surgery requires specialized skills and has a steeper learning curve than traditional open surgery [36, 37, 38]. In LMICs, a shortage of trained personnel adds pressure on non-specialized surgeons [39, 40, 6], highlighting the importance of training programs [21]. However, many trainees fail to complete courses, and even those who succeed rarely adopt laparoscopy due to limited access to tools and equipment [1, 41].

Carbon dioxide pneumoperitoneum

In conventional laparoscopic surgery, carbon dioxide gas inflates the abdominopelvic region to create operational space, resulting in unwelcome side effects. An increase in intraabdominal pressure occurs due to the CO_2 pneumoperitoneum, which pushes the diaphragm upward, resulting in decreased total lung volume, reduced pulmonary compliance, and hypoventilation [20, 42, 43]. The CO_2 pneumoperitoneum also induces hypercapnia and side effects such as CO_2 embolus, pain from diaphragmatic stretching, and physiological complications such as respiratory infections and renal problems [44, 45]. Consequently, laparoscopic surgery using CO_2 gas might be a limited option for elderly or cardiopulmonary-compromised patients [20].

Other disadvantages related to the CO_2 pneumoperitoneum are abdominal-wall collapse, arising from over-suction or gas leakage, and plume formation, which blocks the surgeon's vision [20, 45, 46]. During and after surgery, the gas is released into the environment unfiltered, which is dangerous to surgeons, nurses, and patients [45]. Not to mention, the healthcare sector contributes 7% of the entire U.S. CO_2 emission, and this percentage is increasing due to the expansion of MIS [45, 47]. Furthermore, valved trocars with small diameters and laparoscopic instruments specifically designed for surgeries using CO_2 pneumoperitoneum are expensive, delicate, and often single-use items [16].

Abdominal Wall Lift Devices

In GILLS, the abdominal wall is physically raised by an AWL device, creating operational space without CO_2. Since research began in 1991 [48], numerous AWL device iterations have been developed and tested. These are listed in Section A.2. Loop-shaped AWL devices are the current state-of-the-art (Figure 1.2). These devices require a single incision, have no moving parts, and are easily mounted on retractor arms. Since the Abdo-Lift, tenting - where lifting is localized near the device, restricting visibility and causing high tissue tension - has been significantly reduced [49]. These devices were optimized for low-resource settings, and recent designs like the Keyloop [50], RAIS [9], and STAAN [51] were successfully tested in LMICs.

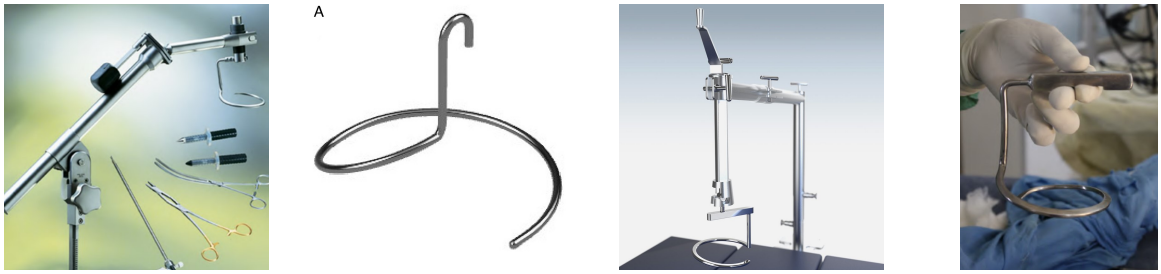

(a) Abdolift (2007) [49] **(b)** Keyloop (2022) [50] **(c)** RAIS (2022) [9] **(d)** STAAN (2022) [51]

Figure 1.2: Loop-shaped AWL devices

2

Project Definition

After recognizing the need for GILLS in LMICs, the project was defined. This chapter specifies the outlook of the project and delineates the boundaries. First, the problem was analyzed. Consequently, a design goal was set within a certain scope.

2.1. Problem Analysis

Nevertheless, adoption in rural hospitals remains limited, partly due to a shortage of staff who can assist in operating laparoscopes. Furthermore, the quality of laparoscopes available in low-resource settings is unmatched by the standards in HICs. Hence, GILLS expert Dr. Gnanaraj identified the need to integrate an AWL device and imaging system.

The primary function of any AWL device is to lift the abdominal wall. Various solutions are outlined in Section A.2, ranging from experimental concepts to practical devices. A major challenge with many designs is tenting, where the device lifts only the area near it, forming a tent-like structure. This reduces surgeon visibility and increases tissue tension. Tenting is common in wire-based, balloon-based, some loop-shaped, and most mechanically expanding designs.

Well-designed mechanically expanding devices address tenting but come with other drawbacks. According to expert GILLS surgeon J. Gnanaraj, they are costly and uncomfortable to use. Other designs are difficult to set up or require too many or large incisions.

Loop-shaped AWL devices, which require only one small incision and have no moving parts, emerged nearly 30 years ago and have seen significant improvements. Newer models with larger loops reduce tenting and connect easily to a single retractor arm, minimizing interference with laparoscopic instruments. These circular lifting devices have been clinically tested in LMICs and represent the current state of the art.

Alternative designs, such as external suction or motorized devices, have been explored but were not promising. While unconventional designs might theoretically improve wall lifting, outperforming current loop-shaped devices was deemed unlikely. After consulting from a biomedical engineer from India and Deborah Maufi[1], the decision was made to focus on a circular loop shape early in development, enabling a deeper exploration of its potential.

[1] CEO of Loresa, a health venture working on the commercialization of the RAIS system

Previous study

This project was a continuation of Robbert den Butter's master thesis project [30]. His work introduced the integration of an imaging system in a loop-shaped lifting device. The final design is presented in Figure 2.1. The key feature of the design is the cheap but high-quality camera module. The raw materials cost less than € 60, and only conventional production techniques were used.

Although the concept was excellent and has great potential, certain aspects require improvement. Foremost, the shape of the loop should be modified. The loop's size should be decreased to reduce the risk of injury, and it should have a twist to make insertion easier. Additionally, the diameter at the incision point should be reduced to allow for single-incision laparoscopic surgery (SILS).

A different camera position was required to accommodate SILS and common laparoscopic procedures (Appendix A). Furthermore, the LED lighting system generated excessive heat, and the sealing technique was insufficient. These improvements should be considered for the next iteration. That is the starting point of this project.

Figure 2.1: The final lifting device design from a previous study [30].

2.2. Project Goal

With the potential and challenges of GILLS evaluated, the project goal was established. The overall aim was fairly broad and will be quantified in Section 4.2. The goal of this thesis project was:

> *Design, build, and validate a next-generation abdominal wall lift device with an integrated imaging system for gas insufflation-less and single-incision laparoscopic surgery in a low-resource setting.*

2.3. Project Scope

As described, the project focused on designing a loop-shaped AWL device. Current AWL devices, shown in Figure 2.2, consist of two parts: a lifting device and a retractor arm. This project only focused on the lifting device part, which should be compatible with existing retractor arms.

The most outstanding feature of the previous design by Den Butter was the high-quality camera, especially for its low price point. The camera module was validated, which will be described in depth in Section 9.1. The decision was made to begin the design process with this module as a starting point.

The decision set constraints to the shape and dimensions of the lifting device. On the other hand, it created time for other aspects of the design, such as finding the optimal camera position. The lifting device targets GILLS procedures in rural areas of LMICs, addressing challenges such as restricted budgets, limited access to maintenance, personnel shortages, and different sterilization techniques (Appendix B). Engaging local users through collaborative prototyping ensures the design is context-appropriate [28].

Figure 2.2: A render of the RAIS AWL system. The red part is the lifting device, which is connected to the retractor arm.

2.4. Project Outline

The thesis is divided in four parts. This part, the problem statement, described the need for GILLS and defines the project; a survey was conducted in Chapter 3 to construct the lifting device's design drivers and requirements, which are presented in Chapter 4.

Part II describes the process of concept design. Based on the design drivers and requirements, three concepts were made in Chapter 5. The concepts were evaluated based on a force analysis (Chapter 6), a camera position analysis (Chapter 7), and other criteria. The best-rated concept was selected in Chapter 8.

The next design phase is presented in Part III. Chapter 9 outlines the final design. The dimensions, materials, and production steps are described in Chapter 10. Chapter 11 discusses the production process and reviews the prototypes.

Part IV is the validation of the lifting device. It consists of verification tests (Chapter 12) and a user test (Chapter 13). Lastly, the lifting device's performance and design process are discussed in Chapter 14, and a conclusion is made in Chapter 15.

3

Survey: Gasless Laparoscopy

A list of design drivers and requirements was constructed from observations of local-end GILLS surgeon J. Gnanaraj, feedback from an Indian biomedical engineer, findings from the previous study by Den Butter and other literature, and responses from a survey. This section discusses the survey.

It was conducted to retrieve information about unforeseen problems of current AWL devices, the importance of the design drivers, and missing design requirements. The goal of the survey was to obtain new insights and use those to update the design requirements and criteria. Considering the small expected respondent size, the survey did not aim to draw statistically significant conclusions.

Method

The survey was distributed on the 11^{th} of July 2024 for two weeks. Respondents with at least some knowledge of laparoscopic surgery were sought, preferably with experience in GILLS. Hence, the survey was distributed via Prof. Dr. Jenny Dankelman's global surgery network. Twelve respondents participated in the survey.

The survey was anonymous by default, but respondents could leave their contact details by choice. It included a mix of closed and open questions. This approach was taken to keep the survey duration short while allowing respondents to provide new insights in the open questions. After the survey, two follow-up conversations were held with a GILLS expert surgeon from an LMIC and a laparoscopic surgeon from a HIC.

The questionnaire was not identical for all respondents. Depending on the level of experience in performing GILLS, questions about the used AWL device(s) were presented. These involved questions about the performed laparoscopic procedures and the performance of the AWL device. The next part of the questionnaire was presented to all respondents. These questions involved ranking relevant criteria for an AWL device with an integrated imaging system and which laparoscopic procedures should be performed with such a device. The descriptions of the design criteria can be found in Section 4.1 and the full questionnaire in Appendix F.

Results

A total number of 12 respondents participated in the survey, residing in India (1), Kenya (4), Madagascar (1), the Netherlands (4), and Tanzania (2). The participants included nine surgeons, two biomedical engineers, one medical student, and one biomedical engineering student. All respondents had at least some knowledge of laparoscopy (7) or were experts in the field (5). Seven of the eight surgeons performed laparoscopic surgery regularly, and one had some experience. Experience in performing GILLS was lower, with four surgeons performing GILLS regularly and two surgeons having some experience.

The AWL devices used by surgeons with experience in GILLS were RAIS (4), STAAN (2), Abdolift (1), and a string device[1] (1). Procedures performed with those devices can be seen in Figure 3.1. Statements were presented to the surgeons regarding the devices used, the results are shown in Table 3.2. In the open section, surgeons mentioned that port positioning is a problem and that there is limited vision in obese patients.

The next part was presented to all participants, although one surgeon from Kenya failed to complete it. The participants were asked to rank relevant criteria for a hypothetical AWL device with an integrated imaging system; Table 3.1 displays the outcome. The score is the average rank given by the eleven respondents. The laparoscopic procedures that should be performed with this device, according to respondents with knowledge of laparoscopic procedures, are presented in Figure 3.1.

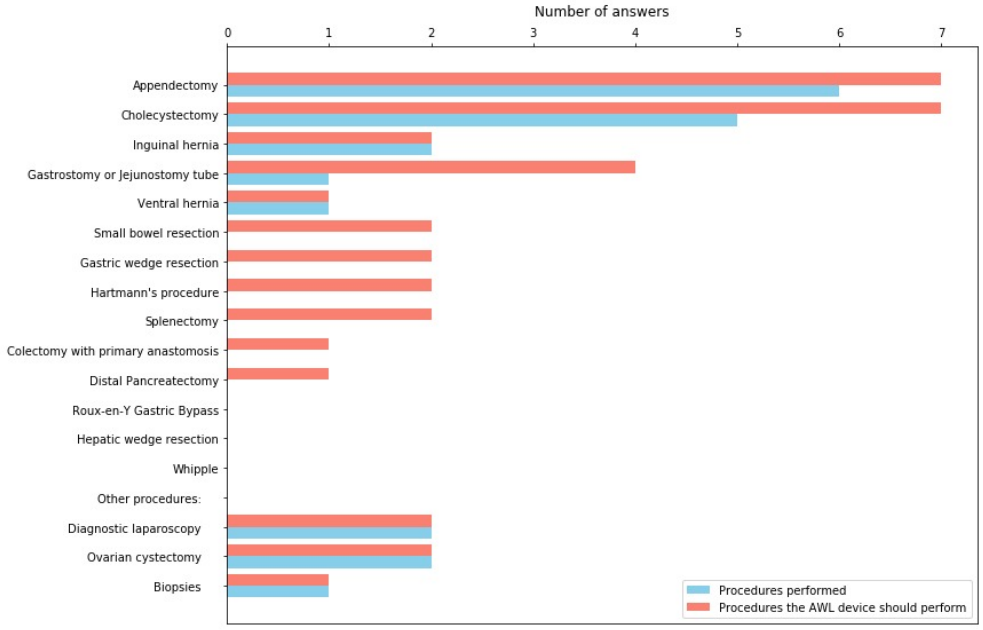

Figure 3.1: The number of respondents who have performed certain procedures and those who believe the AWL device should perform specific procedures.

Table 3.1: Ranking of design criteria by eleven respondents. The score is the average rank given by the respondents, i.e. the lower the score, the more important the design criterion

	Criteria	Rank					Score
		1	2	3	4	5	
1	Surgeon's visibility	11	0	0	0	0	1.0
2	Patient safety	0	5	3	1	2	3.0
3	User-friendliness	0	3	5	1	2	3.2
4	Costs	0	1	3	3	4	3.9
4	Robustness	0	2	0	6	3	3.9

[1] A device similar to Hashimoto et al. Figure A.5a.

Table 3.2: Surgeon opinions about AWL devices. A=Agree, N=Neutral, D=Disagree

	Statement	Abdolift (1)	RAIS (4)				STAAN (2)		String device (1)
1	The device is easy to insert	A	A	A	N	N	A	N	N
2	The device is easy to adjust	A	A	N	N	N	A	D	A
3	The device is easy to remove	A	A	A	A	A	A	N	A
4	The device is easy to connect to a retractor arm	A	A	A	N	N	A	N	D
5	It is easy to position the laparoscope while using the AWL device	A	A	A	N	N	N	N	D
6	During blind entry of the device, patient tissue is damaged sometimes	A	A	N	D	D	A	N	N
7	Frames or wires interfere movement of surgical instruments	N	A	A	N	N	A	N	N
8	The operational volume* is large enough (i.g. no tenting occurs and there is enough space to operate)	N	A	A	N	D	A	N	A
9	More fogging occurs when using this device compared to standard gas laparoscopy (disagree if less fogging occurs)	N	D	D	D	D	A	D	N
10	The device can be used on patients of all sizes	A	N	D	D	D	A	D	A

Conversation with a GILLS expert surgeon

In a follow-up conversation with a surgeon, the differences between the RAIS and STAAN devices were discussed. The RAIS device is easier to adjust, remove from the abdomen, and connect to the retractor arm than the STAAN device. This is due to the STAAN device being heavy, whereas the RAIS device is smaller and lightweight. Additionally, the STAAN device does not react well to the autoclave. According to the surgeon, it was designed for chemical immersion sterilization, and the material is unsuitable for multiple autoclave cycles.

The surgeon was one of the two participants who responded that patient tissue is sometimes damaged during the device's blind entry. However, this statement was nuanced since it only happened once. There will always be a blind entry in laparoscopy, yet feeling the inside of the abdominal wall with your finger before inserting the AWL device is sufficient to avoid tissue damage. In the survey response, he mentioned that port positioning was a problem. However, the positioning of the ports was not the actual problem; it was the interference of the retractor arm and AWL device with other surgical instruments. Consequently, the surgeon ends up in ergonomically challenging positions.

Moreover, the AWL devices are unsuitable for patients with a higher BMI of around 26 to 27. The abdominal wall thickness due to excessive fat is a better measure of obesity [52]. A thick abdominal wall is less compliant, reducing the operational space significantly.

The importance of the design criteria for an AWL device with an integrated imaging system was also discussed. The surgeon's visibility is the most important criterion. The operational space is especially crucial, whereas the image quality, although important, is less significant. User-friendliness should not be underestimated since this reduces operation time and shortens the learning curve. Essential factors determining user-friendliness are the device's weight, the ease of insertion, and the connection to a retractor arm. The surgeon considered the costs of the device the least important criterion. He believes it will inevitably be expensive because it will not be mass-produced.

The surgeon believes this AWL device will only be useful for simple surgeries, such as appendectomy. The fixed camera position limits the view around target tissues, restricting the types of surgeries that can be performed. He has completed research concluding that GILLS is non-inferior to conventional laparoscopic surgery [19, 51]. Nevertheless, when both conventional laparoscopy and GILLS are

available, he would choose conventional laparoscopy because 90% of the abdominal surgeries can be done with the conventional technique, in contrast to only 25% with the gasless technique. Fewer types of surgeries can be performed gasless due to the smaller operational space.

Discussion

Appendectomy (6/6) and cholecystectomy (5/6) are the procedures performed by most surgeons. This was expected, as both are among the most common laparoscopic procedures [53, 54, 55, 56]. Diagnostic laparoscopy and ovarian cystectomy were both answered in the open option by two surgeons, indicating these procedures may be more important than expected.

The surgeons' feedback on current AWL devices (Table 3.2) indicates that all devices are easy to insert, adjust, and remove from the abdomen. The string device, however, is more difficult to set up, and with this device, positioning the laparoscope is more difficult.

There are three reports of tissue damage during blind entry by the Abdolift, RAIS, and STAAN devices. In the concept design, this problem should be considered to minimize tissue damage. Nevertheless, it is of minor importance since feeling the inside of the abdominal wall with your finger before inserting the AWL device is sufficient to avoid tissue damage.

The AWL devices certainly interfere with the movement of other surgical instruments to some extent. Consequently, surgeons end up in ergonomically challenging positions. Yet, most surgeons are neutral on this topic. Therefore, interference will have low priority.

The surgeons agree that the operational volume is large enough, even though fewer types of surgeries can be performed gasless due to the smaller operational space. Furthermore, less or the same amount of fogging occurs with all AWL devices compared to conventional laparoscopy; one surgeon stated that more fogging occurs.

The opinions about the last statement vary greatly. It was reported that the Abdolift and string device can be used on patients of all sizes, while the RAIS device cannot. This is mostly due to limited vision in obese patients. However, the shape and size of the Abdolift and RAIS device are similar, so the discrepancy in answers is inexplicable.

Table 3.1 shows that all respondents find surgeon visibility the most important design criterion. The operational space is especially crucial, whereas the image quality, although important, is less significant. Patient safety is the second most important criterion, followed closely by user-friendliness, as this determines the operation time and the learning curve. The costs and robustness are ranked as least important. This does not imply these criteria should be ignored.

In the open section, respondents emphasized the importance of image quality and operational space and mentioned that cost-effectiveness and user-friendliness will increase the adoption in LMICs. Other important features of the AWL device are the time needed to install it and the ability to clean it. All respondents with knowledge about laparoscopic procedures (7/7) agree that appendectomy and cholecystectomy should be performed with the AWL device and, according to most respondents (4/7), it should be capable of performing gastrostomy or Jejunostomy.

Conclusion

The survey provided valuable insights into the design drivers and requirements for the lifting device. Surgeon visibility emerged as the most important criterion, emphasizing the need for adequate operational space and acceptable image quality. Patient safety and user-friendliness were also prioritized, with factors like ease of use, reduced operation time, and compatibility with retractors. While cost and robustness were ranked lower, they remain critical for adoption and use in LMICs. Feedback highlighted challenges in treating obese patients. Appendectomy and cholecystectomy must be performed with the lifting device.

Besides the survey results, observations of Dr. Gnanaraj, feedback from an Indian biomedical engineer, findings from the previous study by Den Butter and other literature were used to specify the design drivers and requirements for the lifting device, which are detailed in Chapter 4.

4

Design Specifications

4.1. Design Drivers

Design drivers are factors that motivate the design process of the lifting device. These involve the functions of the product, the problems the product fixes, the reasons for making a product, and the look and feel of a product [57]. The development of the lifting device that addresses the particular needs of rural hospitals in LMICs was guided by six key design drivers, which are based on scientific literature, interviews with surgeons, and the conducted survey. The design drivers, along with their rationale, are listed below. The precise requirements resulting from the drivers will be provided in Section 4.2.

- **Surgeon's visibility:** This is the most fundamental design driver for the lifting device. The driver consists of the device's two core functions: creating operational space and viewing inside the abdomen. Good visibility is essential to perform laparoscopic procedures successfully. Nonetheless, it is often inadequate in low-resource settings for various reasons, as detailed in Section 2.1. By enhancing visibility, surgeons can make well-informed decisions, lower the risk of mistakes, and achieve better patient outcomes.
- **Patient safety:** For this design driver, patient safety is defined as a safe surgery with few symptoms and side effects. As laparoscopic surgery is invasive, it always has a minimum level of physical effects. The patient safety can be decreased further by accidents or misuse of the product. A well-designed product has a low minimum level of physical effects while minimizing the risk of accidents and misuses.
- **User-friendliness:** The usability of the lifting device is vital for ensuring its successful adoption in practice [28]. The device should be intuitive to use and easy to operate. To accommodate often undertrained staff in low-resource hospitals, the user interface should be designed for simplicity. Furthermore, ensuring compatibility with existing mechanical retractors is essential for seamless integration into current surgical setups.
- **Cost-effectiveness:** Considering the financial barriers to accessing healthcare in LMICs, cost-effectiveness is a crucial design driver. Minimizing the device's initial, operational, and maintenance costs allows for greater adoption and implementation. This design driver only considers the direct costs of the product. Reduced indirect costs are accomplished by the device's performance.
- **Robustness:** The device must be capable of enduring the rigorous conditions and demands of laparoscopic surgery in low-resource settings. A strong, durable, and reliable design that can be sterilized many times and can cope with power fluctuations is essential for this device.
- **Manufacturability:** Design for manufacturing (DFM) entails incorporating manufacturing considerations early in the design process to create parts and products that can be produced more easily and economically [58]. Manufacturing the device locally constraints advanced production techniques. Therefore, the design should be manufactured using simple production techniques and materials that are affordable and available around the globe.

4.2. Design Requirements and Aims

A list of functional requirements and aims directs the development of the lifting device. Design requirements *must* be met, whereas design aims are more flexible ambitions. Using a context-driven design approach for surgical equipment for safe surgery [28], contextual factors were collected to establish context-specific design requirements and aims for the lifting device. Contextual factors in the design approach are (A) hospital and surgery types, (B) availability of equipment, (C) procurement, (D) infrastructure (water, electricity, etc.), (E) team composition and training, (F) maintenance, (G) sterilization, (H) storage, and (I) daily usage. These are described in detail in Appendix B.

The requirements (in bold) and aims (with subscript A) are explained below. These are categorized conforming to the design drivers: **V** is surgeon's visibility, **P** is patient safety, **U** is user-friendliness, **C** is costs and resources, and **R** is robustness. Note that the costs and manufacturability are grouped as both focus on simplicity and widely available resources. The design requirements are summarized in Table 4.2a.

$V1$ **Abdominal wall lifting:** The first core function of the device is lifting the abdominal wall. The abdominal wall will be lifted with a maximum load of $140\,\mathrm{N}$. Therefore, the lifting device must sustain a load of $140\,\mathrm{N}$ without permanent deformation, i.e., with a 2.0 factor of safety (FOS). The explanation for this specific load is provided in Chapter 6. *(Contextual factor A)*

$V2$ **Camera position:** The camera must be positioned and oriented such to accommodate the most common laparoscopic procedures as described in Section A.1. Eye-hand coordination problems must be reduced by positioning the camera adequately. This will be elaborated in Chapter 7. *(Contextual factor A)*

$V3$ **Operational volume:** A considerable part of the surgeon's visibility is determined by the operational volume. This is the space created inside the abdomen, which is also the surgeon's working space. In conventional laparoscopy, this volume is created by carbon dioxide. The operational volume created by the lifting device must be at least equal to the operational volume created in conventional laparoscopy. The calculation of the specific volume is provided in Section 10.1. *(Contextual factor A)*

$V4_A$ **Imaging quality:** The second core function of the device is viewing inside the abdomen. Expert feedback from GILLS surgeon J. Gnanaraj suggests that the imaging quality should match the standards of state-of-the-art laparoscopes from a decade ago. The light intensity also influences the imaging quality. *(Contextual factor A)*

$P1$ **Insertion diameter:** Laparoscopes and AWL devices are inserted in the abdomen through small incisions. Currently, an incision with a diameter of $12\,\mathrm{mm}$ at the umbilicus is needed to insert an AWL device and a laparoscope [50]. The insertion diameter must be a maximum of $12\,\mathrm{mm}$ to avoid compromising patient safety. *(Contextual factor I)*

$P2$ **Product surface temperature:** To prevent tissue damage from heat burns, the device must be designed to have a maximum surface temperature of $41\,^{\circ}\mathrm{C}$. This limit complies with IEC 60601-2-37, which provides guidelines for *Particular requirements for the basic safety and essential performance of ultrasonic medical diagnostic and monitoring equipment* by the International Electrotechnical Commission (IEC). *(Contextual factor I)*

$P3_A$ **Biocompatibility:** The device is an externally communicating medical device in contact with tissue for a limited duration (<$24\,\mathrm{h}$). The device should be biocompatible according to the ISO 10993-1 2018 standards. *(Contextual factor A)*

$P4_A$ **Single-incision laparoscopic surgery:** The device should be able to accommodate single-incision laparoscopic surgery (SILS). This new technique decreases the physical effects on the patient and thereby increases patient safety, as all instruments are inserted through only one incision. For this aim, an adequate camera position and a smaller insertion diameter are crucial. *(Contextual factor A)*

$U1$ **Compatibility with retractors:** Ensuring compatibility with existing mechanical retractors is essential for seamless integration into current surgical setups. The focus for this lifting device will be on compatibility with the RAIS retractor arm. *(Contextual factors B & E)*

$\boldsymbol{U2}$ **Weight:** A heavy lifting device increases the difficulty for surgeons to position it during procedures. Based on recommendations from expert GILLS surgeon J. Gnanaraj, the maximum weight is limited to $0.5\,\mathrm{kg}$. *(Contextual factor I)*

$\boldsymbol{U3}$ **Data and power connection:** To ensure compatibility with low-resource infrastructure, both the power and data connections should use a USB-A port. This universal connection enables surgeons to operate the lifting device using a standard laptop. *(Contextual factor B & D)*

$U4_A$ **Intuitive use & interface:** The lifting device should be intuitive and easy to use. It should feature a straightforward interface to accommodate often untrained personnel in low-resource settings. *(Contextual factor E)*

$\boldsymbol{C1}$ **Low production costs:** Cost-effectiveness is partly determined by the initial costs. The current price of a complete AWL device, such as the RAIS system, is approximately $1500. The cheapest context-specific laparoscope in the market costs $300 [59]. To ensure a competitive market position, the maximum production cost of this lifting device is set to $400. *(Contextual factor C)*

$\boldsymbol{C2}$ **Use of supplies:** Sourcing single-use items and supplies is a significant challenge for rural hospitals in LMICs. Appendix B also highlighted a lack of constant electricity and often a shortage of sterile water. Accordingly, no other resources than water and electricity may be utilized. Sterile water should not be required, and the device also should not need constant electricity from the grid to function. *(Contextual factors B & D)*

$\boldsymbol{C3}$ **Local production:** Manufacturing the device locally in LMICs constraints advanced production techniques but is crucial for an inexpensive product. Therefore, the device should be manufactured using simple production techniques that are affordable and available around the globe. *(Contextual factors B & C)*

$\boldsymbol{R1}$ **Cleaning & sterilization:** Sterile equipment is essential to reduce the risk of infection and cross-contamination. Reusable equipment – which this lifting device is – must be cleaned and sterilized in between every surgery. Autoclaves are often not available or used in low-resource settings. Rural hospitals typically use immersion in chemicals to clean reusable devices instead. This lifting device must be sterilizable with chemical immersion. *(Contextual factors B, G, & H)*

$\boldsymbol{R2}$ **Dust- & waterproof:** The device is consistently exposed to human bodily material (HBM). No HBM may enter the device to be sterilizable. Furthermore, during the chemical immersion sterilization process, no liquid may enter the device. Therefore, the device must be completely dust- and waterproof to maintain functionality, prevent damage, and reduce the risk of infection and cross-contamination. The device must meet the IP67 standard, requiring it to be submerged in water for 30 minutes with its highest point at least $150\,\mathrm{mm}$ below the surface[1]. *(Contextual factors G & I)*

$R3$ **Maintenance:** To increase the lifespan of the lifting device, the electronic parts must be replaceable when defective. *(Contextual factor F)*

$R4_A$ **Durability:** The device should be able to do a thousand cycles. This is a common practice for laparoscopic instruments, according to Dr. Gnanaraj. The durability is determined by the material strength, the lifetime of electronics, and the resistance to chemical immersion. *(Contextual factor F)*

[1] https://clarionuk.com/resources/ip-ratings/

Table 4.2: Design requirements and aims with corresponding performance criteria.

(a) Design requirements

ID	Requirement	Performance criteria
$V1$	Abdominal wall lifting	The device must sustain a load of $140\,\mathrm{N}$ with a 2.0 FOS
$V2$	Camera position	The camera view must accommodate common procedures
$V3$	Operational volume	The operational volume must equal the pneumoperitoneum
$P1$	Insertion diameter	The device must fit through a $12\,\mathrm{mm}$ diameter circular incision
$P2$	Product surface temperature	The surface temperature may not exceed $41\,°\mathrm{C}$
$U1$	Compatibility with retractors	The device must be compatible with RAIS retractor arm
$U2$	Weight	The device must weight a maximum of $0.5\,\mathrm{kg}$
$U3$	Data and power connection	An USB-A port must be used for power and data transmission
$C1$	Low production costs	The production must cost a maximum of $€400$
$C2$	Use of supplies	Only the basic supplies: water and electricity may be used
$C3$	Local production	The device must be manufactured locally in LMICs
$R1$	Cleaning & sterilization	The device must be sterilizable by chemical immersion
$R2$	Dust- & waterproof	The device must be IP67 level dust- and waterproof
$R3$	Maintenance	The electronic parts must be replaceable when defective

(b) Design aims

ID	Aim	Performance criteria
$V4_A$	Imaging quality	The image should match state-of-the-art quality of a decade ago
$R4_A$	Durability	The device should be able to do a thousand cycles
$P3_A$	Biocompatibility	The device should be biocompatible according to ISO 10993-1 2018
$P4_A$	SILS	The device should be able to accommodate SILS
$U4_A$	Intuitive use & interface	The device and interface should be intuitive and easy to use

Part II

Concepts

“Define what the product will do before you design how the product will do it.”

Alan Cooper
The Essentials of Interaction Design

5

Concept Generation

This part, describes the concept design process based on the drivers and requirements. This chapter is the first step of the process: concept generation. Section 5.1 presents a morphological analysis, leading to the creation of three distinct concepts in Section 5.2. Based on analyses in Chapter 6 and Chapter 7, and other criteria a concept was selected in Chapter 8.

5.1. Morphological Analysis

In a morphological analysis, ideas are analytically and systematically generated by focusing on product functions [60]. Solutions to these functions form components in the morphological chart, resulting in a matrix of functions and components. An idea emerges from carefully selecting and combining components. This idea represents a principal solution: a thoughtfully chosen combination of elements that create a conceptual solution.

The AWL device has two main functions: lifting the abdominal wall and viewing inside the abdomen. A morphological analysis of these functions has already been done in previous research [30], which yielded four conceptual solutions. After a systematical evaluation, the circular loop concept was selected.

This process was not repeated, and the design was based on the circular loop concept, for the reasons stated in Chapter 2. Hence, the parameters of the morphological analysis are not the functions of the product but can be seen as design configurations. The morphological chart is shown in Table 5.1. The configurations are the loop shape (a top view of the device), the base shape (a side view), the diameter of the tube, the position of the camera in the loop, the type of lighting, and the heat dissipation system. Carefully selecting combinations of components led to the three conceptual solutions described in the following section.

5.2. Three Concepts

Three conceptual solutions were developed using the configurations in the morphological chart. Mixing various different components yielded unique concepts with logical pairings – such as the combination of optical fibers and airflow because these generate but also dissipate the least heat. However, most combinations of components are interchangeable.

Concept 1

The first concept's frame is a circular loop (option 2) with a flat base (option 1) and a constant outer diameter of $10\,\mathrm{mm}$. The camera is located in a specially designed tip at the extension of the circular loop (option 4). The lighting is accommodated by optical fibers (option 3), and the heat will be dissipated by airflow (option 1).

Since the camera is positioned in a designated tip, only the wires have to pass through the tube. The optical fibers only need one or two small openings in the tube, which is beneficial for the strength of the frame. Hence, a narrow tube of $10\,\mathrm{mm}$ diameter can be used for this concept. Optical fibers do not generate heat as the light (and heat) source is outside the human body. Therefore, airflow, which is the least efficient option for heat dissipation, will be sufficient to prevent the device from overheating.

Table 5.1: A morphological chart for generating conceptual solutions of a loop-shaped AWL device with an integrated camera.

Configuration	Option 1	Option 2	Option 3	Option 4	Option 5
Loop shape	Spiral	Circular			
Base shape	Flat	Helix			
Diameter	One diameter	Swaged	Multiple tubes		
Camera position	At start	In the middle	At the end	In the tip	
Lighting	LED standard	LED one resistor	Optical fibers		
Heat dissipation	Airflow	Water cooled	Heat pipe	Heat sinks	Vapor chamber

Concept 1
Concept 2
Concept 3

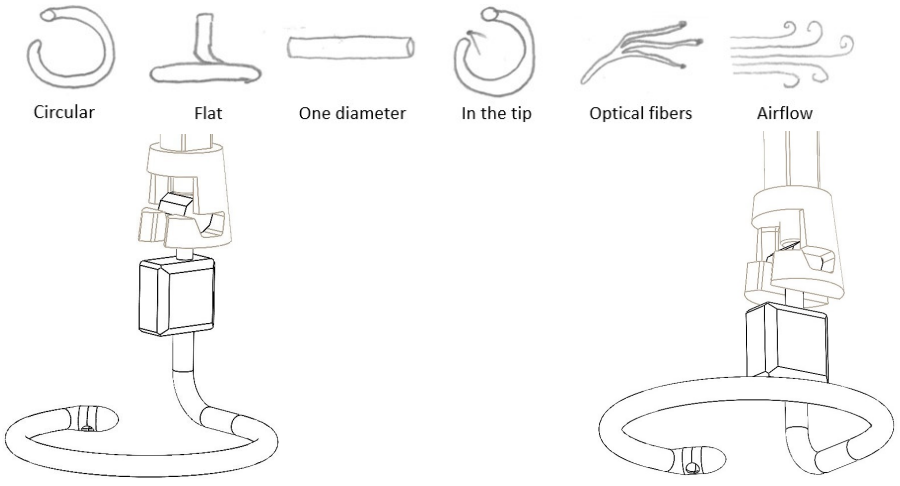

Figure 5.1: Concept 1: A circular loop with a flat base, a $10\,\mathrm{mm}$ diameter, the camera in a specially designed tip, optical fiber light, and airflow heat dissipation.

Concept 2

The frame of the second concept consists of a spiral loop (option 1) and a helical base (option 2). The tube has an outer diameter of $10\,\mathrm{mm}$, which is swaged to $12\,\mathrm{mm}$ at the end of the loop. That is where the camera is located (option 3). An LED circuit with one resistor (option 2) produces lighting around the loop, and heat will be dissipated by a heat pipe (option 3).

The inner diameter of the swaged end of the loop is larger than the rest of the tube. The camera is positioned in that part, and only the wires must pass through the tube. The LED circuit has only one resistor, which is placed outside the body; the bulk of the heat will be produced outside the abdomen. Nevertheless, some heat will be generated in the loop, which a heat pipe will dissipate.

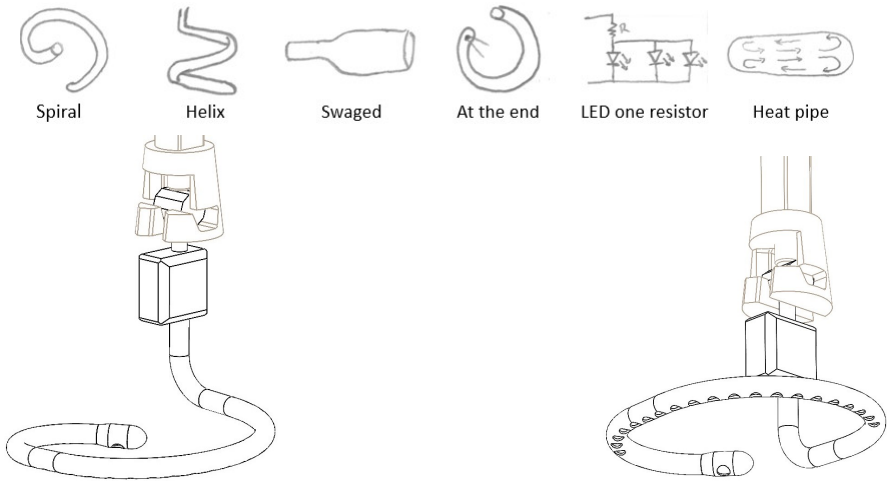

Figure 5.2: Concept 2: A spiral loop with a helical base, a $10\,\mathrm{mm}$ diameter swaged at the end with the camera inside, standard LED lighting, and a heat pipe.

Concept 3

The third concept's frame is a circular loop (option 2) with a helical base (option 2) and is swaged at the start of the loop (option 2). The camera is located in the middle of the loop (option 2), surrounded by standard LED light (option 1) and a water cooling system (option 2).

The camera has to fit in the middle of the tube. Consequently, the tube diameter around the loop is $12\,\mathrm{mm}$, and it is reduced to $10\,\mathrm{mm}$ before the upward curve. The standard LED strip will generate much heat, but it will be dissipated by a water cooling system, which is known for its extremely efficient heat transfer technology.

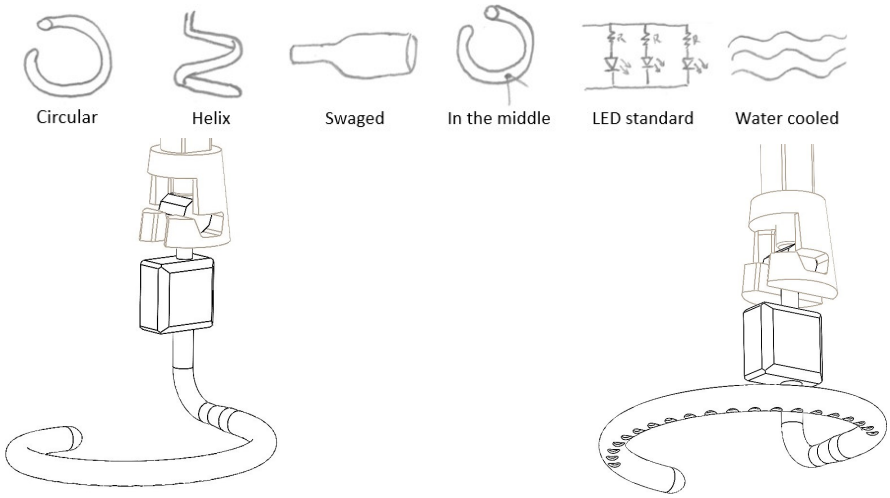

Figure 5.3: Concept 3: A circular loop with a helical base, a $12\,\mathrm{mm}$ diameter around the loop and $10\,\mathrm{mm}$ at the upward bend, the camera in the middle, LED lighting with one resistor, and a water cooling system.

6

Force Analysis

The three concepts of the previous chapter will be assessed on seven criteria, detailed in Chapter 8. The two most important criteria required thorough analyses. The first is discussed in this chapter.

Lifting the abdominal wall

Lifting the abdominal wall is a core function of this device. The abdominal wall comprises five layers, arranged from superficial to deep: skin, subcutaneous tissue, abdominal muscles, transverse fascia, and parietal peritoneum [61]. When operational space is created in the abdominal cavity, these layers are stretched, resulting in mechanical stress on the tissue, obstructing the further expansion of the abdominal wall [62].

The pneumoperitoneum in conventional laparoscopy is created with a standard intra-abdominal pressure setting of $15\,\mathrm{mmHg}$ ($0.02\,\mathrm{kg/cm^2}$). To provide adequate surgical exposure in morbidly obese adults, this may need to be increased up to $20\,\mathrm{mmHg}$ ($0.027\,\mathrm{kg/cm^2}$) [63, 64]. The largest abdominal radius recorded on CT was less than $120\,\mathrm{mm}$ [50]. Assuming a hemispherical shape for the abdomen, this equates to a maximum abdominal surface area of $452\,\mathrm{cm^2}$. With an intra-abdominal pressure of $15\,\mathrm{mmHg}$, the load would be equivalent to $9\,\mathrm{kg}$, while at $20\,\mathrm{mmHg}$, the load would be $12\,\mathrm{kg}$.

However, other studies report a $13.6\,\mathrm{kg}$ maximum load on the abdominal wall [65, 66, 67]. This aligns with research findings that the maximum acceptable force on the abdominal wall is $130\,\mathrm{N}$ and that trauma occurs from $150\,\mathrm{N}$ to $170\,\mathrm{N}$ [68]. For safety, the lifting device should be designed to lift a maximum load of $140\,\mathrm{N}$ without incurring any permanent deformation.

Permanent deformation, also known as plastic deformation, occurs when the strain in a material becomes so significant that the tensile stress exceeds the material's yield strength. This is known as the Von Mises yield criterion for ductile materials. When this criterion is exceeded, the deformation is irreversible; whereas deformations that remain below the yield strength, elastic deformations, are reversible.

The load of $140\,\mathrm{N}$ by the abdominal wall will deform the lifting device. Depending on the type of material, size, and geometry of the device, this will be an elastic or plastic deformation. The circular lifting device is assumed to create a truncated cone shape of the abdomen. The stretching of the abdominal wall results in internal forces along the direction of the layers, which translates to forces acting on the lifting device. The resulting forces acting on the lifting device are illustrated in a simplified 2D representation in Figure 6.1. A finite element analysis (FEA) tool was used to model the load and calculate the resulting deformations and Von Mises stress.

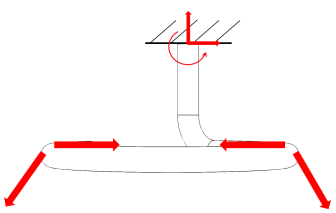

Figure 6.1: Resulting forces of the abdominal wall acting on the lifting device

Verification of the FEA tool

The SolidWorks Simulation tool [69] was verified by comparing the FEA deformation and stress results of a simple cantilever under distributed load to the analytical solution. An $10\,\mathrm{x1\,mm}$ stainless steel 17-4PH tube, with an elastic modulus E of $200\,\mathrm{GPa}$ and a length L of $300\,\mathrm{mm}$ was subjected to distributed loads of 100, 150 and $200\,\mathrm{N}$, as displayed in Figure 6.2. The default mesh size from SolidWorks was used. Additionally, a FEA was performed on a bent tube with identical characteristics and a bend radius of $60\,\mathrm{mm}$.

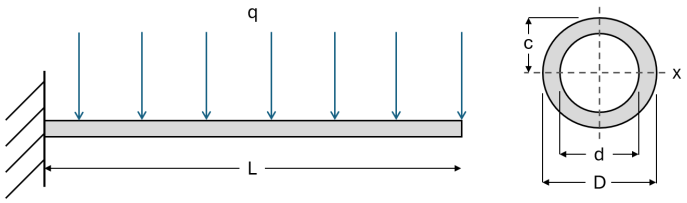

Figure 6.2: Cantilever beam under distributed load and the cross-section of a tube

The moment of inertia I_x for a tube is described by Equation 6.1 [70]. According to the Euler-Bernoulli beam theory, for a cantilever beam that is subjected to a distributed load q, the maximum deflection $\delta_{y_{max}}$ is described by Equation 6.2, and the maximum stress σ_{max} by Equation 6.3 [71].

$$I_x = \frac{\pi}{64}(D^4 - d^4) \qquad (6.1) \qquad \delta_{y_{max}} = -\frac{qL^4}{8EI_x} \qquad (6.2) \qquad \sigma_{max} = \frac{Mc}{I_x} = \frac{qL^2c}{2I_x} \qquad (6.3)$$

A visualization of the FEA results for a load of $100\,\mathrm{N}$ is displayed in Figure 6.3. These results were compared to the analytical solution. The maximum deformations and stresses from the analytical analysis and FEA for given loads are presented in Figure 6.4. By comparing Analytical (straight) and FEA (straight), it is evident that the maximum deformation results are exactly the same for both the analytical analysis and FEA. The maximum stress results, however, are overestimated by $2.7\,\%$ by the SolidWorks FEA tool. The discrepancy could be due to the mesh and solver imperfections. The FEA tool is thus not perfect. However, the discrepancy is minor and conservative, as it overestimates the maximum stress.

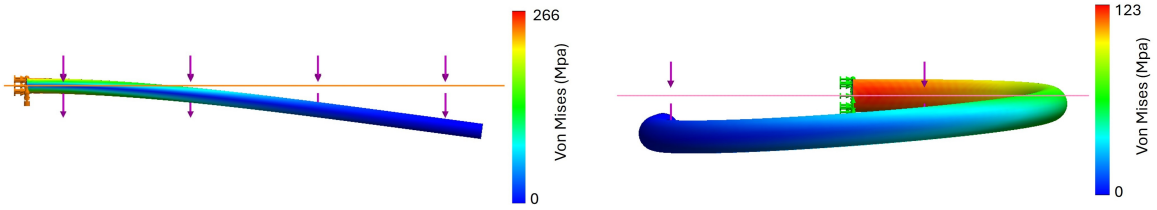

(a) Von Mises stress in straight tube

(b) Von Mises stress in bent tube

Figure 6.3: Visualization of the FEA results for a load of $100\,\mathrm{N}$.

When the tube is bent, see FEA (bend), the maximum stress in the material decreases by a factor of 2. The moment acting on the fixation point is lower, due to the shorter moment arm. The maximum stress is measured at this point, hence the lower moment makes this an unfair comparison between the straight and bent tube. Nonetheless, the circular shape causes part of the bending load to be converted into torsion. Since tubes are excellent at handling torsion, this conversion enhances the overall strength of the structure [70].

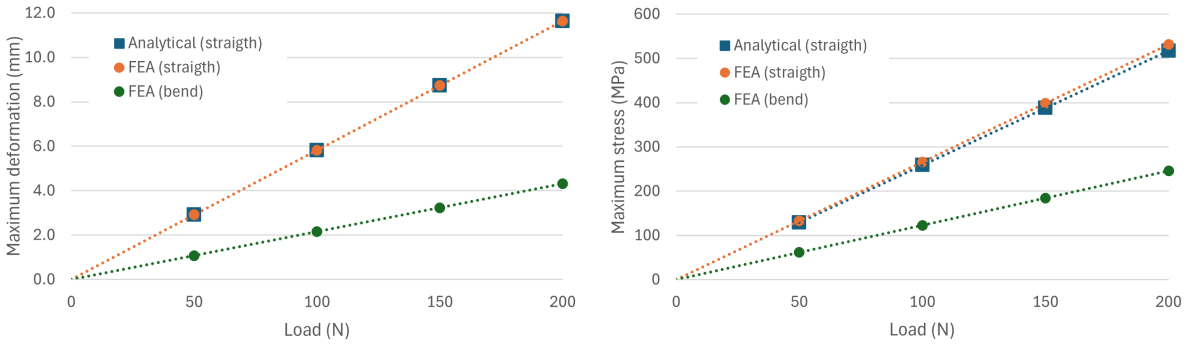

Figure 6.4: Comparison of analytical and FEA results for straight and bent cylindrical tubes.

Method

The frames of the three concepts discussed in Section 5.2 vary in three aspects. Firstly, the tube diameter can be $12\,\mathrm{mm}$, $10\,\mathrm{mm}$, or swaged from $12\,\mathrm{mm}$ to $10\,\mathrm{mm}$. Secondly, the frame base can be a flat or a helical shape. Thirdly, the frame base can be bent with one or two bending radii. The concepts are combinations of these aspects, which are shown in Figure 6.5. The influence of the aspects on the maximum Von Mises stress in the material was examined by executing finite element analyses for all possible configurations.

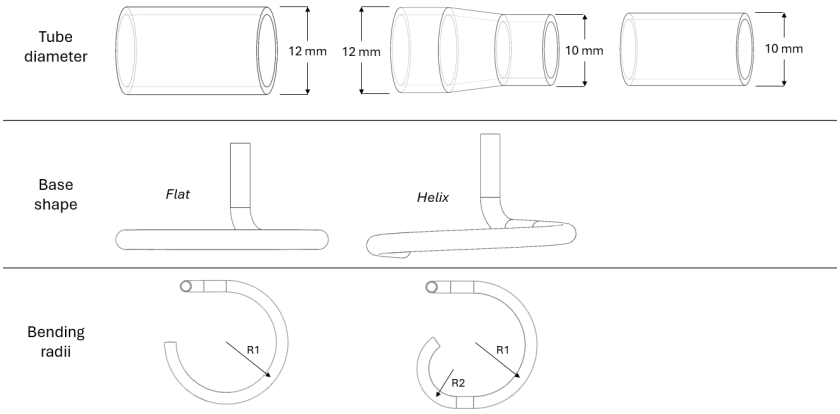

Figure 6.5: Configuration aspects of the tubular frame. Combining makes a total of $2\text{x}2\text{x}3 = 12$ distinct configurations.

The strengths of the frame configurations were calculated using the SolidWorks Simulation tool for finite element analysis [69]. A vertical static load of $140\,\mathrm{N}$ was distributed over the circular parts of the concepts. The material used for the simulation was stainless steel 17-4PH, which has a yield strength of $870\,\mathrm{MPa}$ [72]. The resulting tensile stress, or Von Mises stress, was computed.

To transfer light from the electronics inside the tube to the abdomen, a pattern of holes is drilled in the tube. Many holes are needed for the concepts with LED lighting, whereas the concepts with optical fiber light only need one hole. Stress concentration occurs at these holes because the stress is not uniformly distributed, which presents strong stress gradients in a few localized small areas [73]. Transverse holes in a tube can drastically increase the maximum Von Mises stress. The aforementioned FEA was also executed on all frame configurations with transverse holes for lighting to examine the resulting maximum tensile stress on the frame configurations.

The frames of the three concepts, including the transverse holes for lighting, were examined in terms of their strength. The first concept has a flat base, one bending radius, a $10\,\mathrm{mm}$ tube diameter, and one hole for optical fiber light. The second concept has a helical base, two bending radii, a $10\,\mathrm{mm}$ tube diameter, and twenty holes for LED lighting. The third concept has a helical base, one bending radius, a $12{-}10\,\mathrm{mm}$ tube diameter, and twenty holes for LED lighting. Similar finite element analyses were executed for the three concepts.

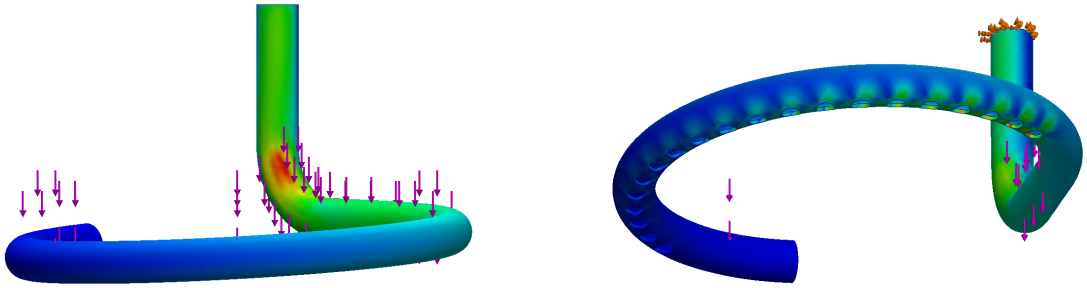

(a) A configuration without transverse holes

(b) A configuration with transverse holes

Figure 6.6: Visualization of the Von Mises stress under a static $140\,\mathrm{N}$ load. The maximum Von Mises stress is colored red.

Results

The location of the maximum tensile stress is similar for all twelve configurations without holes. The Von Mises stress is highest inside the upward bend; the location is displayed in Figure 6.6a. The results of the FEA of the twelve distinct configurations are shown in Figure 6.7. The configurations are grouped per tube diameter. The Von Mises stress is lower in all $12\,\mathrm{mm}$ diameter frames than in $10\,\mathrm{mm}$ and $12-10\,\mathrm{mm}$ diameter frames. Having multiple bending radii in the frame does not significantly influence the maximum tensile stress. Furthermore, the helical base results in a slightly lower Von Mises stress. Especially for the $12\,\mathrm{mm}$ diameter frame with one bending radius, the helical base results in lower stress. That particular configuration results in the lowest Von Mises stress.

Similar finite element analyses were executed on all frame configurations with transverse holes for lighting. The maximum tensile stress is measured in the first or second transverse hole, depending on the configuration (Figure 6.6b). The results of the FEA of the twelve distinct configurations with transverse holes are shown in Figure 6.8 . Again, the configurations are grouped per tube diameter. The figure shows that $12\,\mathrm{mm}$ diameter frames result in the lowest maximum tensile stress, followed closely by $12-10\,\mathrm{mm}$ frames. Having multiple bending radii reduces the Von Mises stress. The helical base does not significantly influence the maximum tensile stress in $12\,\mathrm{mm}$ and $12-10\,\mathrm{mm}$ diameter frames. The Von Mises stresses in $10\,\mathrm{mm}$ diameter helical base frames, however, are lower than in the flat base frames.

Figure 6.9 shows the results of the FEA on the three concept frames. The maximum Von Mises stress is $260\,\mathrm{MPa}$, $415\,\mathrm{MPa}$ and $303\,\mathrm{MPa}$ for concept 1 to 3, respectively. The corresponding factors of safety for this material are 3.3, 2.1, and 2.9. The Von Mises stress is highest inside the upward bend in concept 1. In concept 2, the stress is highest at the second of the twenty holes, and, in concept 3, at the first hole.

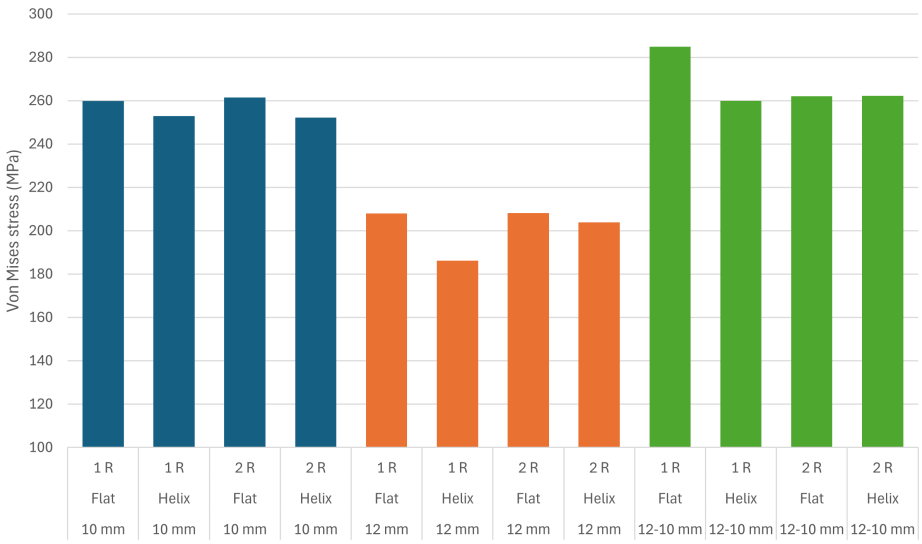

Figure 6.7: FEA results of twelve frame configurations without transverse holes.

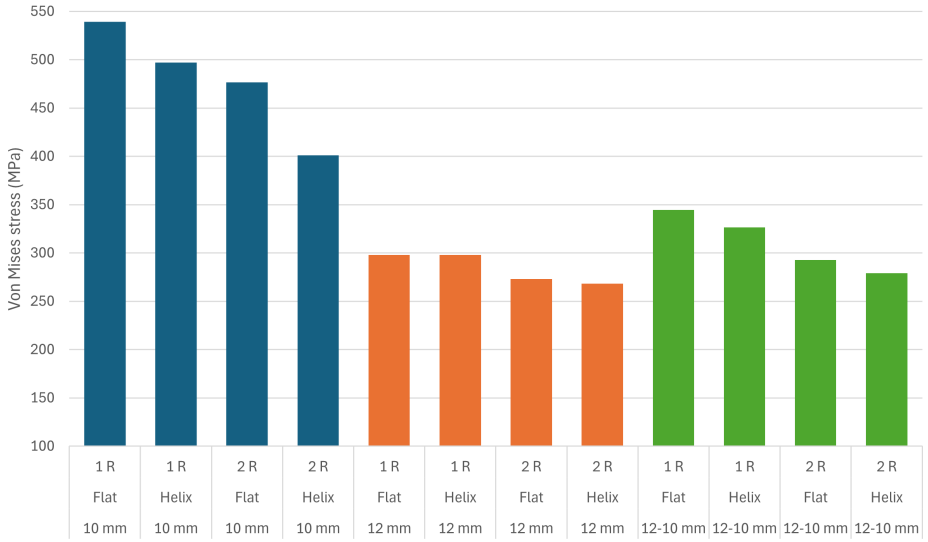

Figure 6.8: FEA results of twelve frame configurations with transverse holes.

Discussion

The tensile stress is maximal, where the strain in the material is the largest. In the case of configurations without transverse holes, the stress is uniformly distributed over the materials. Hence, the Von Mises stress decreases linearly along the loop of the frame. Consequently, the tensile stress is maximal at the upward bent since the largest bending moment is acting on that area. At this specific area, a combination of high tension and torsion occurs due to the upward bent. In the configurations with transverse holes, the stress is not uniformly distributed, resulting in high stress concentration. As the stress decreases linearly along the loop of the frame, the highest stress concentration occurs at the first or second hole.

Examining the FEA of frame configurations without transverse holes, it was observed that the Von Mises stress is lowest in $12\,\mathrm{mm}$ diameter frames. This is because the moment of inertia increases with increasing diameter, as denoted in Equation 6.1. The distance from the neutral axis to the outermost fiber – c in Equation 6.3 – also increases with increasing diameter. However, this scales linearly, whereas the moment of inertia scales to the third power. Therefore, a larger diameter results in lower tensile stress. Furthermore, the presence of two bending radii does not significantly affect the maximum Von Mises stress since the length of the tube is the same. Hence, the bending moment and resulting tensile stress are similar. The helical base results in a slightly lower maximum Von Mises stress. It is expected to be due to the $2.3°$ smaller upward bent, although this was not proven.

Likewise, the maximum tensile stress for frame configurations with transverse holes is lowest in $12\,\mathrm{mm}$ diameter frames. The helical shape is less important due to the maximum stress being concentrated in the holes instead of the upward bent. However, it has a significant influence on the $10\,\mathrm{mm}$ diameter configurations. Furthermore, the presence of two bending radii reduces the Von Mises stress. This is likely due to the transverse holes being arranged differently. The number of holes and hole diameter are identical for all frame configurations, but the spacing is slightly different due to the varying frame shapes. The $5.5\,\mathrm{mm}$ hole diameter results in a considerably higher Von Mises stress for $10\,\mathrm{mm}$ diameter frames since the holes are relatively larger with respect to the tube diameter. The hole arrangement is of substantial importance and should be optimized for a specific frame configuration.

Considering the aforementioned findings, the FEA results from the three concepts were as expected. Although concept 1 has the smallest frame diameter, it has the lowest maximum Von Mises stress because it has only one transverse hole for lighting. Concept 2 results in the highest Von Mises stress, due to the transverse holes in the smaller diameter frame. When many transverse holes are required for lighting, a $12\,\mathrm{mm}$ diameter frame is favored, either with a flat or helical base.

To conclude, although differences in Von Mises stress are significant, these are well within the elastic deformation. All concepts have a factor of safety larger than 2 of the yield stress for the specific

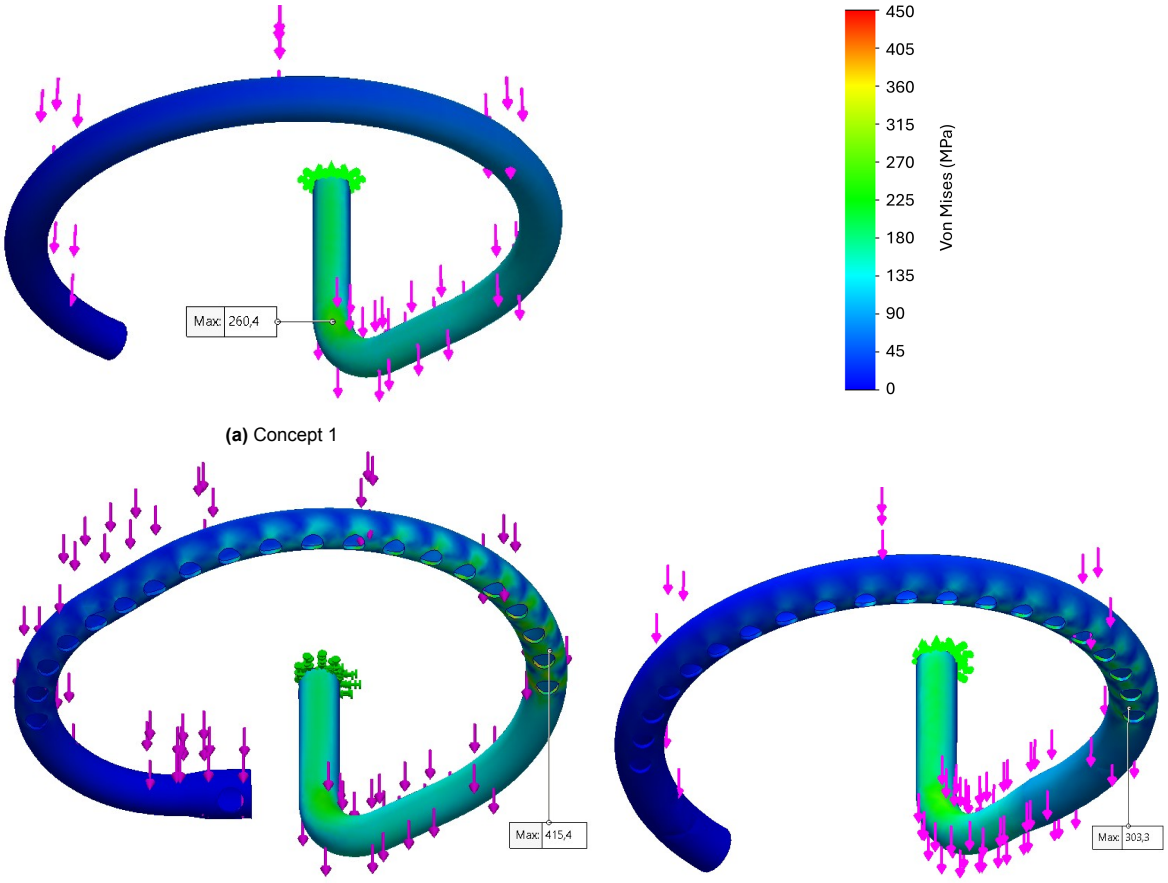

(a) Concept 1

(b) Concept 2

(c) Concept 3

Figure 6.9: Visualization of the Von Mises stress in the three concepts for a load of $140\,\mathrm{N}$.

material. Nonetheless, a larger tube diameter is favorable; flat and helical bases are comparable, as well as having one or two bending radii. Moreover, the effect of transverse holes is considerable, and the arrangement should be optimized. Arranged from best to worst are concept 1, concept 3, and concept 2, with the side note that all are well under the yield stress.

Limitations

The Von Mises stress computed by the SolidWorks FEA tool is overestimated by $2.7\,\%$. Mesh and solver imperfections may be causing the discrepancy. Although the FEA tool is not perfect, the difference is minimal and conservative, as it overestimates the maximum stress. A second limitation is the type of load that is applied in the FEA tool. Figure 6.1 showed a simplified representation of the resulting forces of the abdominal wall acting on the lifting device. This was further simplified to a $140\,\mathrm{N}$ load acting vertically.

The freedom in design makes it difficult to draw indisputable conclusions. For example, the radius of the upward bend, the length of the loop, and the pitch of the helical frames affect the amount of Von Mises stress and potentially the maximum tensile stress. Moreover, the transverse hole arrangement is based on the previous prototype described in Section 2.3. The location of the first hole, the number of holes, the spacing between holes, and the hole diameter are major factors determining the Von Mises stress in the material. The range of design choices makes it challenging to draw firm conclusions.

7

Camera Position Analysis

The second analysis aimed to find the most favorable camera position for common laparoscopic procedures. First, the answer was sought in literature (Appendix C). Although the literature provided interesting insights into eye-hand coordination problems, no notable distinction between the concepts could be made. Hence, a box trainer experiment was executed.

This experiment aimed to determine the effect of camera position and orientation on the surgeon's performance during laparoscopic tasks. The study combined quantitative test results with participants' perceived experience to make an informed decision on the most favorable camera position.

Method

The Lapron box trainer from ForceSense and Amsterdam Skill Centre was used to simulate the laparoscopic tasks. ForceSense has a strong scientific foundation with 17 publications supporting its validity [74]. The sensor system, integrated into the box trainer, automatically tracks the participant's performance. The objectives it measures are the time taken to complete an exercise, the forces applied to the tissue, and the motion of the instruments.

(a) Task 1: Zig-zag Loop

(b) Task 2: Wire Chaser (Two Hands)

Figure 7.1: Tasks performed by the participants

Various laparoscopic tasks, ranging from simple to advanced, can be performed to evaluate the participant's performance. Choosing the right level of difficulty was crucial to obtain useful data output. In explanation, the measured objectives should vary due to the different camera positions. If a task is either too easy or too hard, the difference in measured objectives will not be determined by the camera position. After performing multiple pilot tests, two tasks were selected based on their level of difficulty. The first task is the zig-zag loop, Figure 7.1a. The goal is to thread a rope through the loops on the first and second rows in a zig-zag pattern. The second task is the wire chaser (two hands), Figure 7.1b. The goal is to move three rings, with decreasing diameters, one by one, to the other side of a wire using the left and right hand alternately.

Another factor that influences the output data is the participants' learning curve. A certain period is required to get used to the new environment, especially for participants with little to no experience handling laparoscopic instruments. As described in Section C.1, the impaired eye-hand coordination, effects of the incision point, impeding effects on observation, and impaired perception of depth influence

the participants' performance. Giving the participants time to get used to the environment will reduce the variance in the output data due to the learning curve.

Three camera positions will be used in the experiment based on the concepts from Section 5.2. The position of the cameras relative to the incision point varies between the concepts, and their view is displayed in Figure 7.2. The first concept has the camera positioned on the right side of the incision point; in the second concept, it is placed in front of and close to the incision point; and the third concept also has it positioned in front of the incision point, but further away. Thus, the camera positions are, respectively, (a) from the right side, (b) in direct line-of-sight, and (c) a top view. All cameras are oriented so that the target is in the center of the view.

(a) Camera position A **(b)** Camera position B **(c)** Camera position C

Figure 7.2: The view of the camera in each position. The first subfigure displays the zig-zag loop task, and the second and third subfigures show the wire chaser task.

So, the participants are asked to perform two tasks. These tasks are repeated for each camera position, adding up to six trials per participant. The duration of a trial is set to a maximum of three minutes. The experiment has a duration of approximately 50 minutes per participant, and seven participants performed the experiment. The order of tasks was identical for all participants. On the other hand, the order of camera positions was randomized for each participant. This was done to reduce the influence of experience, i.e., to cancel out the participants' learning curves. The experiment protocol of participant C is provided as an example in Section C.2.

The participants were assessed quantitatively on the time it took to complete the task or part of the task, the path length of the instrument tips, the number of misgrasps, the maximum force, the number of force threshold exceedance, and the longitudinal movement of the left and right instruments. The longitudinal instrument movement directly correlates to the perception of depth [75]. A low task time, few unnecessary movements and misgrasps, and little force applied are measures of favorable performance. Consequently, the concept corresponding to low objectives measured is considered superior. A brief interview obtained qualitative user experience.

Experimental Setup

The experimental setup, shown in Figure 7.3, consists of three parts: the Lapron box trainer (1), a 3D-printed camera holder (2), and a second monitor (3). The Lapron box trainer is a plug-and-play mobile device that allows using any $5\,\mathrm{mm}$ laparoscopic instrument (4). The functions of the box trainer can be divided into three elements. The first is a cavity where the target task (7) is located. This part cannot be seen directly because it is covered by a black sheet (5).

The black sheet acts as the abdominal wall. Two laparoscopic instruments and a laparoscope are inserted through this sheet. The baseball diamond port positioning (Figure 7.4) is applied to this box trainer [76]. This means a $60°$ angle between the two instrument tips, a tangential approach to the target site, and an appropriate working distance. The laparoscopic instruments are inserted through trocars (6), which measure the movement and force on the tips.

Although the Lapron box trainer has an integrated laparoscope and monitor, these cannot be utilized for the experiment. Lapron's standard laparoscope cannot be used to simulate the three different camera positions due to dimensional constraints. Hence, the much smaller OV5693 camera module was used.

This module has a digital USB video output, whereas the integrated monitor has an uncommon analog 3.5 mm jack input. Converting USB video to an analog 3.5 mm jack involves using a combination

Figure 7.3: The experimental setup and the inside of the box trainer.

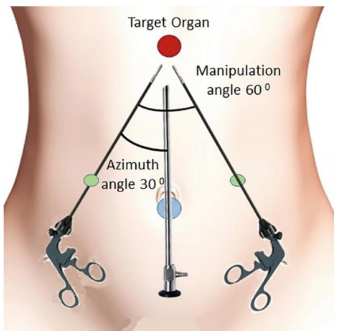

Figure 7.4: The baseball diamond port positioning principle [76, 77].

of USB video adapters, digital-to-analog converters, and A/V cables. Consequently, the signal would be degraded, and delay would be introduced. Therefore, an external monitor was added to the setup. The benefit of the external monitor is the higher-definition display due to the better quality of the camera and digital signal.

As described before, three camera positions will be used in the experiment based on the concepts from Section 5.2. A 3D-printed assembly was designed to resemble these camera positions. The third and final iteration is shown in Figure 7.5. The main part (1) is fixed to the laparoscope's incision point by tightening part 2. The camera module is placed in position A, B, or C, and parts 3, 4, and 5 fixate the module. The different camera orientations result in the views displayed in Figure 7.2.

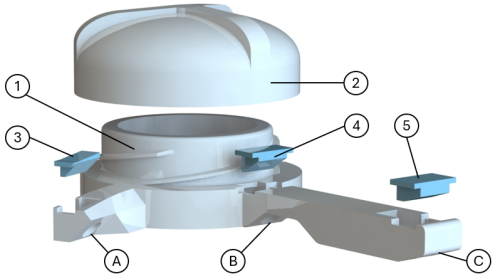

Figure 7.5: The 3D-printed camera holder assembly. (1) is the main part; (2) is a lid to fix the device to the box trainer; (3), (4), and (5) are caps to fixate the camera module in position; (A), (B), and (C) are the positions of the camera module.

Results

The participants performed a total of 42 trials, 21 for each task. They were assessed on six objectives. The most essential is the time to complete the task. However, the task was not always completed since a maximum of $180\,\mathrm{s}$ was set. For those, the task time was corrected for the percentage of progress. Hence, the task time in Figure 7.6a and Figure 7.7a can be higher than $180\,\mathrm{s}$. The path length of the instrument tip is corrected likewise.

The other objectives are the number of misgrasps, the maximum applied force, the number of times the force threshold is exceeded, and the longitudinal movement of the left and right instruments. The force exceedance only applies for the second task, and the threshold was $2\,\mathrm{N}$. As explained before, a low task time, few unnecessary movements and misgrasps, and little force applied are measures of favorable performance. Consequently, the concept corresponding to low objectives measured is considered superior.

Task 1: Zig-zag loop

The results of Task 1 are displayed in Figure 7.6, ordered from most to least important. The means are included in the figures to give a more comprehensive overview. Considering the task time, it is observed that the medians of positions B and C are slightly below the central box of position A. However, the central box of position A completely overlaps boxes B and C. There is no significant shift between the whole box plots. The variance in task time of positions A and B are enormous, with relative standard deviations (RSD) of 58% and 51%, respectively, and the RSD of position C is 28%. No distinction between the three camera positions can be made based on the modest differences and extensive variances.

The second most essential objective is the number of misgrasps. The complete central box of position A is below boxes B and C. The whole box plot of position A is shifted down compared to positions B and C, despite one far outlier. The medians of position B and C are identical and the central boxes overlap considerably. The means show the same trend. Again, the variance is considerable, with RSDs of $70\%, 40\%$, and 54%, respectively. Nevertheless, it can be observed that there is a difference in the number of misgrasps, and position A is more favorable in that sense.

The path length is the absolute distance the tips of both instruments move. All medians are within the central boxes of the other positions, and the boxes have considerable overlap. The box plot of position B is slightly shifted up compared to positions A and C, albeit it is difficult to compare considering the outlier from position A. The RSDs are $54\%, 50\%$, and 31% for positions A, B, and C, respectively. Conclusively, there is no significant distinction between the positions regarding path length.

The longitudinal movement was measured for the left and right instruments. For the left instrument, the median of position A is below the central boxes of positions B and C, but the central boxes do overlap noticeably. The means positions A, B, and C are ordered from lower to higher, and the box plots are shifted accordingly. There is less variance with RSDs of $26\%, 13\%$, and 23%, respectively. For the right instrument, positions A and B have similar medians, means, and spread. The medians of positions A and B are just above box C. The whole box plot of position C is shifted down, and the mean is as well. However, there is an overlap between the three central boxes. The variance is similar to the left instrument with RSDs of $23\%, 19\%$, and 16%. It can be observed that the longitudinal movement of the left instrument is slightly less with camera position A, while for the right instrument, it is slightly less with position C.

Considering the maximum applied force, it can be observed that the median of position B is above boxes A and C. The central boxes do, however, have vast overlap. The box plot of position B is slightly shifted up compared to positions A and C, albeit it is difficult to compare considering the outlier from position C. The RSDs are $28\%, 39\%$, and 54%, respectively. With the relatively minor differences and the considerable deviations, no distinction between the positions can be made.

Task 2: Wire Chaser

The results of Task 2 are shown in Figure 7.7. The participant had more difficulty in completing this task within the $180\,\mathrm{s}$ time limit, consequently the (corrected) task times are higher. The median of position B is slightly below boxes A and C, and the upper quartile of position B is equal to the medians of A and C. The whole box plot of position B is also shifted down compared to A and C. The means follow the same trend, where position B's mean is 20% lower. The variances are comparable with RSDs of $29\%, 20\%$, and 23%, respectively. All in all, the task time is lower with camera position B.

Considering the number of misgrasps, the median of position A is well above boxes B and C. Those two box plots are comparable in medians, means, and spread. The whole box plot of position A is shifted up, and the mean is 52% higher than position B and 63% higher than C. The variance between participants is large with SPDs of $58\%, 41\%$, and 32%, respectively. Thus, there are more misgrasps with camera position A, although the difference might be smaller than at first glance.

The median path lengths of all positions are within the central boxes. Nonetheless, the whole box plot of position B is shifted down compared to positions A and C. Accordingly, position B's mean is approximately 20% lower than A and C. The variances are similar with RSDs ranging from $23\,\%$ to $27\,\%$. No distinction between positions A and C can be made. Position B, on the other hand, has a moderately shorter path length.

The longitudinal movement is slightly larger for Task 2. For the left instrument, the means are similar, all medians are within the central boxes, and these overlap considerably. The variance is relatively low with SPDs of $23\%, 14\%$, and 12%. For the right instrument, the medians of positions A

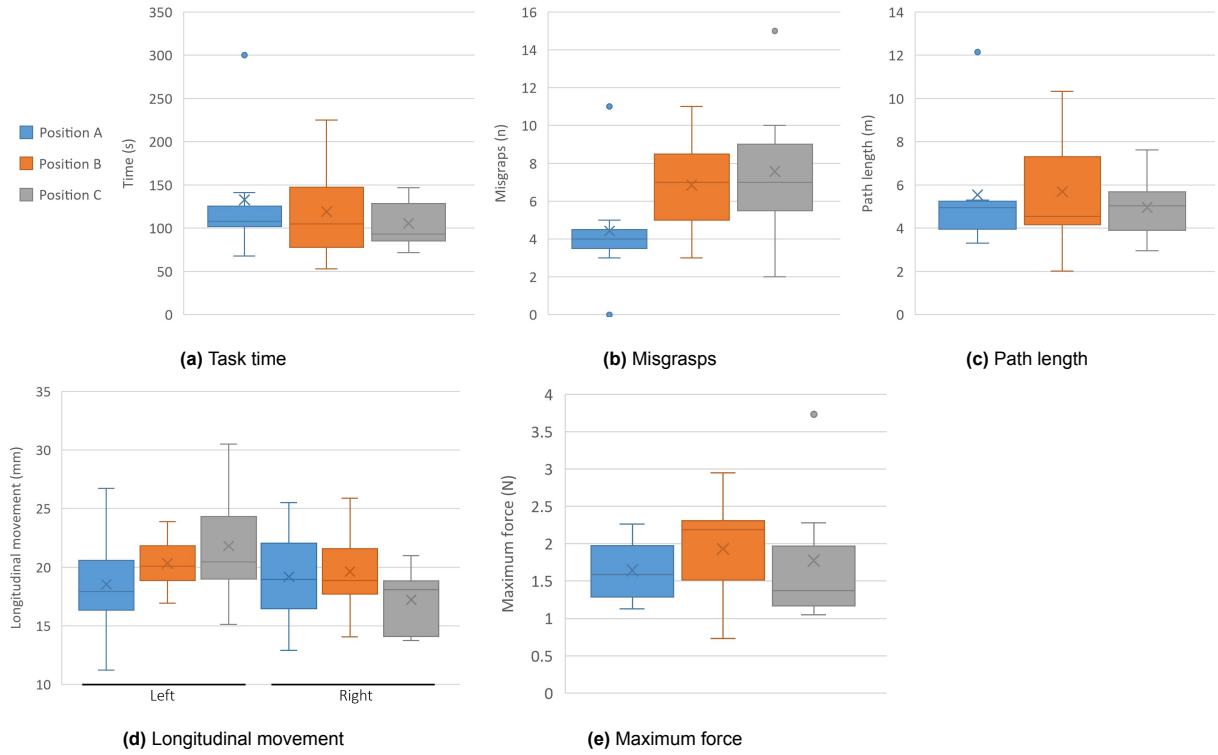

(a) Task time **(b)** Misgrasps **(c)** Path length

(d) Longitudinal movement **(e)** Maximum force

Figure 7.6: Results of Task 1: the zig-zag loop. The mean values are included in the box plots. The quartiles are calculated with the median included.

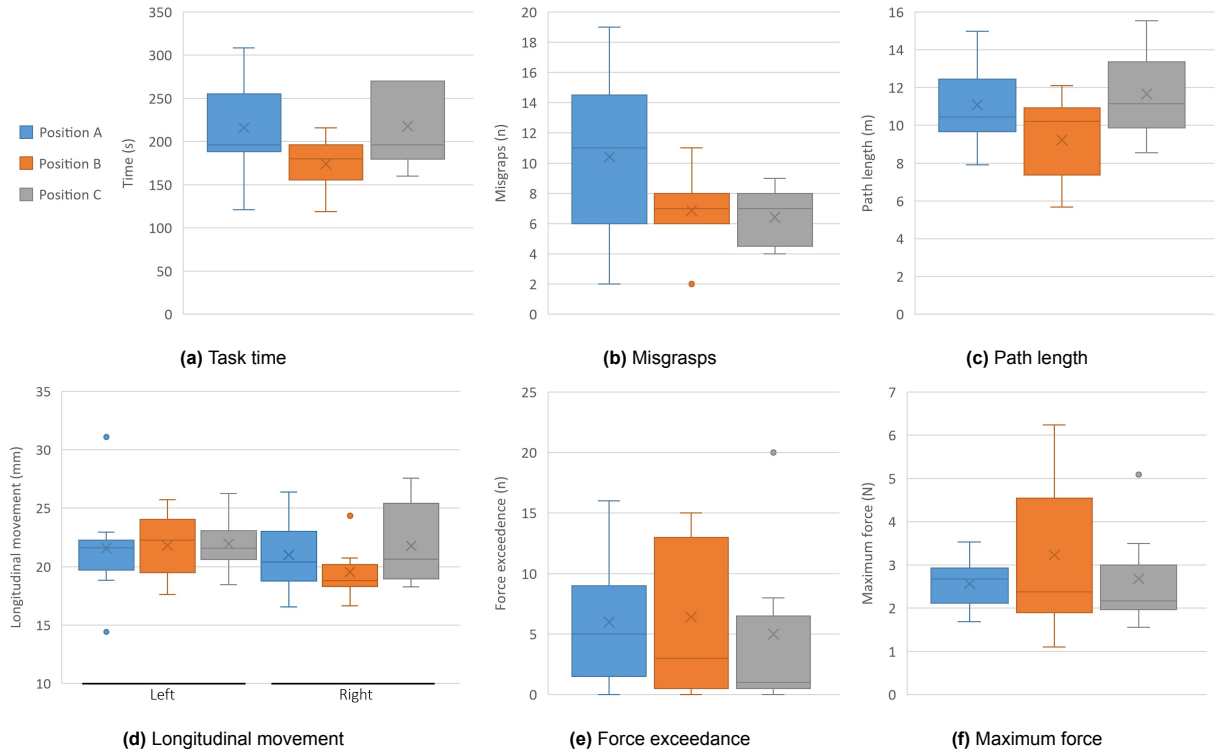

(a) Task time **(b)** Misgrasps **(c)** Path length

(d) Longitudinal movement **(e)** Force exceedance **(f)** Maximum force

Figure 7.7: Results of Task 2: the wire chaser (two hands). The mean values are included in the box plots. The quartiles are calculated with the median included.

and C are slightly above box B, and the median of position B is slightly below boxes A and C. However, there is considerable overlap between the central boxes, especially between boxes A and C. The whole box plot of position B is marginally shifted down. With SPDs of $17\%, 13\%$, and 16%, the variances are similar to the left instrument. Conclusively, no distinction between the camera positions can be made for the left instrument. The longitudinal movement of the right instrument is lower to some extent with camera position B, although this might be insignificant.

The number of force exceedance was only applicable to the second task. All medians are within the central boxes, the boxes overlap substantially, and the means are comparable. As can be seen at first glance, the variance is enormous (RSDs $95\%, 107\%$, and 49%). Thus, no distinction between the camera positions can be made.

The same applies to the maximum force. Although the variance is lower (RSDs $25\%, 65\%$, and 46%), all medians are within the central boxes, and the boxes overlap significantly. The whole box plot of position B is shifted upward, and the mean is 20% higher than A and C. Nevertheless, the differences are relatively small compared to the variance, so no distinction between the camera positions can be made.

Table 7.1: Ranking of the camera positions by the quantitative results. The numbers indicate the number of times a camera position is rated better or worse, or no distinction could be made. The score is a rating from one to ten; where the better rank weights triple, identical weights double, and worse weights once.

(a) Task 1: Zig-zag loop

	Camera position	Rank			Score
		Better	Identical	Worse	
1	Position A	2	3	1	7.2
2	Position C	1	3	2	6.1
3	Position B	0	3	3	5.0

(b) Task 2: Wire chaser (two hands)

	Camera position	Rank			Score
		Better	Identical	Worse	
1	Position B	4	3	0	8.6
2	Position C	1	3	3	5.7
3	Position A	0	3	4	4.8

The results of the objectives in Figure 7.6 and Figure 7.7 are summarized in Table 7.1 and a score is given to the camera positions. Note that the importance of the objectives is not reflected in these tables. For Task 1, no distinction between the camera positions could be made from the task time, path length, and maximum force. Therefore, the difference in score is based on the number of misgrasps and the longitudinal movement. For Task 2, the difference is based on the task time, number of misgrasps, path length, and longitudinal movement of the right instrument. Although these tables do not give a comprehensive overview, they give insight into which camera position is favorable. For Task 1, camera position A is ranked best and position B worst. For Task 2, it is exactly the opposite.

Interview

The participants were also examined on their opinions about the tasks and influence of the camera position. Four of the seven participants found Task 2 (The wire chaser) the most difficult task. They reported that grabbing the rubber ring and transferring it between the instruments was challenging because the ring was round and often slipped out the instrument tip. ”Getting the stiff rings around the corners was difficult and forcing them will cause them to slip out of the claw.” Executing Task 2 well and neatly was demanding. Participants often dropped the rings, sometimes forward and sometimes backward. The setbacks were demotivating.

The other participants (3/7) found this task the easiest. In their experience, it was easier to understand; it was clearer how the ring moves (compared to the rope) since it was more rigid. They reported that their hands felt when the ring was grabbed. There were fewer obstacles in the way of the instruments, which gave them the feeling there was more space to operate. One participant reported: ”In this task, there was a better view of whether the gripper had reached the ring.”

These three participants found the zig-zag loop (Task 1) more difficult because it was hard to see if the rope went through the loops, which obliged them to guess it went through. Other loops were in the way of the instruments, forcing the participants to grab the rope in the right place with the right orientation. This required experience and a strategy.

The majority (4/7) found this task easier. They reported that grabbing the rope and transferring it between the instruments is easier than the rings. Less rotation of the rope and instruments was

required, and less precision was necessary to complete the task. Pulling the rope through the first loop was the easiest because there was the most space. The final loop gave the most trouble.

The participants were asked to rank the camera positions from best to worst for both tasks. An rankings overview is given in Table 7.3. Camera position B is rated best for both tasks. The participants gave remarks about their ranking. Their quotes are summarized below.

Task 1: Zig-zag loop	Task 2: Wire chaser (two hands)
Position A	
• Hard to see the depth toward the rope and the instrument's tip. (4x) • Least natural and intuitive movement, the orientation was difficult to understand. (2x) • I could clearly see if the rope would go in the loop. (2x) • The motion I saw on the screen was different than expected. • There is a large variation between the motion of the left and right instruments. • The last loop is very difficult to see. • I saw the loops from the side and could see the y and z directions better. • I could not see or understand what loops were in the way of the instrument; I kept bumping into them.	• When the instrument was in line with the image, I could not see how far the tip was, and it blocked part of the view. (2x) • Looking at it from an angle was difficult; I got a bit dizzy because of it. • Understanding the orientation was hard. • It seemed like the angle I could make with the instrument was smaller, like there was less room to move. • I frequently bumped into the wire. • I often grabbed the iron wire. • Transferring the ring between instruments was easier • I could easily see how the ring was twisted.
Position B	
• I easily and quickly saw if the rope was through the loop. (3x) • Direction x and z are clearly visible, direction y – the distance between the row of loops – is difficult to see. (2x) • It was harder to see if the rope would go into the loop. • It felt the most natural how you saw the instruments and how they moved. • I had the best sense of the working field's depth. • Grabbing the rope and correcting it if I didn't grab it properly was the easiest.	• I easily saw how the rings were twisted. (2x) • I saw the graspers clearly, and transferring between instruments was easier. (2x) • I saw all corners clearly, and I saw depth in all directions. • The image I saw was correct with the movement I made. • The instrument did not get stuck. • It was more difficult to see how I held the rings and how they were twisted.
Position C	
• It was hard to estimate the height of the loops and the instrument's tip. (3x) • Grabbing the rope and transferring between the instruments was more difficult (2x) • I had to look twice where the instrument's tip actually was. • I often grasped before the instrument's tip was at the rope. • I could easily see if the rope was through the loop. • This was the easiest position to determine the x and y directions.	• I could estimate depth the best, and I understood the image best. (2x) • It was hard to see where the corner was and if the ring passed it. (2x) • I missed height perception. • It felt like 2D-vision. • The ring got stuck sometimes, but I did not understand how.

Table 7.3: Ranking of the camera positions by seven participants. The numbers indicate the number of times a camera position is rated first, second, or third. The score is a rating from one to ten; where 1^{st} rank weights triple, 2^{nd} weights double, and 3^{rd} weights once.

(a) Task 1: Zig-zag loop

	Camera position	Rank 1^{st}	Rank 2^{nd}	Rank 3^{rd}	Score
1	Position B	3	3	1	7.6
2	Position C	2	3	2	6.7
3	Position A	2	1	4	5.7

(b) Task 2: Wire chaser (two hands)

	Camera position	Rank 1^{st}	Rank 2^{nd}	Rank 3^{rd}	Score
1	Position B	4	3	0	8.6
2	Position C	2	1	4	5.7
3	Position A	1	3	3	5.7

Discussion

All participants were completely new to the laparoscopic environment. Therefore, there was a substantial variance in performance between the participants. The learning curve was steep, which resulted in better performance at later trials. Although the order of trials was randomized, it could have contributed to the large variance. Nonetheless, the following conclusions can be carefully drawn.

The measured objectives do not result in an unambiguous favorite camera position. No distinction between the camera positions could be made from the task time, path length, and maximum force of Task 1. The difference in score is based on the number of misgrasps and the longitudinal movement. Camera position A is clearly favorable, although the variance is considerable. The variance in longitudinal movement is smaller, but the differences between camera positions are minor.

Table 7.1a shows that camera position A is favorable. However, the importance of the objectives is not reflected, and the differences between camera positions are more nuanced than the table suggests. In explanation, the only clear distinction can be made based on the number of misgrasps, which is just one of the five measured objectives. In conclusion, for Task 1, camera position A is slightly favorable, although the difference is insignificant.

For Task 2, the distinction between camera positions is based on task time, number of misgrasps, path length, and the longitudinal movement of the right instrument. The first three are the three most important objectives. Camera position B certainly results in the shortest task time. The distinction between camera positions is less evident for the other objectives. The number of misgrasps is higher with position A; however, the variance is substantial. Camera position B results in a moderately shorter path length and a slightly shorter longitudinal movement (right), although this might be insignificant.

Table 7.1b reflects that camera position B is favorable for Task 2. Though the table has the aforementioned limitations, the distinction between camera positions is based on four objectives and, therefore, yields a more relevant distinction.

The participants expressed that camera position B is more favorable in their experience. However, the impressions vary considerably, especially for Task 1. Generally, the participants understood the camera view best with position B. They mentioned that it felt the most natural and that the image they saw reflected their movements.

Most participants indicated that depth perception and understanding of the orientation and motion was difficult with camera position A. On the other hand, some actually preferred this camera position. With camera position C, understanding the orientation and movement was less complicated. However, the participants missed height perception with the top-view camera.

For Task 1, the participants' experience does not correspond to the measured results. As mentioned, the distinction between camera positions with quantitative results is only based on the number of misgrasps. Therefore, the measured results are insignificant, and the disparity with the participants' experience is understandable.

On the contrary, the measured results and the participants' experience for Task 2 do align. The quantitative results of Task 2 are more meaningful, and there is more consensus in participants' opinions. Nevertheless, participants' opinions should be interpreted with caution and not be regarded as absolute facts since they were new to the laparoscopic environment.

In conclusion, the box trainer experiment aimed to evaluate the effects of camera positioning on laparoscopic task performance. Overall, while the experiment reveals slight performance differences across camera positions, the results do not distinctly favor one position. Camera position B shows a modest advantage in Task 2, with faster task completion and fewer misgrasps. However, high participant variability and limited distinctions in Task 1 suggest that these findings should be interpreted cautiously.

The overall findings are presumably mixed due to eye-hand coordination challenges inherent in laparoscopic surgery. Camera position B aligns better with the surgeon's line of sight, improving coordination and offering benefits in specific tasks. Nevertheless, the variation among participant experiences and performance results underscores the need for further research to optimize the fixed camera positioning in laparoscopic procedures.

Limitations

The most essential limitation of the experiment was the participants' lack of laparoscopic experience. People with no laparoscopic experience are prone to the most basic eye-hand coordination problems and effects of the incision point. Consequently, the differences in performance could be due to factors other than the camera position. Allowing participants to get familiar with the environment helped, but having participants with far more experience will yield more realistic and useful results. Then, differences in results will be irrefutably due to changes in camera position.

As concluded, the optimal camera position is task-dependent. The experiment should be repeated for a variety of tasks to obtain a more comprehensive overview. Moreover, the tasks are created to train laparoscopy students' skills rather than mimicking real surgery. Therefore, the tasks are located in the center of the box and oriented in the line of the original laparoscope. Such conditions are typically uncommon in actual laparoscopic surgery. So, the experiment should consist of various more realistic tasks.

The number of trials should be increased to decrease the uncertainty of the results. The box plots are now made with only seven data points each. Increasing the number of trials would not necessarily decrease the variance, but it would yield more reliable results. This can be achieved by inviting more participants or conducting more trials per participant.

Resolving these limitations would allow for a more numerical comparison of the camera positions. In the experiment, conclusions are based on box plots, which are crude visual representations of the data. With data constraints this significant, it was unreasonable to attempt explicit numerical conclusions. Having more data points that are more realistic and directly reflect changes in camera position will deepen understanding of its influence and allow for unambiguous conclusions.

8

Concept Selection

8.1. Criteria

This chapter evaluates the three concepts based on the design drivers. A graphical representation of the strengths and weaknesses of the concepts - the so-called Harris Profile - is used to evaluate these systematically [60]. Each concept will receive a visual rating of its potential. An informed decision will be made to select the most promising concept.

The rating of the concepts is attributed to seven criteria. These criteria are established from the six design drivers. The most fundamental driver, surgeon's visibility, is divided into two criteria: lifting capability and camera position. Patient safety is evaluated on one aspect: the product surface temperature. The rating indicates a concept's potential to meet certain criteria. Below are the seven criteria ranked by their level of importance:

1. Lifting capability: The concept should have the potential to sustain a $140\,\mathrm{N}$ lifting force.
2. Camera position: The camera position should accommodate common procedures and reduce eye-hand movement problems.
3. Patient safety: The concept should have the potential to keep the product surface temperature below $41\,^{\circ}\mathrm{C}$ and not to injure the patient during surgery.
4. Manufacturability: The concept should use simple production techniques and materials that are available around the globe.
5. User-friendliness: The concept should be intuitive and easy to operate.
6. Cost-effectiveness: The concept should be inexpensive, with a maximum production cost of $\$400$.
7. Robustness: The concept should be strong, durable, and reliable.

8.2. Evaluation

The three concepts earn a quantitative rating for each criterion; those are bad (- -), moderate (-), good (+), and excellent (++). The following list outlines the rationale behind the concepts' ratings for every criterion. The results are visualized in the Harris Profile in Figure 8.1.

1. Lifting capability was evaluated as excellent (++) when the factor of safety (FOS) was greater than 2.5, good (+) for a FOS higher than 2.0, moderate (-) for a FOS above 1.5, and bad (- -) for a FOS below 1.5. Consequently, concepts 1 and 3 are rated as excellent (++) and concept 2 as good (+).
2. Camera position was evaluated as excellent (++) when there were few impeding effects on observation and a minor loss of depth perception. A bad (- -) rating was assigned when the impeding effects were so severe that no surgical procedure could be performed. During the box trainer experiment, the participants experienced impeding effects but could perform the tasks successfully. However, no unambiguous distinction between the concepts could be made. Therefore, all concepts are rated as good (+).

3. Patient safety ratings were partly based on the potential to keep the product surface temperature below $41\,^{\circ}\mathrm{C}$. I.e., a standard LED strip produces substantial heat, an LED with one resistor generates the bulk of heat outside the abdomen, and optical fibers produce practically no heat. Heat dissipation is expected to be most efficient with a water cooling system, followed by heat pipes, and dissipation via airflow is expected to be insignificant. Furthermore, the concepts should not injure the patient. The camera tip in concept 1 has a odd shape that could be a safety hazard. The combinations of these aspects result in the following ratings: concepts 2 is excellent (++), and concepts 1 and 3 are good (+).
4. Manufactureability was evaluated as excellent (++) when only simple production techniques are needed, and materials are easily available across the globe. It was rated as bad (- -) when the opposite was true. Concept 1 has a frame that is easy to manufacture and no demanding cooling system. However, the camera tip has a complex shape that is difficult to manufacture. Concept 2 has the most complex frame shape and requires a custom LED strip and a curved heat pipe, which is not widely available. Concept 3 has a reasonably complex frame shape and requires a water-cooling system. These are available around the globe but are challenging to manufacture. Consequently, concepts 1 and 3 are rated as good (+) and concept 2 as moderate (-).
5. User-friendliness was based on the shape of the frame. A helical base shape will create less friction with the inside of the abdominal wall compared to a flat base, which results in easier insertion in the abdomen. According to GILLS expert Dr. Gnanaraj, the spiral loop shape of concept 2 will not be intuitive to use, and the location of the tip makes insertion challenging. Due to the required size and shape of concept 2's specially designed camera tip, it is more difficult to insert the device through the abdominal wall. Hence, concepts 1 and 2 are rated as moderate (-) and concept 3 as excellent (++).
6. Cost-effectiveness was evaluated as good (+) when the production costs are below $\$400$. The frame of concept 1 is the simplest to manufacture, resulting in lower labor costs. The airflow cooling system is inexpensive, but the specially designed camera tip and optical fiber lighting are high-priced. Concept 2's frame is the most difficult to manufacture with the spiral and helical shape and swaged end. Together with the custom LED strip and heat pipe, this will be the most costly product. The manufacturing costs of Concept 3's frame will be higher than those of concept 1 and lower than those of concept 3. The cost of a standard LED strip is negligible. However, the water cooling system will add to the price. All aspects added up, concept 1 and 2 are rated as moderate (-) and concept 3 as good (+).
7. Robustness was based on the strength, durability, and reliability of the device. Optical fiber lighting is more reliable than LED lighting. Especially with one resistor, LED burnout is a hazard. Moreover, the camera tip of concept 1 was not expected to be strong and durable. Ultimately, all concepts are rated moderate (-).

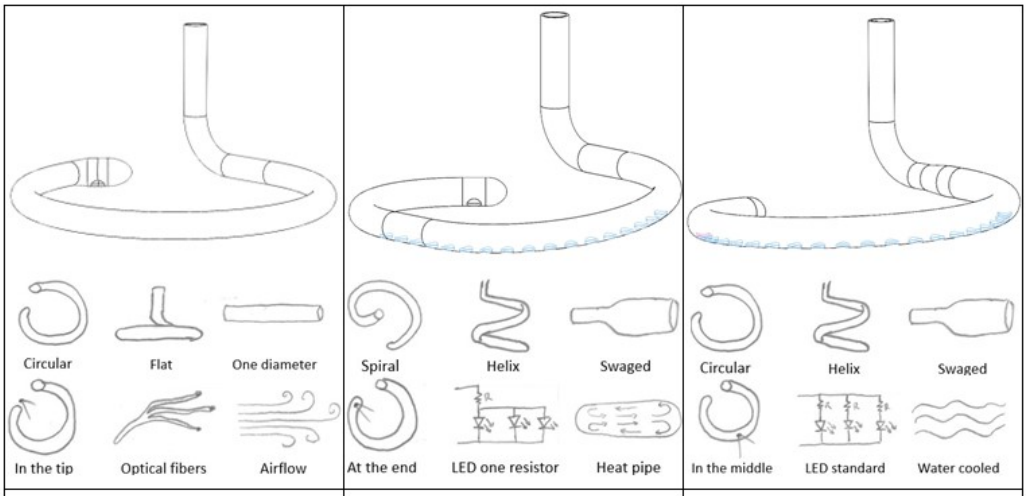

	Concept 1				Concept 2				Concept 3			
	–	– –	+	+ +	–	– –	+	+ +	–	– –	+	+ +
Lifting capability												
Camera position												
Patient safety												
Manufacturability												
User-friendliness												
Cost-effectiveness												
Robustness												

Figure 8.1: Harris Profile of the three concepts.

8.3. Selection

The Harris Profile shows that concept 2 is definitely inferior. In contrast, concepts 1 and 3 are more comparable. Nonetheless, concept 3 is most favorable, scoring excellent or good on six of the seven criteria. The shape of the frame mostly causes the advantage; it has a circular loop and a helical base and does not require a special part for the camera. The LED lighting is also beneficial, making this concept superior.

Despite that, most components of the design configurations – shown in Table 5.1 – are interchangeable. For example, the helical shape can be applied to all concepts, and all types of lighting and heat dissipation methods are compatible with each concept.

In conclusion, the combination of concept 3's features is superior. The selection process was discussed with GILLS expert Dr. Gnanaraj. He favored the camera position in the middle of the loop. Though a different combination could yield a more optimal conceptual solution, this concept was selected for further development for its frame shape, camera location and inexpensive electronics. The following chapters in Part III provide the next element of the design process: prototyping.

Part III

Prototypes

“Simplicity will stand out, while complexity will get lost in the crowd.”

Kevin Barnett

9

Design Outline

The final design of the lifting device is illustrated in Figure 9.1. The design includes a stainless steel hollow circular loop with a 5 MP camera module and integrated LED lighting, functioning as a replacement for traditional lifting devices and current laparoscopes.

In this chapter, these design features are discussed. Chapter 10 describes the dimensions and materials of the final design along with the production and assembly steps to manufacture the device. The prototypes are discussed in Chapter 11.

Figure 9.1: Render of the lifting device.

9.1. Structure

The lifting device comprises five elements: the load-bearing frame, the RAIS connector joint, the electronics, the housing, and the sealing. A brief introduction of each element is given below.

Load bearing frame

The load-bearing frame is a 12x$1\,\mathrm{mm}$ diameter tube with a circular loop shape and a helical base. At the end of the circular loop, the tube is bent vertically; this part is called the upright. The circular loop is the section of the frame that is inserted into the abdomen. The upright remains outside the human body. The two sections are visualized in Figure 9.2.

The tube diameter is different from concept 3. The selected concept has a $12\,\mathrm{mm}$ diameter tube around the loop, which is swaged to $10\,\mathrm{mm}$ before the upright. The reduction of tube diameter is necessary to satisfy design aim $P4_A$, allowing single-incision laparoscopic surgery (SILS). Due to manufacturing constraints, tube swaging was not available. Therefore, the final design has a constant tube diameter of $12\,\mathrm{mm}$.

The frame is the most fundamental element of the device as it lifts the abdominal wall to create operational volume. Its hollow shape allows for electronics inside the frame. In the middle of the circular loop, there is a transverse hole for a camera. On both sides of the central camera hole, there are ten transverse holes for lighting. In the upright section, there is a hole for the insertion of electronics.

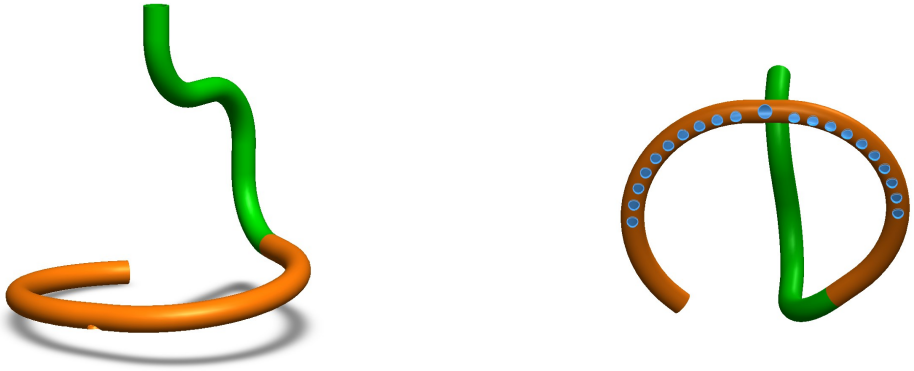

Figure 9.2: The two sections of the load-bearing frame. The loop section is orange, the upright section is green, and the transverse holes are blue.

RAIS connector joint

The second element of the device is joined to the frame at the top endpoint of the upright. This part connects the lifting device to the RAIS retractor arm. It is a ten-sided polygon. Hence, the device can be pitched with $36°$ increments. The joint satisfies design requirement $U1$, compatibility with retractors.

Figure 9.3: The RAIS connector joint and its connection to the retractor arm.

Electronics

The third element is the electronics to view inside the abdominopelvic cavity. The imaging system comprises a 5 MP camera module and an LED strip. In Section 9.2, these will be discussed in detail. A small 3D-printed part with a magnet is attached to the camera sensor for assembly purposes.

Housing

The electronics exit the tubular frame at the upright. At that location, there is a housing for the electronics with two output cables. The housing has a right and a left side, as shown in Figure 9.4. These are connected to each other and the frame by three M3 bolts.

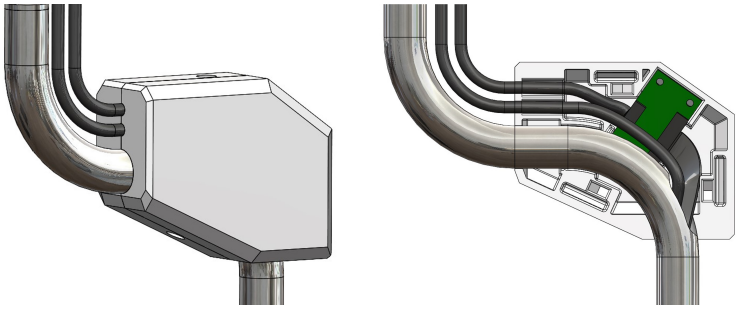

Figure 9.4: Housing of the electronics.

Sealing

A transparent polyolefin heat shrink seals the holes in the frame. This heat shrink allows light from the LED strip to pass through while making the device waterproof. A copolyester lens covers the camera module. The opening at the end of the circular loop is closed with an endcap. It has a spade shape to minimize injury.

Note that there is a difference between concept 3 and the final design. Originally, a water cooling system was incorporated into the frame to keep the product surface temperature below $41\,^{\circ}\mathrm{C}$. The water cooling system requires a flexible hose inside the frame for the water stream. Outside the frame, a reservoir, pump, radiator, and cooling fans would be needed for a functional system. However, due to a low priority, this component was left out of the final design.

9.2. Imaging system

The most outstanding feature of this device compared to other AWL devices is the integration of an imaging system. The system has two electric elements: a camera module and a LED strip, which are shown in Figure 9.5. Both electronic elements are commercially available and inexpensive. This subsection describes the camera module and LED strip that were used in the prototype.

(a) The OmniVision 5693 camera module.

(b) The LED strip.

Figure 9.5: The electric elements used for final prototyping.

A camera module consists of two parts: a camera sensor and a printed circuit board (PCB). The camera sensor produces an analog signal, which is converted into a digital signal inside the sensor. The PCB converts this signal from its RAW format to JPEG. A huge variety of such camera modules is available online.

The main hardware distinction between camera modules is the type of sensor. There are two types of technologies commonly employed in digital camera sensors: Charge Couple Device (CCD) and Complementary Metal-Oxide Semiconductor (CMOS) [78]. Generally, CCD sensors have superior sensitivity and lower noise than CMOS sensors. They excel in capturing high-quality images in low light conditions [79]. On the other hand, CMOS sensors are smaller, have lower power consumption, and faster readout speeds. They are the standard in the smartphone and tablet industry [80]. Due to the large-scale use and production, the quality gap to CCD sensors was narrowed, and reliable sensors are available at very low cost. For this device, a CMOS sensor was used as they are cheaper, smaller, faster, and generate less heat.

As explained before, a PCB is necessary to convert the camera sensor's signal. It can be connected to the camera sensor directly or by a Flat Flex Cable. The PCB is the camera element that generates the most heat and is larger than the camera sensor. Therefore, splitting the PCB from the camera sensor is beneficial. The camera sensor can be located in the abdomen, whereas the PCB is in a part of the lifting device outside the abdomen. Most heat is generated outside the human body, and the dimensions of the lifting device inside the abdomen are smaller.

The focusing mechanism in camera sensors is crucial for capturing sharp images. Two common types are fixed-focus and auto-focus. Fixed-focus has a preset focal distance, making the design compact and vibration-resistant, which is ideal for consistent shooting distances but limited for varying ranges. Auto-focus dynamically adjusts for different distances using methods like phase or contrast detection, but it is more complex, costly, and generates extra heat. Given the known shooting distance range and the need for cost and heat efficiency, fixed-focus is more suitable for the lifting device.

The World Laparoscopy Hospital (WLH) states that Full HD imaging (1920 x 1080 pixels) offers a superior viewing experience for surgeons [81], corresponding to a resolution of at least 2 MP. Furthermore, according to WHL, a frame rate of 30 frames per second (FPS) is sufficient for this lifting device. Although more FPS reduces motion blur, the camera will remain mostly stationary during procedures. Additionally, 30 FPS offers better video quality in low light, produces less heat, and is more cost-effective. Lastly, a camera sensor with a wide field of view (FOV), which captures a larger area of the surgical field in a single frame, improves the surgeon's visibility.

The camera module used in the prototype is displayed in Figure 9.5a. It features an OmniVision 5693 CMOS sensor with a resolution of 5 MP and a fixed-focus $120°$ FOV lens[1]. It records Full HD 1080p at 30 FPS or 720p at 60 FPS, consuming up to $300\,\mathrm{mW}$ at $5\,\mathrm{V}$. The sensor size measures 8.5 x 8.5 x $5.8\,\mathrm{mm}$ and is connected to the PCB by a $300\,\mathrm{mm}$ long, $8\,\mathrm{mm}$ wide FFC cable.

The compact sensor and long FFC make this camera module ideal for the lifting device: the sensor can be placed inside a small instrument within the abdomen, generating minimal heat, while the PCB remains outside. As of October 2024, the module was available from China for about € 30. The module was used for prototyping for its small sensor size, affordability, and high-quality image, which was validated in previous research [30], demonstrated in Figure 9.6.

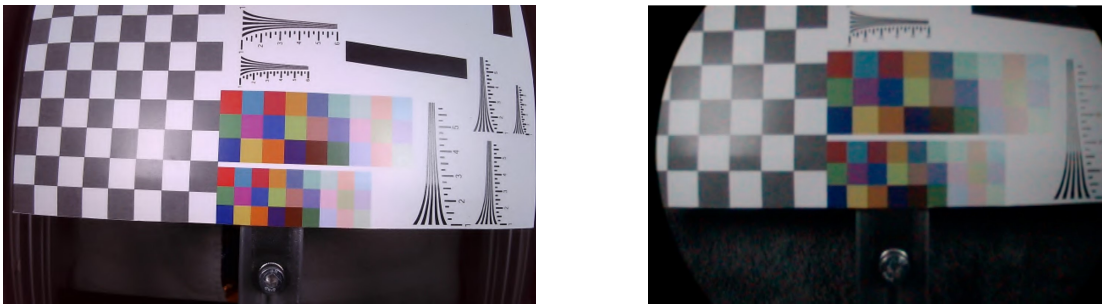

(a) OV5693 capture of the test chart.

(b) OTV-S7 capture of the test chart.

Figure 9.6: Image quality comparison between the OV5693 and the benchmark Olympus OTV-S7 laparoscope reveals visible differences in sharpness, noise, color accuracy, distortion, and FOV [30].

The second electric element for lighting the abdominopelvic cavity is shown in Figure 9.5b. It is a $12\,\mathrm{V}$ chip on board (COB) LED strip with $480\,\mathrm{LEDs/m}$. The LED strip is $8\,\mathrm{mm}$ wide and features a beam angle of $180°$. With a power consumption of $11\,\mathrm{W/m}$, it has a color temperature of $6000\,\mathrm{K}$ and a light intensity of $1250\,\mathrm{lm/m}$. As of October 2024, it can be imported from China for around € 10 per five meters[2].

Both electric elements have a male USB-A output. Using a male cable simplifies chemical sterilization of the lifting device and allows for connection to nearly any laptop, the standard monitor choice in low-resource settings. Feedback from Indian rural surgeons revealed that they highly favor a single USB-A plug cable. This requires many bulky components or designing a custom circuit, exceeding the project's scope. As a result, two USB-A cables are used in the prototypes-—one dedicated to the camera and the other to the LED strip.

[1] OmniVision 5693 CMOS camera module
[2] LED strip

10

Dimensions, Materials & Production

10.1. Dimensions

This section describes the factors that have driven the dimensions of the lifting device. These dimensions involve the size and shape of the loop, the camera position, the tube diameter, the dimensions of the upright, and the transverse hole dimensions. Table 10.1 summarizes these parameters.

Operational volume

The principal function of AWL devices is to create operational volume, which is achieved using carbon dioxide pneumoperitoneum in conventional laparoscopic surgery. Design requirement $V3$ specifies that the volume created by the lifting device must match that of the pneumoperitoneum. The required operational volume and corresponding loop size were derived from previous research [50, 82].

The models of the operational volume created using carbon dioxide and a lifting device are shown in Figure 10.1. There is no consensus about the actual shape of the abdominopelvic cavity. The following calculations are based on observations on an abdominal laparotomy model [50]. The pneumoperitoneum was modeled as a hemisphere, and the lifting device's operational volume was modeled as a truncated cone.

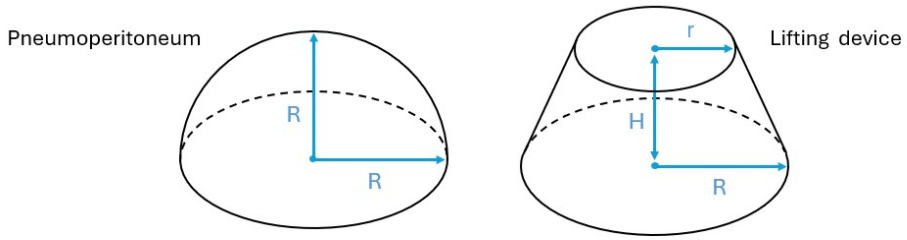

Figure 10.1: The operational volume models from a pneumoperitoneum and a loop-shaped lifting device. The pneumoperitoneum was assumed to be a perfect hemisphere with radius R. The lifting device's volume was assumed to be a truncated cone with base radius R, top radius r, and height H.

The operational volume created by the pneumoperitoneum, V_P, was determined using Equation 10.1, where R represents the base radius of the hemisphere. It is defined as the transverse abdominal radius – the linear distance from the midpoint of the abdomen to the peritoneal edge of the lateral abdominal wall.

$$V_P = \frac{2\pi}{3} R^3 \tag{10.1}$$

The operational volume created by the lifting device, V_L, was calculated with Equation 10.2. Again, R was defined as the transverse abdominal radius. H is the height of the lifting device's loop, and r is the radius of the loop.

$$V_L = \frac{\pi}{3} H(R^2 + Rr + r^2) \tag{10.2}$$

The lifting height, H, is typically $100\,\mathrm{mm}$ to $150\,\mathrm{mm}$ with the STAAN device, according to GILLS expert Dr. Gnanaraj. By altering the height of the lifting device, the surgeon can alter the camera position to their preference. The volume created by the lifting device must match that of the pneumoperitoneum, i.e., $V_P = V_L$. Combining Equation 10.1 and 10.2 gives the required height H as a function of the base radius R and the loop radius r (Equation 10.3).

$$H = 2R^3(R^2 + Rr + r^2)^{-1} \tag{10.3}$$

The transverse abdominal radius differs with age and between persons. Research with CT scans determined that children have an average transverse abdominal radius of $60\,\mathrm{mm}$ and adults average $105\,\mathrm{mm}$ [50]. Another CT scan experiment measured an average radius of $103\,\mathrm{mm}$ for adults. As the lifting device is designed for adults, a mean transverse abdominal radius of $104\,\mathrm{mm}$ was used for further calculations.

As the range of lifting height and the transverse abdominal radius were known, Equation 10.3 was plotted in Figure 10.2. The lifting device's loop radius r should be above the blue line to satisfy requirement $V3$. Consequently, when the lifting height is at its lowest point ($H = 100\,\mathrm{mm}$), the loop radius should be $72\,\mathrm{mm}$.

However, surgeons prefer a smaller loop radius of $\leq 60\,\mathrm{mm}$. Before the blind entry of the device, surgeons do a so-called finger test, where they examine the inside of the abdominal wall for irregularities. The lifting device should not be larger than their fingers can reach. Therefore, the loop radius is set to $60\,\mathrm{mm}$. This reduces the visibility and working space for lower lifting heights but is necessary for performing safe surgery.

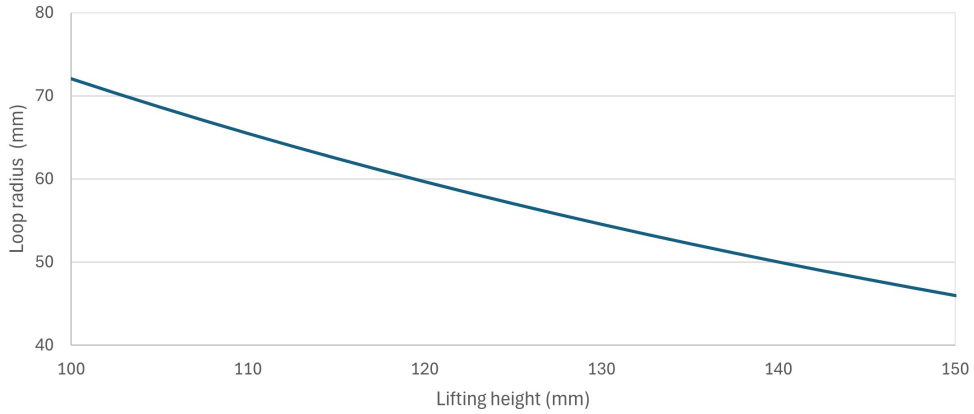

Figure 10.2: The required loop radius r to satisfy the operational volume requirement for the lifting height H range.

Loop shape

Thus, the loop radius was set to $60\,\mathrm{mm}$. The next loop parameter is the circle circumference. Figure 10.3 presents three circumference configurations. A longer loop provides better support to the abdominal wall, forming the truncated cone shape, which results in a larger operational volume.

Izumi *et al.* found that a shorter loop decreases friction during insertion [82]. Additionally, it drastically decreases the probability of peritoneal injury; the $5/6$ loop had a 45% injury rate, the $3/4$ loop 13%, and the $1/2$ loop 0%.

The effects of the circumference are conflicting. To provide sufficient visibility while minimizing the risk of peritoneal injury, the loop circumference is set to approximately $3/4$.

The insertion friction can be reduced by introducing a helical base shape. The recently developed RAIS and STAAN lifting devices incorporate this downward twist, as shown in Figure 1.2c and Figure 1.2d. Both devices have a $5/6$ circumference, typically resulting in a high insertion friction. Nevertheless, the helical shape reduces the resistance to an acceptable level for surgical use. No peritoneal injury rates were published. However, it was expected to decrease the risk as insertion is easier to control.

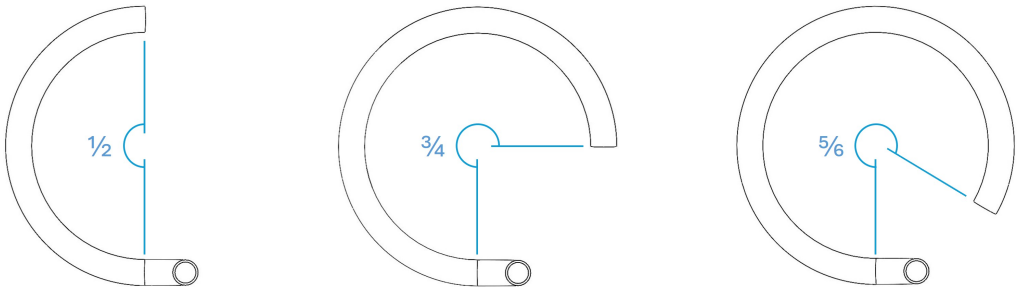

Figure 10.3: Three loop circumferences used to determine peritoneal injury risk [82]. The fraction represents the portion of the full $360°$ covered by the loop.

The actual loop is not perfectly helical. It consists of two $140°$ bends α, of which the planes are rotated $\theta = 10°$ compared to each other. This mimics the helical shape, as shown in Figure 10.4. Two planar bends were introduced to simplify the manufacturing process, which will be discussed in Section 11.2. There is a straight section d of $15\,\mathrm{mm}$ between the two loops.

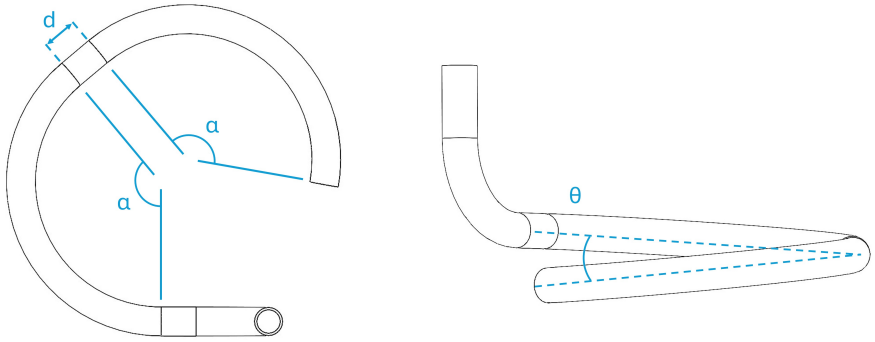

Figure 10.4: The shape of the loop with two planar bends, $\alpha = 140°$. The planes are rotated $\theta = 10°$ compared to each other.

Tube diameter

The camera module is positioned in the small straight section between the two bends of the loop. The module, with a size of 8.5 x 8.5 x $5.8\,\mathrm{mm}$, had to fit through the tube. Hence, the inner diameter of the tube was a constraint; it must be at least $10\,\mathrm{mm}$.

The tube's outer diameter should be minimized and must not exceed $12\,\mathrm{mm}$, as specified by requirement $P1$. Furthermore, a design driver was the use of readily available materials. Therefore, opting for a $12\,\mathrm{mm}$ tube with a $1\,\mathrm{mm}$ wall thickness was sensible as it is a standard type of tube that meets both constraints. The tube and camera module are shown in Figure 10.5.

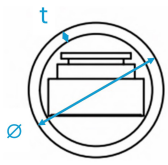

Figure 10.5: Cross-sectional dimensions of the tube and the camera module. $\varnothing = 12\,\mathrm{mm}$ and $t = 1\,\mathrm{mm}$.

The upright

The upright is the section of the frame that remains outside the abdominopelvic cavity, acting as a bridge between the RAIS retractor arm and the circular loop. The incision point, which marks the transition from the loop to the upright, was preferred at the loop's edge (indicated in Figure 10.6a). Placing it on the edge maximizes the loop surface in front of the incision and makes insertion easier.

The preferred connection point with the RAIS retractor arm is at the center of the circular loop, as shown in Figure 10.6b. In the current RAIS ring, the connection is also at the center of the loop. It makes the device easier to operate. Consequently, the upright is not merely a vertical section. It has a shape that accommodates both requirements.

The upright has three $90°$ bends β_1, β_2, and β_3, which are indicated in Figure 10.6b. The first bend β_1 results in a vertical section d on the edge of the loop. The second bend β_2 is rotated clockwise around the z-axis by $\phi = 57°$, directing it toward the circular loop's center. The third bend β_3 forms a vertical segment at the loop's center, serving as the endpoint for the RAIS connector joint.

(a) Side view. **(b)** Top view.

Figure 10.6: The upright section's angles. Bends β_1, β_2, and β_3 are all $90°$ and $d = 15\,\mathrm{mm}$. Bend β_2 is rotated clockwise around the z-axis by $\phi = 57°$. (1) is the incision point, (2) is the center of the circular loop.

Hole placement

The camera sensor is located in the middle of the circular loop, for which $7\,\mathrm{mm}$ diameter transverse hole is drilled (Figure 10.7a). Surgeon J. Gnanaraj stated that the ideal viewing angle $\angle_v$ ranges from $45°$ to $60°$. Hence, the viewing angle of the lifting device was set to $60°$, as presented in Figure 10.7b. However, it can be adjusted as desired by pitching the whole lifting device.

On both sides of the camera sensor are ten $5.5\,\mathrm{mm}$ diameter holes for LED lighting, which are presented in Figure 10.7b. These are evenly spread around the camera sensor for an even light distribution. They span $\gamma = 180°$ of the circular loop and have a spacing s of $9.6\,\mathrm{mm}$. This configuration was established from several FEA simulations.

The simulation parameters were the hole size (5.0 and $5.5\,\mathrm{mm}$), spacing (8.7, 9.6, and $11.9\,\mathrm{mm}$), and a corresponding amount of holes (18, 20, and 22). To emit as much light as possible, the total surface area of the holes should be as large as possible. On the other hand, the resulting stress in the material should not exceed the factor of safety (FOS). This configuration was found to have a relatively large surface area while maintaining a FOS greater than 2.5.

Please note that the analysis was quick, and a limited amount of simulations were executed. A more extensive analysis should be considered to optimize the emission of LED light. Nevertheless, this configuration was used for prototyping.

(a) Transverse hole distribution. **(b)** Viewing angle.

Figure 10.7: The transverse hole placement in the tubular frame. (1) is a $7\,\mathrm{mm}$ diameter hole for the camera. (2) are twenty $5.5\,\mathrm{mm}$ diameter holes for LED lighting. The hole spacing $s = 9.6\,\mathrm{mm}$, the span $\gamma = 180°$, and the viewing angle $\angle_v = 60°$.

Table 10.1: Summary of the twelve dimension parameters.

Parameter	Value	Rationale	Illustration
R	$60\,\mathrm{mm}$	The radius of the circular loop.	Figure 10.4
α	$140°$	The angle of the two loop bends.	Figure 10.4
θ	$10°$	The rotation between the two loop bends.	Figure 10.4
d	$15\,\mathrm{mm}$	The straight segments' distance.	Figure 10.4
r	$30\,\mathrm{mm}$	The radius of the three upright bends.	Figure 10.6
β	$90°$	The angle of the three upright bends.	Figure 10.6
ϕ	$57°$	The rotation between bends β_1 and β_2.	Figure 10.6
$\varnothing$	$12\,\mathrm{mm}$	The outer diameter of the tube.	Figure 10.5
t	$1\,\mathrm{mm}$	The thickness of the tube.	Figure 10.5
$\angle_v$	$60\,\mathrm{mm}$	The camera's viewing angle.	Figure 10.7
n	20	The number of holes for lighting.	Figure 10.7
γ	$180°$	The span of the holes.	Figure 10.7
s	$9.6\,\mathrm{mm}$	The spacing between the holes.	Figure 10.7

10.2. Materials

This section describes the materials of the lifting device. The materials of the prototype are different from the materials of the final design due to availability and manufacturability. The bill of material is presented in Table 12.1.

Plastics

The housing is an intricate and complex part. It does not require the structural strength of the frame. Therefore, 3D printing was a suitable production technique. Polylactic acid (PLA) was readily available at the Delft University of Technology production facilities. Hence, that material was used for the prototype's housing.

PLA has limited resistance to sterilization chemicals, low heat resistance ($60\,^{\circ}\mathrm{C}$ to $70\,^{\circ}\mathrm{C}$), and limited abrasion resistance [83]. Nylon has superior resistance characteristics, but it costs three times as much and is more flexible than PLA [84]. Resistance to sterilization chemicals is crucial for a medical device in low-resource settings. Therefore, nylon should be used for the final design.

The prototype has two more 3D-printed parts: the RAIS joint and the endcap. Both were designed to be machined out of metal. Especially, the RAIS joint requires structural strength to sustain the $140\,\mathrm{N}$ load. Nonetheless, these parts are made from PLA for the prototype.

A transparent heat shrink seals the LED holes in the frame. It is made of polyolefin, a thermoplastic material. The material is flexible and designed to shrink at moderate temperatures ($70\,^{\circ}\mathrm{C}$ to $100\,^{\circ}\mathrm{C}$) with a maximum ratio of $2:1$, making it suitable for wrapping around the intricate shape of the lifting device, forming a tight, waterproof seal while protecting against abrasion and physical damage. It is resistant to many chemicals, oils, and solvents and provides excellent electrical insulation [85].

A copolyester lens covers the camera hole, ensuring clear and undistorted images. While copolyester can be thermoformed, this process may introduce distortions. Therefore, the lens is a simple, laser-cut flat circle of copolyester placed directly over the camera sensor.

Frame

The load-bearing frame should be made of strong material to sustain a $140\,\mathrm{N}$ distributed load. The FEA was executed with stainless steel 17-4PH, resulting in a 2.8 FOS. This steel has a yield strength of $870\,\mathrm{MPa}$. Therefore, the frame's material should have a yield strength of at least $620\,\mathrm{MPa}$ to ensure a 2.0 FOS. This has to be verified with FEA, and a higher yield strength is favored.

While the frame is largely protected by heat shrink, the metal should be corrosion- and chemical-resistant to withstand repeated procedures and sterilization cycles. Additionally, it should be commercially available as a tube and be bendable for shaping during production.

A material analysis was conducted to find potential materials. Several filters were applied. The yield strength is at least $620\,\mathrm{MPa}$. The price per volume is maximum $10^6 €/m^3$, corresponding to € 20 for the frame. The minimal corrosion resistance was set to 26 PREN, recommended for medical devices inside the human body [86]. Lastly, the chemical resistance should be excellent. The result is shown in Figure 10.8.

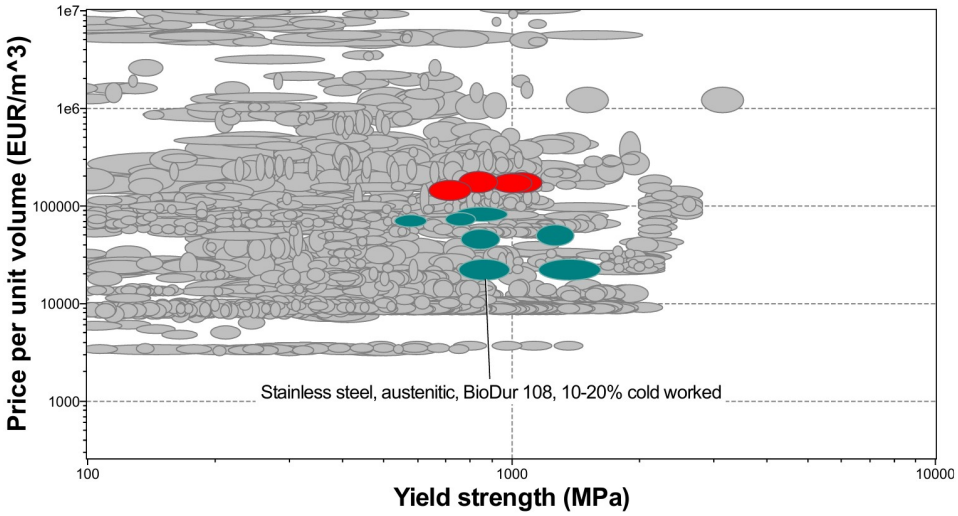

Figure 10.8: The potential materials for the load-bearing frame.

Only one of these materials is available as a tube: stainless steel BioDur 108[1]. It has a yield strength range from $750\,\mathrm{MPa}$ to $990\,\mathrm{MPa}$, depending on the heat treatment [72]. The material is bendable with conventional bending techniques when annealed. It is used for medical implants and is highly biocompatible [87].

Stainless steel tubes require excessive force for manual bending - the production technique used for prototyping (described in Section D.1). Hence, aluminum 6060-T66 was selected for the prototype as it was readily accessible in the required sizes, could be bent manually, and could be annealed to enhance ductility. It has a yield strength of $165\,\mathrm{MPa}$ and a density of $2700\,\mathrm{kg/m^3}$, making the aluminum frame about four times lighter and weaker than one made from stainless steel BioDur 108.

10.3. Production & Assembly

The lifting device was manufactured using conventional production techniques. Appendix D provides an in-depth overview of these techniques, the required forces, custom tools, and production steps.

The desired frame shape was achieved by bending. Bending offers excellent design flexibility and preserves the material's structural integrity [88]. It also produces a smooth surface finish, reducing post-processing needs. These advantages lower material use, labor, and tool costs.

Compression bending was used to make the aluminum prototype. It involves deforming the tube around a fixed bend die using a wiper die. This common, cost-effective technique struggles with small radii bends and precision compared to rotary draw bending.

Rotary draw bending secures the tube with a clamp die and bends it by rotating the bend die. A pressure die holds the tube in place during rotation. This technique provides higher precision and force

[1] Stainless steel BioDur 108

capability than manual methods. Therefore, rotary draw bending should be used to bend a stainless steel frame.

The tube-bending process requires precise management of key variables [89]. A straight section at least 2.5 times the tube diameter is needed for clamping and to minimize slip and kinking at the inner radius. The minimum bend radius is 2.5 times the tube diameter. Smaller radii risk imperfections like flattening or collapse. Elastic recovery after force release (spring back) can cause dimensional inaccuracies. To counter this, the die's bend radius should be designed 3% smaller than the desired tube radius, and the bend angle increased by $1°$ to $2°$ for aluminum and $2°$ to $3°$ for stainless steel.

Smaller bend radii require higher bending forces, which can be reduced by annealing. The required bending moment for a $30\,\mathrm{mm}$ radius bend is $15\,\mathrm{Nm}$ (Equation D.8). This can be achieved by hand using a proper lever tool. The custom tools to manufacture the prototype are presented in Section D.2.

The prototype production took approximately two days, and the custom tools took three days. An overview of the production steps is presented in Figure 10.9. The elaboration of the steps are provided in Section D.3.

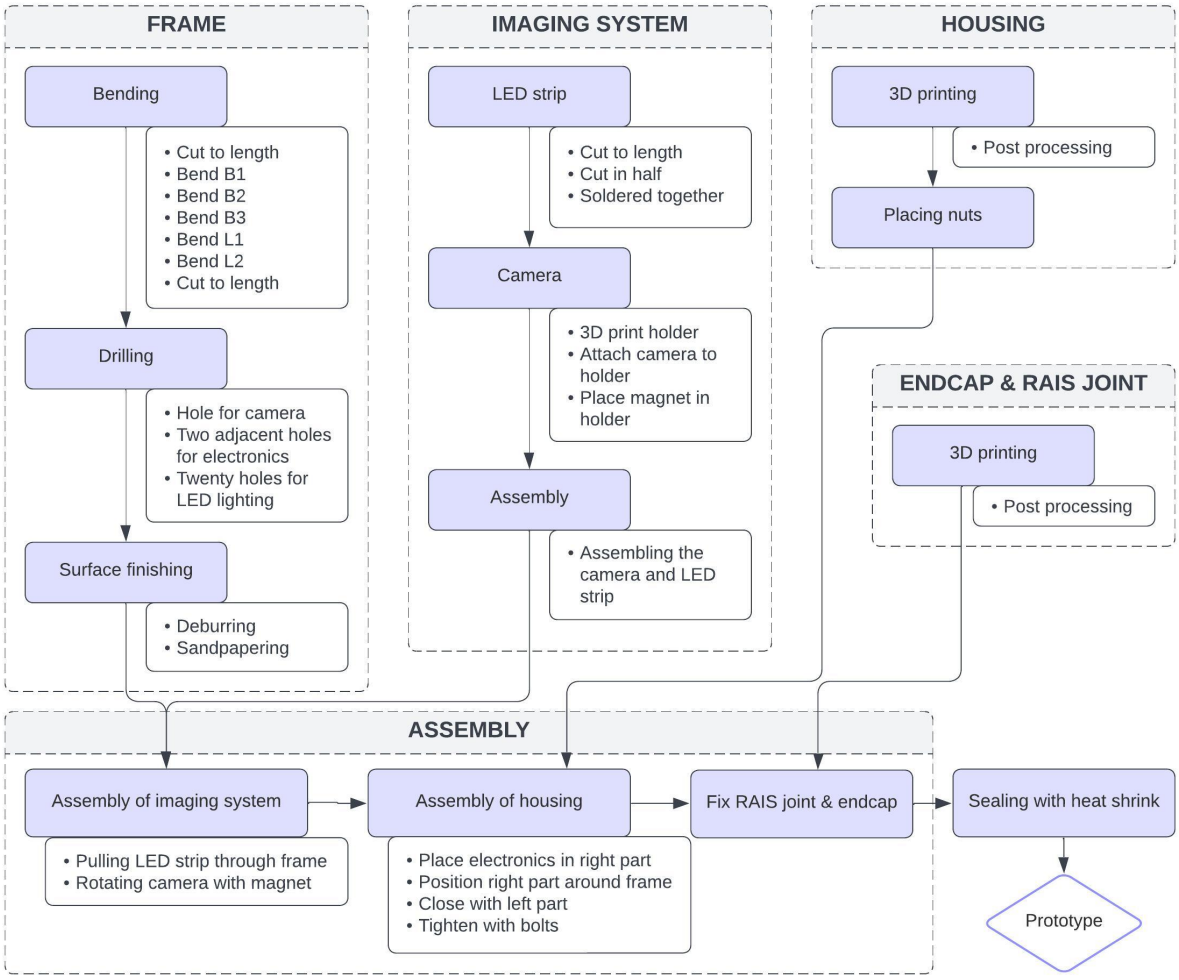

Figure 10.9: Flowchart of the prototype's production process.

11

Prototypes

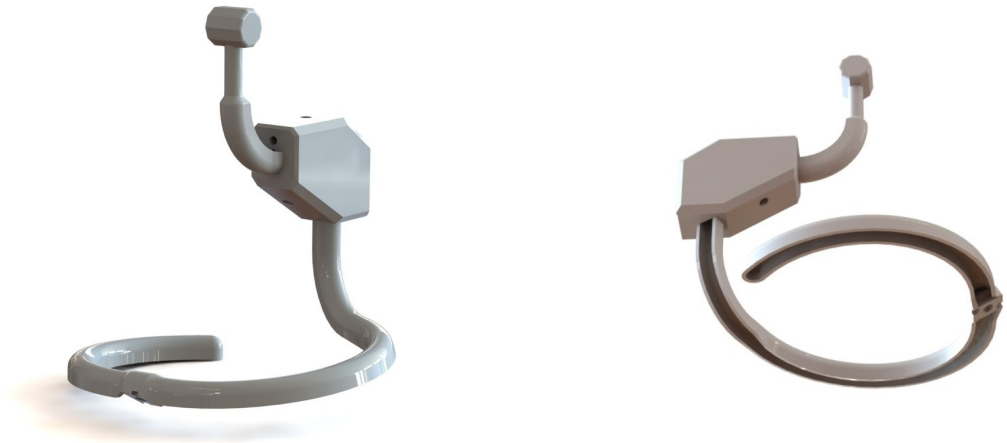

Figure 11.1: Render of the 3D-printed prototype.

11.1. 3D Printed Prototype

A 3D-printed prototype was developed to validate the concept. It was used to evaluate the imaging and lighting functionality and to confirm the fit of the electronics within the frame and housing. Further, the connection to the RAIS retractor was evaluated.

The prototype was a quick proof of concept – only one iteration was made. Most dimensions are identical to the parameters in Table 10.1. However, a fundamental difference between the final design and the 3D-printed prototype is the cross-section of the frame. As tubes are nearly impossible to 3D-print, the prototype's cross-section has an opening at the bottom (Figure 11.1). Consequently, there was no need for lighting holes.

A Sony IMX258 12 MP Autofocus camera module was used in this prototype. It was tested by Den butter [30] and has comparable quality to the OV5693 camera module from the final design, with the advantage of its autofocus. The module was recommended and, therefore, used for this prototype.

Findings

The prototype was fully functional, displayed in Figure 11.2. The camera module's flat cable could be bent to make the required curves, and the PCB could be fitted neatly into the housing. However, the IMX258 module generates noticeably more heat than the OV5693 module, though it was not precisely measured. Additionally, the height of the IMX258 module is 35% larger (8.5 x 8.5 x $7.6\,\mathrm{mm}$ versus 8.5 x 8.5 x $5.8\,\mathrm{mm}$), which is too large for a bent tube with an inner diameter of $10\,\mathrm{mm}$.

The sides of the LED strip can be cut off, which makes it smaller and easier to bend. Nevertheless, the strip can only bend laterally, making the light face sideways instead of downward. Therefore, an LED strip with a beam angle of $180°$ is necessary.

Considerable heat was generated where the camera sensor and LED strip crossed, which can result in overheating. Moreover, the LED strip must be in front of the camera's flat cable to emit light while being behind the camera sensor so as not to block the view. These conflicting constraints require a modification to the LED strip; it has to be cut into two pieces, which two wires will connect.

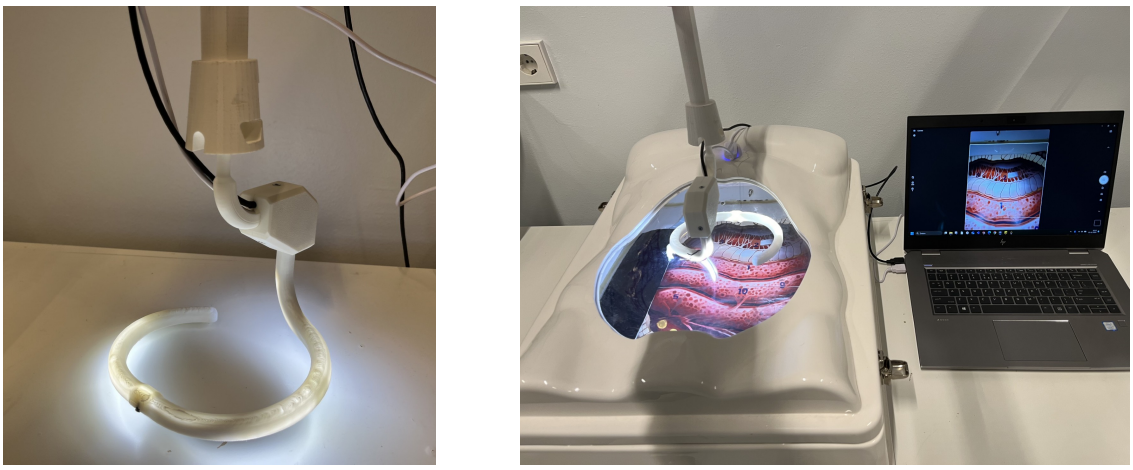

Figure 11.2: The 3D-printed prototype connected to the RAIS retractor arm.

11.2. Final Prototype

The second phase prototype resembles the desired design more than the 3D-printed prototype. This is the prototype referenced in other chapters, and it is shown in Figure 11.3. The frame was made from aluminum 6060-T66 instead of stainless steel for its easier manufacturability. Section D.3 describes the production steps to create the prototype. This section describes the findings from the production process.

As described in Section 9.1, the prototype consists of five elements: the load-bearing frame, the RAIS connector joint, the electronics, the housing, and the sealing. The RAIS connector joint and the endcap were 3D-printed instead of machined from metal. The final prototype is not fully functional. The camera module broke during assembly, which will be discussed later. The key lessons from the production process and recommended improvements are outlined below.

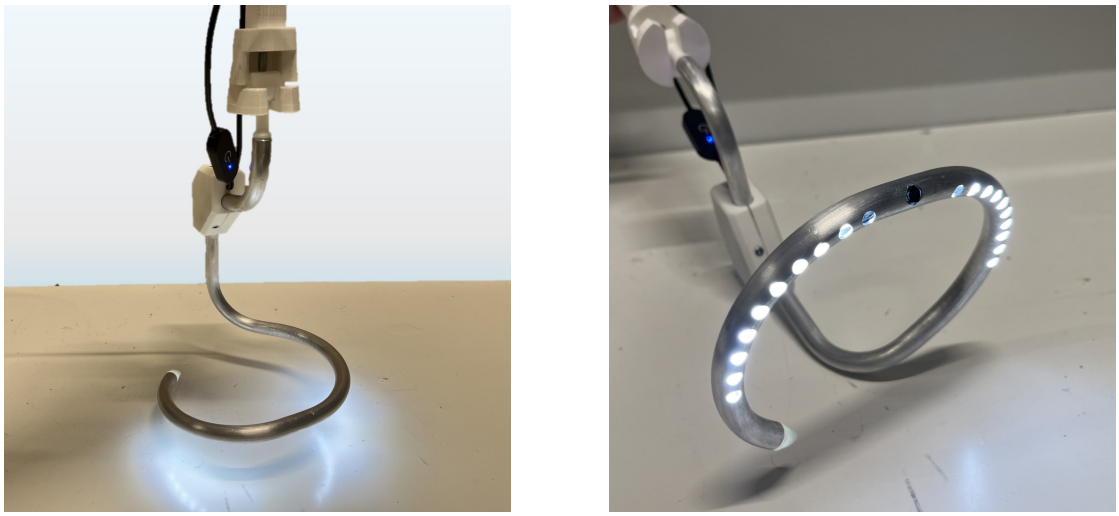

Figure 11.3: The final prototype.

(a) Bending tools for the $60\,\mathrm{mm}$ radius bent

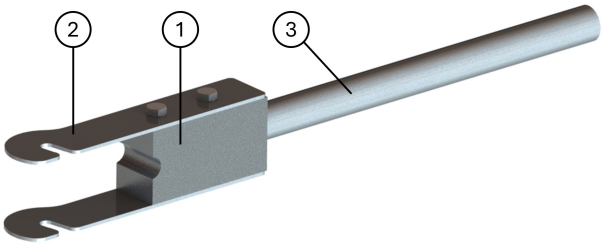

(b) Render of bending handle

Figure 11.4: The custom tools for bending. (1) is the main aluminum milled part, (2) are the laser-cut steel plates, and (3) is the stainless steel lever.

Bending

Bending the aluminum tube with a radius of $60\,\mathrm{mm}$ was successful. It resulted in an accurate bend with limited surface imperfections and negligible flattening. The tools presented in Figure 11.4 were sufficient to make these bends. The required forces were acceptable, as the bends could be made by hand. Nevertheless, some improvements can be made.

The bending die and clamp must be fixed very tightly in a vice to prevent them from slipping. The 3D-printed parts were just strong enough to sustain the pressure, but some minor cracks formed. Therefore, the die and clamp should either be made of a stronger material, or the design should be changed so that no rotation could occur without fixing the tools very tightly in a vice.

Because the handle was a rigid part, its surface slid over the tube's surface during bending. Although the surface was quite smooth – as the handle was a machined part – it resulted in friction, and when not properly used, the handle "bit" into the tube. Thus, the handle should be modified to have a rotating part that rolls over the tube instead of sliding. Like the current handle, that part should enclose the tube to prevent flattening. Furthermore, making the exact rotations for the helical shape was difficult. It was mostly done by eye, resulting in poor precision and repeatability.

A similar tool was created for the smaller $30\,\mathrm{mm}$ bends (Figure 11.5). The forces required to bend the tube were acceptable, as calculated in Section D.1. However, due to the larger forces, the die and clamp had to be fixed more tightly in the vice. Hence, the smaller 3D-printed bending die had to be reinforced to endure the load of the vice and the handle; a stronger material should be used.

More importantly, the tube was significantly flattened during bending, shown in Figure 11.6. Despite annealing and filling it with quartz sand, the tube's walls did not retain its circular shape. Besides ensuring the structural strength, the circular shape is crucial for assembling the camera module. Consequently, the standard pipe bender with a $43\,\mathrm{mm}$ bending radius was used.

It is expected that the flattening occurs because the quartz sand was not sufficiently compressed. The filler material can be pressurized by making a bend that will eventually be cut off. After that bend is made, the tube will not flatten anymore even for small radius bends. This method has to be verified.

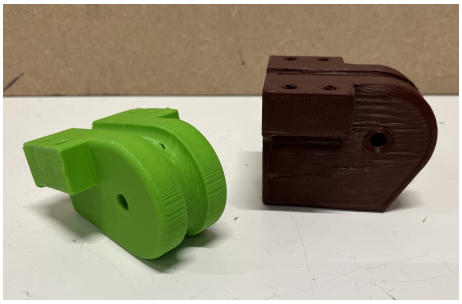

Figure 11.5: Bending dies for the $30\,\mathrm{mm}$ radius bend. The green die tore and the brown die was reinforced.

Figure 11.6: Flattening of the tube after bending with a $30\,\mathrm{mm}$ radius.

Drilling

The second production process, drilling, was accomplished with two custom drill jigs. These ensured the holes were drilled at the tube's center line, avoiding the drill bit to "walk" over the surface. Figure 11.7 displays the jig for the lighting holes. The jig also made precise hole distribution easy, reducing the manufacturing time.

The production of the holes was made easy with the current jigs. Nevertheless, the actual emitted light is not optimal. The holes face downward with respect to the plane of the bends, whereas the camera has a viewing angle of $30°$. Therefore, the light is not parallel to the camera view, and the highest intensity is not at the center of the view.

Thus, a new jig should be designed so that the holes are both parallel to the camera view and on the tube's center line. This will improve the lighting performance but will increase the production time since the holes will not be in one plane.

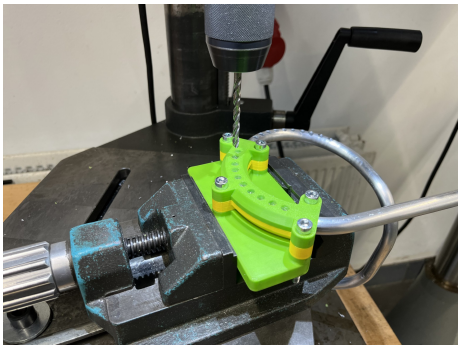

Figure 11.7: The drill jig for the twenty lighting holes.

Figure 11.8: The gap in between the two housing parts.

Housing

The housing of the prototype is overly complex, and the size can be decreased. However, it may be beneficial not to reduce the size but to make it more ergonomic for the surgeon's hand. The housing will be used to operate the device during insertion.

This highlights the importance of the second improvement, the connection to the frame. Three M3 bolts connect the two parts of the housing. These shapes fit around the frame. The connection insufficiently closes the gaps and is not robust. For the prototype, the gaps were closed with glue, which made disassembly difficult. Thus, a more sturdy design that also closes the gaps without glue is necessary.

Assembly

The imaging system comprises two elements: the LED strip and camera module (Figure 11.9), which are pulled through the frame together. A 3D-printed part with a magnet was attached to the camera module, allowing rotation of the sensor from outside with a secondary magnet. This principle worked properly; the camera could be moved through the entire frame and positioned in the designated hole. Nevertheless, it was observed that dimensions are at the limit of what fits through a $12\text{x}1\,\text{mm}$ tube.

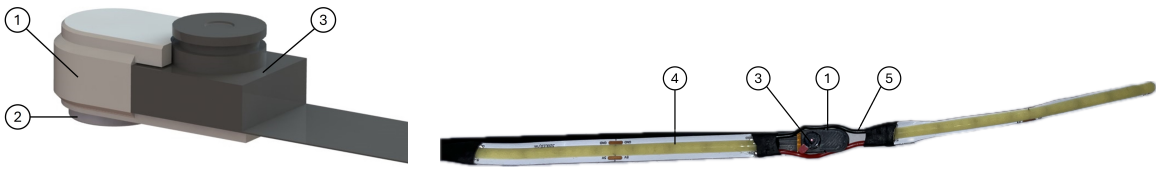

(a) Render of the magnet holder.

(b) Picture of the imaging system assembly.

Figure 11.9: The imaging system. (1) is the 3D-printed holder, (2) the magnet, (3) the camera module. (4) the LED strip, and (5) the wires.

The modified LED strip could easily be pulled through the frame. Together with the camera module and magnet, however, it got stuck. When the imaging system was extracted from the frame, the camera module's flat flex cable was partly torn, making the system defective. Hence, the final prototype is not fully functional.

Later in the project, the camera's flat flex cable was also very fragile. This should be considered for future iterations of the lifting device. Precautionary measures should be taken to protect the cable. For example, reinforcement around the connection between the cable and sensor can be introduced, or only negligible forces can be applied to the cable.

Nonetheless, it does not solve the assembly problem. The problem can be solved in three ways. The first is increasing the tube size, which conflicts with design requirement $P1$. The second is using a smaller camera module, which is undesirable since it will drastically increase the cost. The most straightforward method is decreasing the size of the magnet and magnet holder and using thinner wires for the LED strip.

Sealing

The final production step was to seal the frame with a heat shrink, attach a copolyester lens to the camera sensor, and glue the housing of electronics. Ultimately, the copolyester lens was not used due to the defective camera module. The heat shrink was tried on one frame, shown in Figure 11.10. Placing the heat shrink around the frame was harder than expected, requiring much force and time. The inside of the heat shrink was significantly scratched by the holes in the frame, reducing the transparency. Furthermore, since the heat shrinks are designed for straight materials, the sealing wrinkles at the inside of the loop.

These sealing techniques are irreversible, have low reliability, and poor repeatability. A single tear, such as an accidental cut from a surgical tool, requires the entire heat shrink to be stripped and replaced. Moreover, the shrinking temperature (70–$100\,^{\circ}\mathrm{C}$) surpasses the camera's allowable operating temperature of $70\,^{\circ}\mathrm{C}$.

Therefore, different sealing techniques should be considered. For example, transparent infill resin could be used, or a disposable sealing could be made. The disadvantage of the first option is its irreversibility. The second option simplifies sterilization substantially but introduces a disposable, which conflicts with design requirement $C2$.

Figure 11.10: The wrinkles and scratches on the heat shrink.

Part IV

Validation

“If I had asked people what they wanted, they would have said faster horses.”

Henry Ford

12

Verification

This chapter initiates the validation of the lifting device. The validation comprises quantitative experiments and a qualitative user test. Chapter 13 discussed the findings from the user test. In this chapter, the prototype's design requirements will be verified. The first section discusses the structural strength of the lifting device. In the second section, a surface temperature test was executed. Lastly, five additional requirements are verified.

12.1. Structural load experiment

Lifting the abdominal wall is a core function of the device. According to design requirement $\boldsymbol{V1}$, the lifting device must sustain a load of $140\,\mathrm{N}$ without permanent deformation. The lifting device was designed for stainless steel BioDur 108 with a safety factor (FOS) of 2.8. The prototype was made of a much weaker material, aluminum 6060 T66.

Therefore, the prototype's structural strength was tested and compared to numerical simulations to examine if these remain valid after the production process. With this information, initial predictions can be made about the stainless steel frame's load-bearing capacity.

Methods

The structural load experiment consists of two parts. In practice, the lifting device's frame is exposed to a distributed load by the abdominal wall; the first part evaluated this type of load. The second part was a more regular force-displacement measurement.

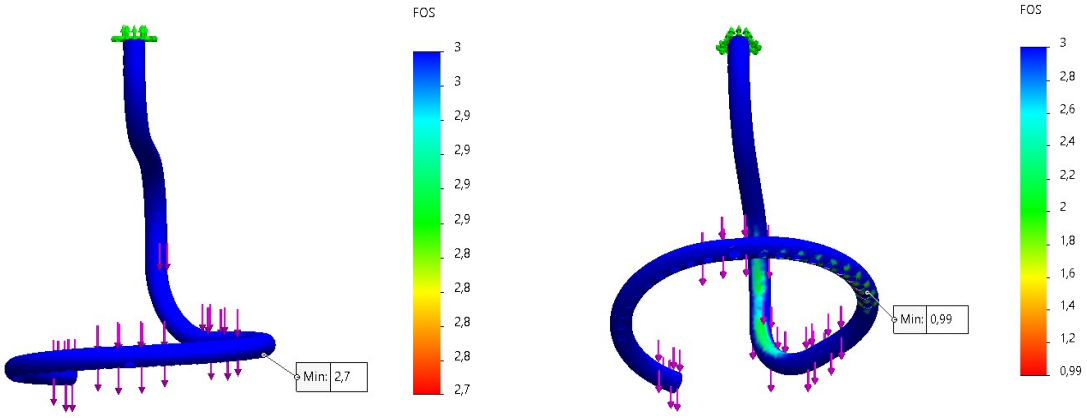

(a) FOS for a distributed load of $26\,\mathrm{N}$.

(b) FOS for a distributed load of $72\,\mathrm{N}$.

Figure 12.1: The FEA simulation results for the aluminum prototype under a distributed load.

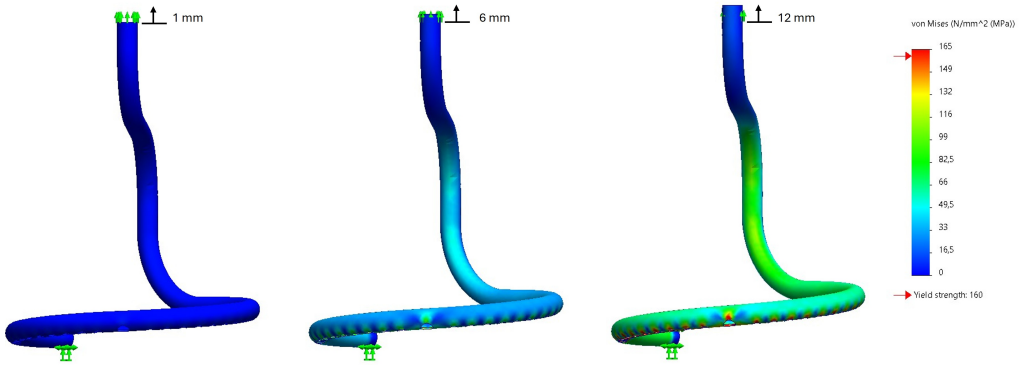

Figure 12.2: Three FEA snapshots of the force-displacement simulation of the aluminum prototype. The red color indicates the material's yield stress is exceeded.

Finite Element Analyses

The load experiments were executed for aluminum 6060 T66 frames with a Young's modulus of $70\,\mathrm{GPa}$, a yield strength of $160\,\mathrm{MPa}$, and an ultimate tensile strength of $215\,\mathrm{MPa}$ (Appendix E). The lifting device was designed for stainless steel with a Young's modulus of $200\,\mathrm{GPa}$, a yield strength of $870\,\mathrm{MPa}$, and an ultimate tensile strength of $1050\,\mathrm{MPa}$ [72].

The SolidWorks Simulation Tool for finite element analysis (FEA)[69] and the model from Chapter 6 were used to determine the resulting stresses for a distributed load. A stainless steel frame under a distributed load of $140\,\mathrm{N}$ has a FOS of 2.8 and will be $4.2\,\mathrm{mm}$ displaced. It will exceed its yield strength at a distributed load of $395\,\mathrm{N}$, after which it is plastically deformed.

The aluminum frame has a 2.8 FOS for a distributed load of $26\,\mathrm{N}$, which is approximately 18% of the design load of $140\,\mathrm{N}$. This corresponds to the yield strength ratio between aluminum 6060 T66 and stainless steel BioDur 108. Yielding will start at a distributed load of $72\,\mathrm{N}$. The results of the simulations are presented in Figure 12.1. The mode of failure was expected to be at the second hole.

For the second part of the experiment, the frame was fixed at the end of the loop section. The frame was linearly displaced upward, and the resulting stress and force were computed. The simulation is displayed in Figure 12.2. With these settings, a stainless steel frame yields at a $10.4\,\mathrm{mm}$ displacement and a $305\,\mathrm{N}$ load. Aluminum will exceed its yield strength at $5.65\,\mathrm{mm}$ and a $55\,\mathrm{N}$ load. Again, the mode of failure was expected to be at the second hole.

(a) Overview test setup.

(b) The custom load cell connection.

Figure 12.3: The test setup includes the Festo linear stage, Futek load cell, and LabVIEW.

Test setups

The linear motion for the tests was provided by the Festo EGSL linear stage, shown in Figure 12.3a. It can withstand a maximum axial load of $300\,\mathrm{N}$. The displacement was set to $30\,\mathrm{mm}$ with a constant velocity of $1\,\mathrm{mm/s}$. A Futek LSB210 FSH03943 load cell was attached to the linear stage, shown in Figure 12.3b. It was calibrated from $-210\,\mathrm{N}$ to $210\,\mathrm{N}$ and has a maximum capacity of $450\,\mathrm{N}$. The

prototype was connected to the load cell by a custom joint with an M3 thread. Data was extracted from the load cell every $100\,\mathrm{ms}$ with LabVIEW.

For the first part of the experiment, the load was distributed over the lifting device's loop by 300x$200\,\mathrm{mm}$ Rayyl artificial skin. A hole was made to insert the lifting device, and it was secured to the Thorlabs base plate by 32 M6 bolts, shown in Figure 12.4a. For the second part, the frame's endpoint was fixed to the base plate as shown in Figure 12.4b.

The load on the lifting device during laparoscopic procedures was simulated in the first part of the experiment. However, the load was distributed by artificial skin, which strained when force was applied. Hence, only the resulting force could be verified with that setup. The second part excluded the artificial skin, which allowed for a force-displacement measurement.

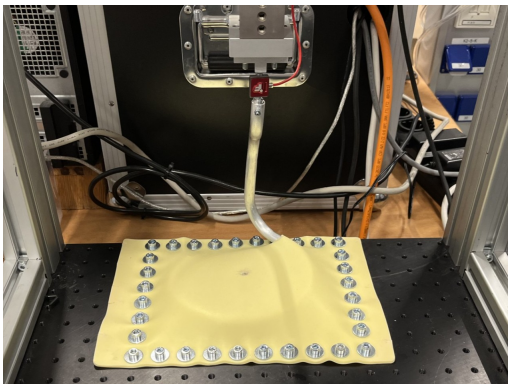

(a) Part 1: a distributed load.

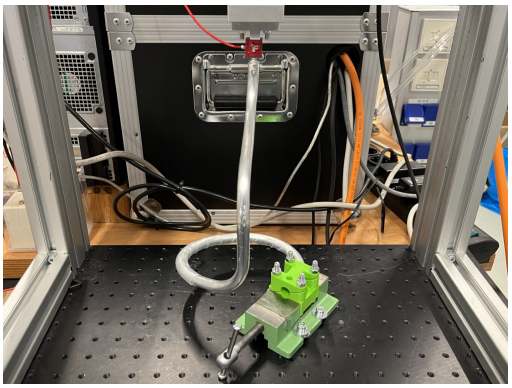

(b) Part 2: a force-displacement measurement.

Figure 12.4: The two setups for the structural load experiment.

Results

The results from the first part of the experiment are plotted in Figure 12.5. The left graph displays time-series data for force (N) and displacement (mm), while the right graph provides the corresponding force-displacement curve. The load cell reached the maximum calibrated value of $210\,\mathrm{N}$ before the $30\,\mathrm{mm}$ stroke was finished. After 41 seconds the downstroke to the starting point started with a velocity of $10\,\mathrm{mm/s}$. The force measurement settles at a value of $-13.2\,\mathrm{N}$.

The slope of the curve decreases from $14\,\mathrm{N/mm}$ to $7.9\,\mathrm{N/mm}$, which indicates the material exceeded its yield strength. This occurs at a load of approximately $69\,\mathrm{N}$, with a vertical displacement of $5.0\,\mathrm{mm}$. The trendlines of the elastic and plastic deformation sections are presented in Figure 12.5b.

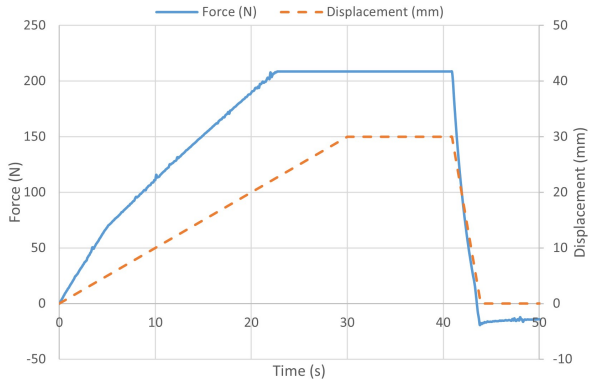

(a) Force and displacement plotted over time.

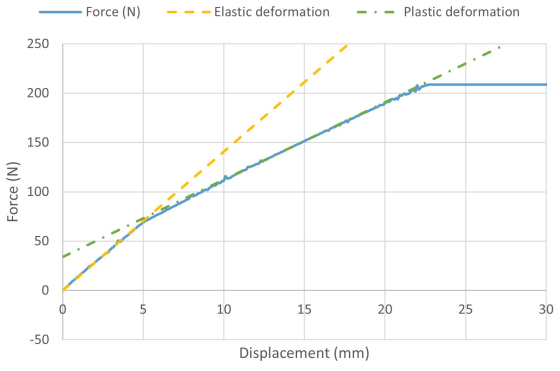

(b) Force-displacement curve of the upstroke.

Figure 12.5: The results of the structural load experiment's first part. The dashed trendlines indicate the elastic and plastic deformation.

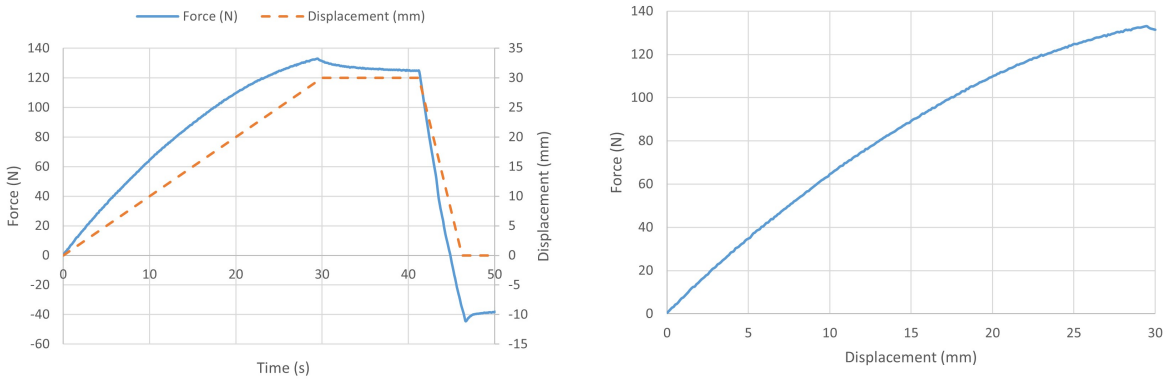

(a) Force and displacement plotted over time.

(b) Force-displacement curve of the upstroke.

Figure 12.6: The results of the structural load experiment's second part.

The results from the experiment's second part are presented in Figure 12.6. In contrast to the first test, this curve is nonlinear and no yielding point was identified. After 41 seconds the downstroke to the starting point started with a velocity of $5\,\mathrm{mm/s}$. The force measurement settles at a load of $-37.6\,\mathrm{N}$.

The permanent deformations of both frames relative to the final prototype are shown in Figure 12.7. No distinct mode of failure was identified in either frame, but it can be observed that the holes for LED lighting did not remain perfectly circular.

(a) No deformation.

(b) Deformation first test.

(c) Deformation second test.

Figure 12.7: The permanent deformations of the tested frames relative to the final prototype.

Discussion

The experiment gives an indication of the structural strength of the aluminum frame. After evaluating the test results, an initial prediction can be made about the load-bearing capacity of a stainless steel BioDur 108 frame.

The results from the experiment's first part strongly suggest that plastic deformation starts at a $69\,\mathrm{N}$ load, as the slope decreased from $14\,\mathrm{N/mm}$ to $7.9\,\mathrm{N/mm}$. This is not allowed according to design requirement $V1$. The transition occurs at a $5.0\,\mathrm{mm}$ displacement. However, this value is meaningless since the artificial skin also deforms.

After the downstroke to the starting position, the measured force was negative, meaning the load cell was compressed. This happened because the frame got pushed against the baseplate by the linear stage, confirming plastic deformation occurred.

The load at which the frame starts to yield was similar to the FEA result, $69\,\mathrm{N}$ and $72\,\mathrm{N}$, respectively. However, the test setup did not perfectly replicate the FEA model. The load was not uniformly distributed over the frame's loop, displayed in Figure 12.8. This may contribute to the 4% difference.

The second part of the experiment aimed to obtain useful deformation data. According to the FEA, the material was expected to yield at a $5.7\,\mathrm{mm}$ displacement with a $55\,\mathrm{N}$ load. However, the force data

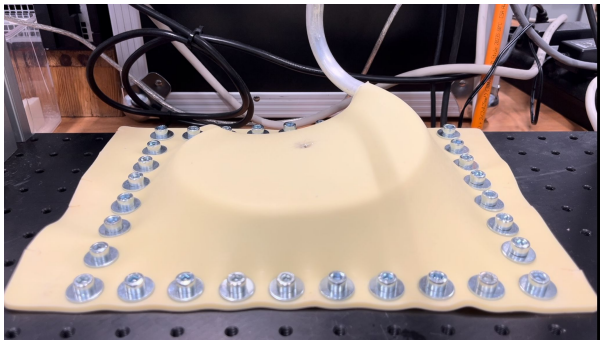

Figure 12.8: The tension in the Rayyl artificial skin. The resulting load in ununiformly distributed over the frame's loop

from Figure 12.6 shows a completely different behavior. No transition from elastic to plastic deformation was identified.

An error in the setup was observed in the video footage of the test. The frame rotated at the fixation clamp. Hence, the force-displacement curve is incorrect, and the second part of the experiment is invalid.

Nevertheless, although there is a 4% discrepancy, the first experiment strongly suggests the FEA model is valid after the production process. Accounting for the discrepancy, the FEA model indicates a stainless steel frame could sustain the design load of $140\,\mathrm{N}$ with a 2.7 FOS. Therefore, design requirement $V1$ is satisfied.

To conclude, it is recommended to use the SolidWorks Simulation Tool [69] to develop a stainless steel frame. Although the FEA model suggests the final design could sustain a $140\,\mathrm{N}$ load with a 2.7 FOS, this should be verified with a similar but improved structural load test.

Limitations

Because both parts of the experiment were performed only once, the results are vulnerable to variability. Each test destroys a semi-finished prototype, which takes a day to manufacture. For future structural strength evaluations, it is advisable to first conduct multiple non-destructive stress tests before proceeding with destructive testing.

As discussed, the first test setup could have been a better replicate of the FEA model. While this could have added to the discrepancy in the results, the conclusion is well within the safety factor. Presumably, the test setup was closer to reality than the FEA model. This implies the FEA model is overly simplified. Therefore, a more realistic force distribution should be considered.

The load cell could be calibrated to $300\,\mathrm{N}$. Although this was not necessary for finding the yielding load, it would result in a more comprehensive measurement. Additionally, the failure load could be determined more precisely using strain gauges.

No useful deformation data was acquainted. The first test used artificial skin, which made the displacement data useless. The second test aimed to exclude the skin's uncertainty but was improperly set up.

12.2. Surface temperature test

In this test, the lifting device's surface temperature was measured. To prevent tissue damage from heat burns, the device must be designed to have a maximum surface temperature of $41\,°\mathrm{C}$, according to IEC 60601-2-37 (design requirement $P2$). The prototype by Den Butter exceeded this temperature by $1\,°\mathrm{C}$.

Den Butter's prototype used a $12\,\mathrm{V}$, $11\,\mathrm{W/m}$ LED strip, whereas this prototype uses a $5\,\mathrm{V}$, $6\,\mathrm{W/m}$ LED strip. Heat was only generated by the LED strip due to the defective camera module. The test aimed to determine if the product surface temperature remains below $41°$ with a less powerful LED strip.

Method

The two most common laparoscopic procedures - appendectomy and cholecystectomy - take approximately 1 to 2 hours. The lifting device will be in a closed and humid environment with an average temperature of $36.6°$ [90]. The test setup, however, was in an open space with a constant room temperature of $19.5°$, shown in Figure 12.9a.

The temperature was measured with a Reed 882 infrared thermometer, Figure 12.9b. It measures temperatures from $-50\,°\mathrm{C}$ to $550\,°\mathrm{C}$, with a $0.1\,°\mathrm{C}$ resolution below $200\,°\mathrm{C}$ and an accuracy of $\pm 2\,°\mathrm{C}$. The temperature was measured every 5 minutes for 1 hour at four locations of the frame, shown in Figure 12.10a.

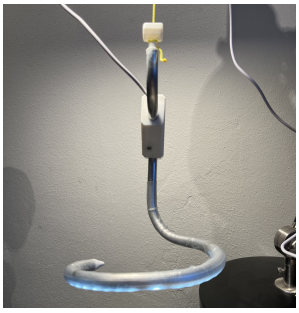

(a) The test frame in an open space.

(b) Reed 882 infrared thermometer.

Figure 12.9: The test setup to measure the product surface temperature.

Results

The results of the measurements are presented in Figure 12.10b. The room temperature of $19.5\,°\mathrm{C}$ is indicated with a gray dashed line. The lifting device heats up in approximately 20 minutes, then settles at a constant temperature; $28.1\,°\mathrm{C}$ at the start of the LED strip, $27.7\,°\mathrm{C}$ at the camera location, and $25.8\,°\mathrm{C}$ at the end of the LED strip. This corresponds to a $6.7, 8.6$, and $8.9\,°\mathrm{C}$ temperature increase. The highest measured temperature was $29.3\,°\mathrm{C}$, which is $11.7\,°\mathrm{C}$ below the maximum surface temperature.

Discussion

Temperature disparities between measurement points indicate that the LED strip's individual resistors generate the heat. There is a heat gradient from the start to the end of the LED strip. This presumably occurred due to inconsistencies in resistor values. Having inconsistencies will result in nonuniform light distribution, which is undesirable. However, no light disparity was visually observed.

The device heats up to its constant temperature in approximately 20 minutes. The quick heating can be attributed to aluminum 6060-T66's thermal conductivity ($150\,\mathrm{W/mK}$) and the direct, uninsulated bonding of the LED strip to the tubular frame. In contrast, stainless steel BioDur 108, with a thermal conductivity of approximately $15\,\mathrm{W/mK}$, heats up more slowly.

The surface temperature was significantly reduced with a less powerful LED strip. The maximum was $29.3\,°\mathrm{C}$ compared to $42°$ in the Den Butter's study. This is $11.7\,°\mathrm{C}$ below the maximum surface temperature from design requirement $P2$.

However, the conditions did not reflect a realistic surgical procedure. The environment should be a closed space with a temperature of $36.6\,°\mathrm{C}$, resulting in lower heat dissipation. The loop's upper

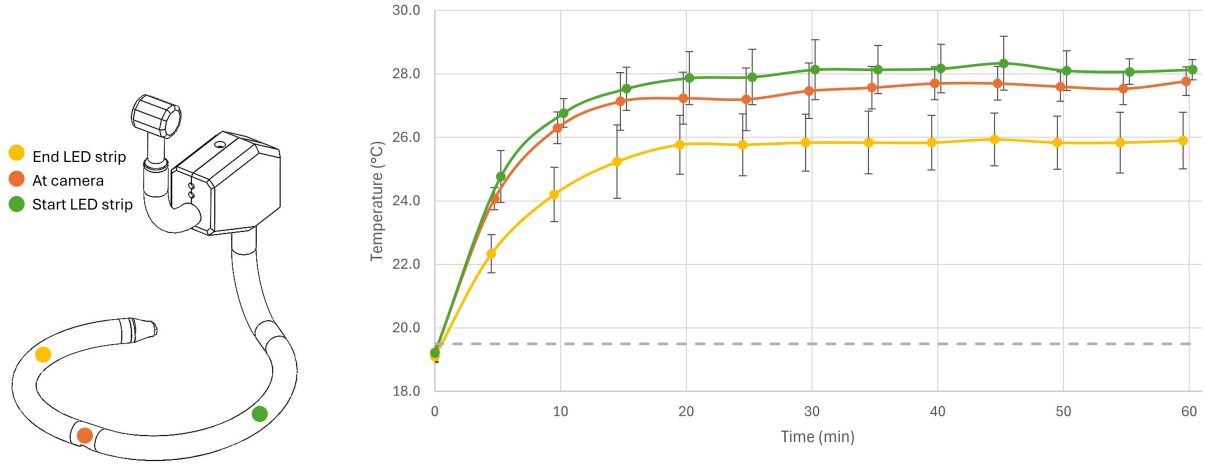

(a) Measurement locations

(b) Temperature results

Figure 12.10: The surface temperature, measured at four locations. The gray line indicates the room temperature of $19.5\,^{\circ}\mathrm{C}$.

side will be in contact with the abdominal wall. Hence, heat will be dissipated via conduction instead of convection, which has a more efficient dissipation. Nevertheless, it is expected that the heat dissipation during surgery will be lower than in the experimental setting.

Since the LED strip will generate the same amount of heat and the camera module will generate additional heat, the temperature is expected to increase with at least $8.9\,^{\circ}\mathrm{C}$. From an ambient temperature of $36.6\,^{\circ}\mathrm{C}$, it will result in a surface temperature of $45.5\,^{\circ}\mathrm{C}$. This stresses the importance of heat management.

To conclude, it is a design trade-off between LED illumination and heat generation. The device should provide sufficient light but not exceed a surface temperature of $41\,^{\circ}\mathrm{C}$. On the other hand, heat dissipation can be increased, and the LED strip can be insulated. Moreover, a custom LED circuit can reduce heat generation; an LED circuit with one resistor outside the human body will produce the bulk of heat outside the abdomen. These alterations will decrease the product surface temperature. Verifying this in a more realistic test environment is recommended.

12.3. Additional Tests

This section verifies design requirements $C1$, low production costs; $R2$, dust- & waterproof; $P1$, insertion diameter; $U1$, compatibility with retractors; and $U2$, weight. The performance of the lifting device on these six requirements was assessed through five short tests, and the outcomes led to suggestions for improving future designs.

Costs

Design requirement $C1$, low production costs, was assessed with this test. Cost-effectiveness was one of the six design drivers for the lifting device. Financial constraints are one of the most significant barriers to accessing healthcare, and purchasing the necessary equipment and supplies can be prohibitively high for many LMICs [91, 8]. Therefore, an inexpensive solution may accelerate the implementation of laparoscopy in low-resource settings [24].

This test estimates the production costs of the aluminum prototype and the final design of the stainless steel. An overview is presented in Table 12.1. The predicted production costs include the raw materials and labor time. The costs of labor differ substantially depending on the location of production. The hourly labor cost is approximately € 40 in HICs and € 10 in LMICs [92]. Expenses for utility, rent, and logistics were excluded.

Furthermore, the costs for custom tools, such as bending dies and drilling jigs, may be significant as the production quantity may be less than 100. An overview of the production costs of the custom tools is presented in Table 12.2. The costs of custom tools for rotary draw bending and the drilling jigs for the stainless steel final design were ignored as these still need to be designed.

Table 12.1: An overview of the weight, costs, and labor time for the lifting device's components. The values are based on the prototype, and values for the final design are in italics

Part	Material	Weight (g)	Costs	Labor time (min)
Frame	Aluminum / *Stainless steel*	$60 \,/\, 148$	€ 2,00 / *€ 14,00*	300
RAIS joint	PLA / *Stainless steel*	$9 \,/\, 51$	€ 0,18 / *€ 4,00*	$10 \,/\, 120$
Endcap	PLA / *Stainless steel*	$4 \,/\, 12$	€ 0,08 / *€ 1,00*	$5 \,/\, 45$
Housing left	PLA / *Nylon*	$20 \,/\, 18$	€ 0,40 / *€ 2,20*	15
Housing right	PLA / *Nylon*	$20 \,/\, 18$	€ 0,40 / *€ 2,20*	15
M3 bolt (3x)	Stainless steel	6	€ 0,15	–
Heat shrink	Polyolefin	14	€ 2,50	20
Camera module	–	5	€ 32,20	15
LED strip	–	10	€ 2,60	30
USB cable (2x)	–	20	€ 2,00	–
Total		$\mathbf{168 \,/\, 302}$	**€ 42,51 / € 62,85**	**400 / 550**

Table 12.2: An overview of the weight, costs, and labor time for the custom tools.

Part	Material	Weight (g)	Costs	Labor time (min)
Bending die	PLA	298	€ 6,00	5
Handle	Aluminum & stainless steel	1010	€ 25,00	960
Axis	Stainless steel	22	€ 0,30	5
M6 bolt and nut (5x)	Stainless steel	35	€ 1,00	–
Drill jig (LEDs)	PLA	160	€ 2,40	5
Drill jig (camera)	PLA	23	€ 0,45	5
Total		$\mathbf{1521}$	**€ 35,95**	**980**

The cost of the materials for the aluminum prototype was approximately € 40 and will be around € 60 for a stainless steel device. The labor costs in HICs are predicted to be € 270 and € 370, respectively. In LMICs, this will be around € 70 and € 90. This stresses the importance of local production. The custom tools materials cost approximately € 40. The labor time will be drastically reduced if an experienced manufacturer produces the handle.

In conclusion, the estimation of production costs indicates that the required maximum of € 400 is satisfied when the lifting device is manufactured locally. However, the estimations were rough, and the costs for rotary draw bending have to be considered.

Weight

Design requirement $U2$, a maximum weight of $0.5\,\mathrm{kg}$, was assessed with this test. The estimation in Table 12.1 shows a weight of $168\,\mathrm{g}$ for the prototype. The measured weight was $168.7\,\mathrm{g}$, which confirms the estimation. Therefore, the expected weight of $302\,\mathrm{g}$ for the stainless steel device is assumed valid. Thus, the lifting device's weight is well below the maximum of $0.5\,\mathrm{kg}$.

Insertion diameter

The lifting device must fit through a $12\,\mathrm{mm}$ diameter incision, as specified by design requirement $P1$. Therefore, the lifting device's cross-section may not exceed a $12\,\mathrm{mm}$ diameter at any point entering the abdominopelvic cavity. Measurements with a digital caliper revealed diameters from $12.3\,\mathrm{mm}$ to $12.5\,\mathrm{mm}$. The discrepancy occurs due to slight flattening in the production process. The overall diameter exceeds the specified limit because the heat shrink was wrapped around a $12\,\mathrm{mm}$ diameter tube. Excessively large diameters were measured at wrinkles in the heat shrink.

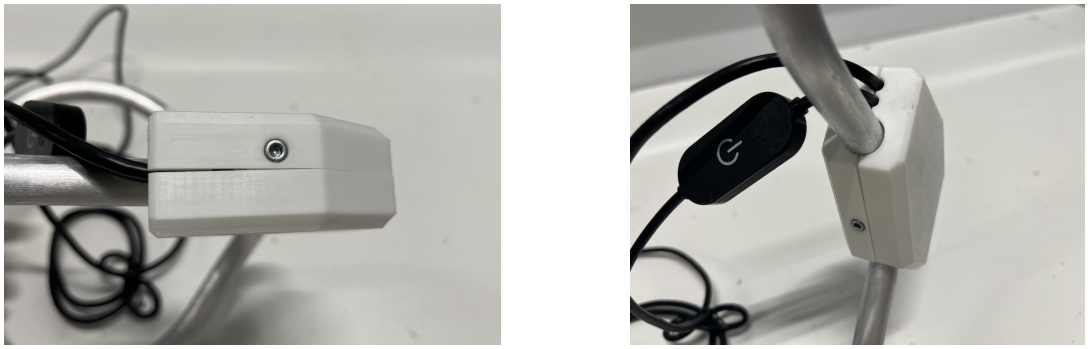

Figure 12.11: The prototype is not waterproof due to large gaps in the housing.

Reducing the diameter could involve using an alternative sealing method or a narrower tube. The current configuration with the camera in the middle of the loop, a narrower tube is impossible. Since an alternative sealing method is most straightforward, that is recommended. Otherwise a completely different design approach should be considered.

Waterproofness

In low-resource settings, medical devices are sterilized by chemical immersion. The lifting device must be IP67 level dust- and waterproof, requiring it to be submerged in water for 30 minutes with its highest point at least $150\,\mathrm{mm}$ below the surface. However, it was visually observed that the device is not waterproof, shown in Figure 12.11.

Therefore, a waterproofness test was executed only for the prototype's loop section. Two semi-finished prototypes were submerged in water up until the housing for two runs of 30 minutes. Waterproofness was evaluated by visual inspection and weighing.

The first prototype was not waterproof. The frame was filled with water after the first trial, shown in Figure 12.12. On the other hand, the second frame was waterproof; no water was observed, and the weight remained the same.

Water breached in the first prototype's frame through the endpoints of the heat shrink. Those were likely insufficiently heated, in contrast to the second prototype. This demonstrates the sealing is inadequate when improperly installed. Furthermore, the highest point was not $150\,\mathrm{mm}$ below the surface due to the gaps in the housing. Hence, it cannot be concluded that the second prototype was IP67 level waterproof.

When the gaps in the housing are fixed, the device should be submerged in water for 30 minutes with its highest point at least $150\,\mathrm{mm}$ to ensure it is IP67-level waterproof. If it is waterproof, it is recommended to assess the chemical resistance to common compounds (hydrogen peroxide, ethylene oxide, and peracetic acid).

Figure 12.12: Water in first test frame.

Compatibility with retractors

Design requirement $U1$ specifies the lifting device must be compatible with the RAIS retractor arm, which is essential for seamless integration into current surgical setups. Figure 12.13 shows the connection between the retractor arm and the prototype.

The joint fits decently in the retractor arm, although the connection is somewhat loose. The width of the joint was designed to be $20\,\mathrm{mm}$, but the actual 3D-printed part is $19.7\,\mathrm{mm}$. This left space to wiggle. However, after the connection screw was tightened, this was undone. The hexagonal sides were the same dimensions as designed, enabling a $36°$ incremental pitch of the device. Deborah Maufi, CEO of Loresa, a health venture working on RAIS system commercialization, verified the compatibility with the RAIS system.

For future iterations, the joint's width should be $20.0\,\mathrm{mm}$ for a slightly better fit. Additionally, the prototype's connector joint was 3D-printed from PLA but should be machined from stainless steel in future iterations. The connection with the retractor arm should be verified after the production process.

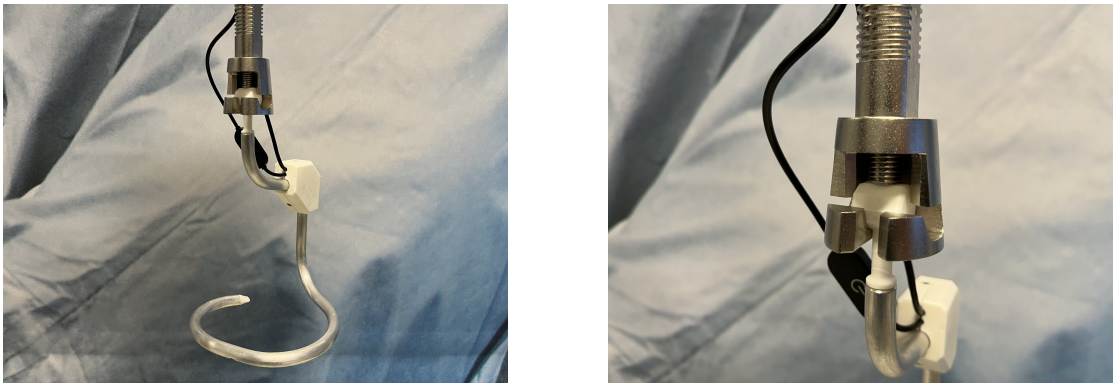

Figure 12.13: The compatibility with the RAIS retractor arm.

13

User Test

13.1. Evaluation by a GILLS surgeon

A user test was conducted to evaluate the three most important design drivers: surgeon's visibility, patient safety, and user-friendliness. The test consisted of two parts. The first included determining the best camera position and examining the quality of the image. The second was discussing the lifting device's physical shape and dimensions and examining if the use was intuitive.

The final design was based on the selection procedure in Chapter 8. However, no clear favorite camera position was identified. Therefore, the three camera positions from Chapter 7 were compared during the user test. The positions are shown in Figure 13.1. The first was at the start of the loop, close to the incision point. The second was a view from the side. The third was in the middle of the loop, which is the camera location of the prototype.

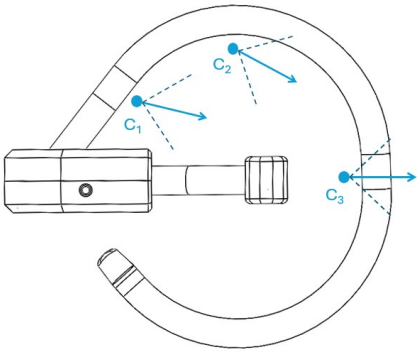

Figure 13.1: The three camera positions for the user test.

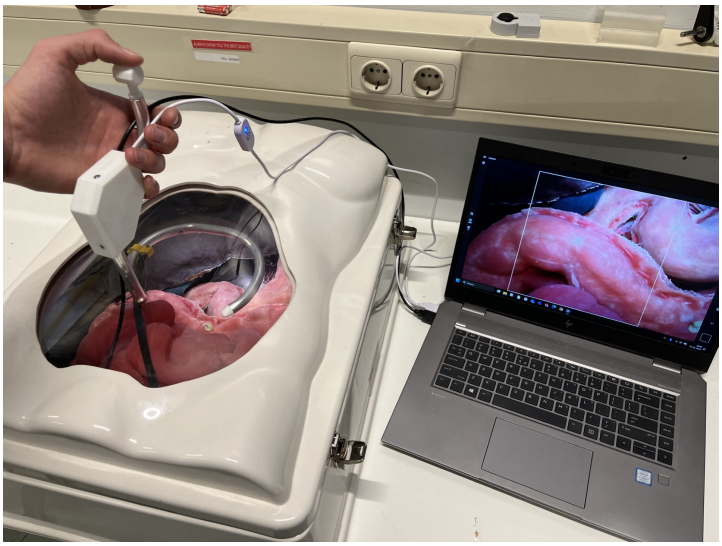

Figure 13.2: The user test setup of an abdomen model with realistically looking organs. During the test, the transparent sheet was replaced with a dark sheet, and two laparoscopic instruments were used.

The setup was a model of the abdomen with realistically looking organs, displayed in Figure 13.2. The prototype was located in the supraumbilical incision. A camera was attached to the outside of the frame to create the three camera views. During the test, the transparent sheet was replaced with a dark sheet to prevent direct vision. Two laparoscopic instruments were inserted from the side following the baseball diamond port positioning principle from Figure 7.4 [76, 77]. The lifting device was held fixed while the surgeon was operating the laparoscopic instruments.

Before the lifting device was fixed, the surgeon oriented it under indirect vision on the laptop screen. The surgeon moved the device to obtain what areas could be seen. Afterward, the camera view was

centered at two target locations. The first was the gallbladder to compare the camera positions for cholecystectomy. The second was the appendix for appendectomy. These are two of the most common laparoscopic procedures [53, 55].

The user test was conducted with Dr. Jesudian Gnanaraj, a renowned GILLS surgeon specializing in low-resource settings. He has dedicated over 30 years to rural healthcare in India. With thousands of surgeries performed and over 30 MIS-capable hospitals established, he leads advancements in underserved areas.

Currently, he serves as president of the Association of Rural Surgeons of India (ARSI), as joint secretary of the International Federation of Rural Surgeons (IFRS), and as an adjunct professor at Karunya University. As editor of the Rural Surgery Journal and author of 45 publications, he actively shapes the field.

In November 2024, during a visit to Delft University of Technology, he evaluated the lifting device prototype against the following design requirements and aims: the imaging quality ($\boldsymbol{V2}$), the camera position ($V4_A$), single-incision laparoscopic surgery ($P4_A$), data and power connection ($\boldsymbol{U3}$), and intuitive use & interface ($U4_A$).

Discussion

The feedback from the user test with Dr. Gnanaraj will be discussed in two parts. The first discusses the image quality and compares the three camera positions. In the second part, the lifting device's physical shape and dimensions will be discussed.

Camera view

In general, the wide-angle camera provides an excellent overview of the abdominopelvic cavity. The quality of the camera module is outstanding. The LED lighting is superior to currently used laparoscopes. Unlike laparoscopes, which emit light from a single point, the lifting device emits light from all directions. Hence, it provides far more light and creates almost no shadows. Laparoscopes often need to be repositioned around the target area to achieve a shadow-free image; this will not be necessary for the lifting device.

The surgeon moved the device to obtain what areas could be seen. By rotating and pitching, the majority of the abdominopelvic cavity can be observed. However, viewing the area straight under the incision point was challenging. The lifting device had to be tilted in an undesirable orientation. Nevertheless, no surgeries are performed straight under the incision point of AWL devices.

Dr. Gnanaraj indicated that, although nearly all areas can be observed, orienting the lifting device was difficult. Changing the orientation will be impossible during operations. Therefore, he suggests having a movable camera such that small adjustments can be made. Furthermore, the camera has a physically defined distance from the target tissue. It cannot be altered as with laparoscopes. As a result, digital zoom is crucial for close-up inspection of tissue.

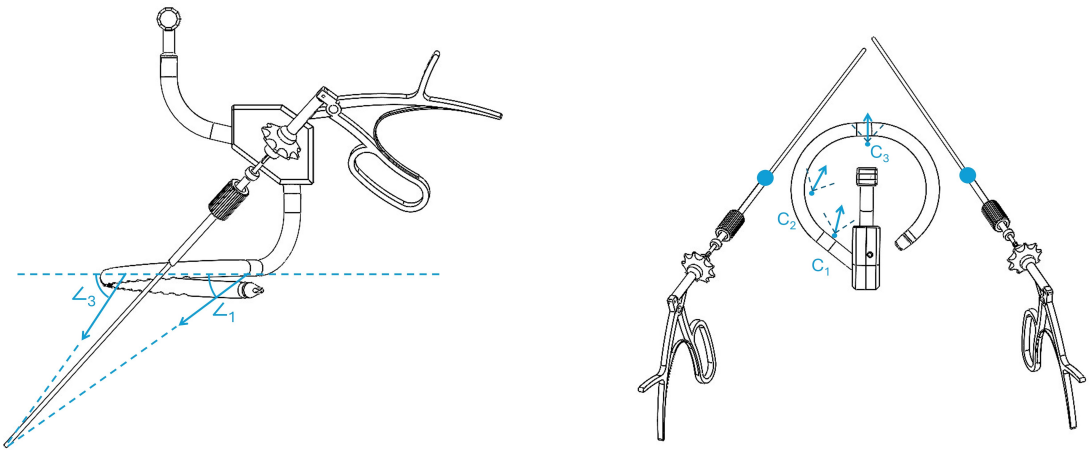

(a) Viewing angles. **(b)** Relative camera positions.

Figure 13.3: The camera positions and orientations with respect to the laparoscopic instruments.

The three aforementioned camera positions were compared. Similar areas can be observed with all camera positions. The surgeon tried some maneuvers from cholecystectomy and appendectomy. The camera positions did not affect the perception of depth, which was sufficient for all views. The viewing angle increases from camera position 1 to 3, as shown in Figure 13.3a.

Camera position 1 – at the start of the loop – was the surgeon's favorite position. It has the smallest viewing angle, which improves the view under lifted tissue. Camera position 2 – from the side – was the worst; the side view was "weird" and impractical. Camera position 3 – in the middle of the loop – was acceptable. The top view gives a clear image, but seeing under tissue was challenging.

Camera position 1 also has the best position with respect to the laparoscopic instruments. It is a little behind the incision points of the laparoscopic instruments, as shown in Figure 13.3b. This yields a view similar to views in conventional laparoscopy. Nevertheless, for single-incision laparoscopy (SILS), position 1 may not be beneficial since it is very close to the incision port.

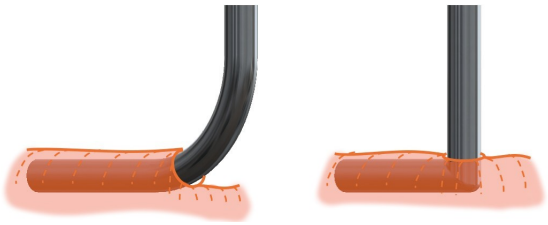

Figure 13.4: The incision in the skin is rotated around the upward bend (left). Without the bend, the incision remains parallel to the skin surface (right).

Shape and dimensions

Dr. Gnanaraj appreciated the helical shape of the frame, which will make insertion easier. He reckoned it has enough pitch. Nonetheless, insertion was challenging due to the diameter of the tube. The diameter at the loop's end should be reduced or flattened to allow smooth insertion.

At the start of the upright, two aspects require improvement. Again, the diameter should be reduced. A smaller diameter is essential for SILS, especially. Furthermore, the upward bend with a $43\,\mathrm{mm}$ radius is too large. For that reason, the 3D-printed prototype from Section 11.1, with a bend radius of $30\,\mathrm{mm}$, was shown to the surgeon. However, that upward bend is also too large, and the skin will slip down the bend. The incision is then rotated inconveniently, as shown in Figure 13.4. Instead, the loop and upright section of the frame should be perpendicular, without a bend.

The lifting device's loop should be smaller. The radius of $60\,\mathrm{mm}$ should be decreased to maximum $50\,\mathrm{mm}$. Before the blind entry of the device, surgeons do a so-called finger test, where they examine the inside of the abdominal wall for irregularities. As the incision point is not in the center of the loop, a finger test does not cover the area of the loop. When the loop size is reduced, the operational volume will be less than the pneumoperitoneum in conventional laparoscopy; according to Dr. Gnanaraj, that is no problem in practice.

Furthermore, the lifting device's helical loop is shaped clockwise, like a corkscrew. This shape complicates the insertion of the device for right-handed surgeons. As the majority of surgeons are right-handed, the loop should be shaped counterclockwise.

The RAIS connector joint is located in the center of the loop, just like the actual RAIS lifting device. However, that is not essential for this lifting device. The RAIS connector joint can be directly above the incision point, making the shape of the upright section less complicated. Nevertheless, the frame's horizontal section and the housing are used to operate the current lifting device. When the horizontal section is removed, the handling of the device should be considered.

Lastly, a single USB A output with a much longer cable is preferred. It will make the device easier to clean and will result in fewer cables in the operating room, which are already challenging to manage [93]. Large commercial available components or a custom circuit are required for this.

14 Discussion

While laparoscopic surgery offers various advantages over open surgery, its implementation in LMICs has been slow due to resource shortages, high costs, and limited infrastructure. GILLS is a cost-effective alternative that avoids reliance on carbon dioxide gas and general anesthetics. However, its use in rural areas is limited by a lack of assisting staff and lower-quality laparoscopes compared to those in high-income countries. Hence, the following project goal was specified:

> *Design, build, and validate a next-generation abdominal wall lift device with an integrated imaging system for gas insufflation-less and single-incision laparoscopic surgery in a low-resource setting.*

This chapter discusses whether the goal was accomplished by reviewing the design drivers and requirements. Additionally, the design process is discussed, and the limitations of the project are described. Lastly, recommendations for future development are presented.

14.1. Discussion

The lifting device's design was driven by the surgeon's visibility, patient safety, manufacturability, user-friendliness, cost-effectiveness, and robustness. A final design and prototype arose from the six drivers, described in Chapter 9 and Chapter 11, respectively. A list of requirements and aims bounded these, Table 14.1. The final design and prototype were evaluated on that list. The last column indicates if the requirements were satisfied based on quantitative tests, calculations, and qualitative assessment.

The prototype is not fully functional, as the imaging system is defective. Nevertheless, the prototype and final design can be assessed on several aspects. This will be done in five sections, each discussing the relevant design requirements.

Camera position

This section assesses design requirement $V2$, the camera position. It was a major focus of the project, as it plays a crucial role in the functionality of the lifting device. Hence, an experiment was executed to determine the effect of camera position and orientation on the surgeon's performance during laparoscopic tasks, shown in Figure 14.1.

The results did not yield one unambiguous favorite camera position. The data suggested that the side view position was slightly favorable for the first task. However, this was due to only one of the seven measured objectives. The outcome of the second task was based on four objectives and the best performance was measured with the front view position.

Despite participants' opinions varying heavily, the front view was preferred. The top view was acceptable, and the side view was inferior. However, the participants' inexperience was a major limitation. The results were task-dependent, and those were not realistic laparoscopic tasks. Therefore, although there was a slight preference for the front view, top view, and side view, respectively, no distinct favorite camera position was identified.

Table 14.1: Design requirements and aims with corresponding performance criteria and result.

(a) Design requirements

ID	Requirement	Performance criteria	Satisfied
$V1$	Abdominal wall lifting	The device must sustain a load of $140\,\mathrm{N}$ with a 2.0 FOS	Yes
$V2$	Camera position	The camera view must accommodate common procedures	No
$V3$	Operational volume	The operational volume must equal the pneumoperitoneum	Yes
$P1$	Insertion diameter	The device must fit through a $12\,\mathrm{mm}$ diameter circular incision	No
$P2$	Product surface temperature	The surface temperature may not exceed $41\,^{\circ}\mathrm{C}$	No
$U1$	Compatibility with retractors	The device must be compatible with RAIS retractor arm	Yes
$U2$	Weight	The device must weight a maximum of $0.5\,\mathrm{kg}$	Yes
$U3$	Data and power connection	An USB-A port must be used for power and data transmission	Yes
$C1$	Low production costs	The production must cost a maximum of $\text{€}400$	Yes
$C2$	Use of supplies	Only the basic supplies: water and electricity may be used	Yes
$C3$	Local production	The device must be manufactured locally in LMICs	Yes
$R1$	Cleaning & sterilization	The device must be sterilizable by chemical immersion	No
$R2$	Dust- & waterproof	The device must be IP67 level dust- and waterproof	No
$R3$	Maintenance	The electronic parts must be replaceable when defective	Yes

(b) Design aims

ID	Aim	Performance criteria	Satisfied
$V4_A$	Imaging quality	The image should match state-of-the-art quality of a decade ago	Yes
$R4_A$	Durability	The device should be able to do a thousand cycles	Unknown
$P3_A$	Biocompatibility	The device should be biocompatible according to ISO 10993-1 2018	No
$P4_A$	SILS	The device should be able to accommodate SILS	No
$U4_A$	Intuitive use & interface	The device and interface should be intuitive and easy to use	No

Consequently, the camera position in the final design was decided based on feedback from Dr. Gnanaraj, who preferred the concept with the camera in the middle of the loop (concept 3 in Section 5.2). A user test aimed to validate the preference.

The user test detected that small viewing angles are beneficial. Hence, the front view was favored, aligning with the experimental box trainer results. The side was impractical and undesirable. The top view – the position in the final design – was acceptable, but looking under tissue was challenging.

So, a camera position closer to the incision point would be favorable. However, Dr. Gnanaraj argued that this may differ for SILS, as the instruments will then be in the camera's direct line of sight.

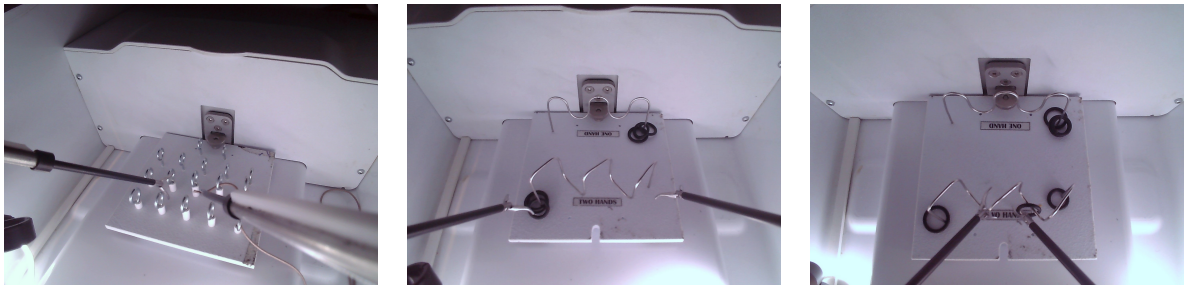

(a) Side view **(b)** Front view **(c)** Top view

Figure 14.1: The box trainer experiment. The effect of three camera positions on two laparoscopic tasks was assessed.

Furthermore, most of the abdominopelvic cavity can be observed with the current camera position. However, the lifting device will often be pitched with an $36°$ increment in practice, shown in Figure 14.2. Hence, the viewing angle should be adjustable to account for the pitch.

In conclusion, the current camera position is acceptable, and it can accommodate common laparoscopic procedures. Nevertheless, it limits viewing under tissues; the $36°$ pitch should be considered, and it is not the optimal position. Because of these limitations and the fact that the imaging system is defective in the prototype, design requirement $V2$ is not satisfied.

(a) $0°$ angle **(b)** $36°$ angle

Figure 14.2: The incremental pitch, altering the camera angle.

Shape & Dimensions

The second discussion points regard the lifting device's shape dimensions. Design requirements $V3, P1$ and aims $P4_A$, and $U4_A$ will be assessed, starting with the operational volume.

The size of the loop determined the operational volume. To provide sufficient visibility while minimizing the risk of peritoneal injury, the circumference was set to $^3/_4$ and the radius to $60\,\mathrm{mm}$.

Nonetheless, the loop size should be reduced to a maximum of $50\,\mathrm{mm}$. Before the blind entry of the device, surgeons do a so-called finger test, where they examine the inside of the abdominal wall for irregularities. The lifting device should not be larger than their fingers can reach. This decreases the operational volume, but that will be no problem in practice, according to Dr. Gnanaraj.

The helical loop shape reduces the friction during the insertion of the lifting device. The $5°$ pitch is sufficient. Nevertheless, insertion was difficult due to the clockwise loop shape. It should be counterclockwise, making insertion easier for right-handed surgeons.

Additionally, smooth insertion can be realized by reducing the tube diameter at the end of the loop to a maximum of $8\,\mathrm{mm}$. No electronics are located in that section, so a reduction should be achievable.

The upward bend requires two improvements. Again, the diameter should be reduced, especially for SILS. Furthermore, the bend radius is too large, causing the skin to slip down and inconveniently rotate the incision. Ideally, the loop and upright section should be perpendicular, without a bend.

With the current electronics, realizing this is highly complicated. The dimensions of the camera sensor determined the tube diameter. The sensor has to fit through the bend, making a $10\,\mathrm{mm}$ inner diameter and a bend necessary. A different approach could be possible. However, the assembly should be considered. This is challenging since the camera module's flat flex cable has a width of $8.5\,\mathrm{mm}$ and a $12\,\mathrm{mm}$ connection at the end.

Lastly, while the RAIS connector joint is centered on the loop, just like in the actual RAIS device, it is not essential. Positioning it directly above the incision could simplify the upright section. However, the current prototype relies on the horizontal section and housing to operate the device. Thus, handling must be considered when the horizontal section is removed.

To conclude, requirement $V3$ was satisfied, but the operational volume and the loop size can be reduced accordingly. Requirement $P1$ and aims $P4_A$ and $U4_A$ were not satisfied

Structure & Materials

Design requirements $V1, U1, U2, R1, R2$, and aim $P3_A$ regard the structure and materials of the lifting device. The structural strength of the frame was evaluated with a load experiment. In that experiment, a distributed load was applied, and the corresponding yielding point was determined.

The aluminum frame exceeded the yield strength at a $69\,\mathrm{N}$ distributed load, aligning with the FEA model (-4%). The model assumed a uniform load distribution over the frame, which does not reflect realistic conditions. This may have contributed to the 4% discrepancy.

Besides the fact that the FEA model could be updated with a more realistic load distribution, the experiment had other limitations. It was only one trial, making it vulnerable to variability. The failure load could be determined more precisely with strain gauges, and no useful deformation data was acquainted.

A second experiment was executed to address the latter. Unfortunately, it was set up improperly, resulting in useless data. Nevertheless, the SolidWorks FEA model could be used to estimate the structural strength of a stainless steel frame.

Finally, accounting for the discrepancy, the FEA model indicates a stainless steel BioDur 108 frame could sustain the design load of $140\,\mathrm{N}$ with a 2.7 FOS, which is well over the required 2.0 FOS. Therefore, design requirement $V1$ is satisfied.

The high FOS implies adjustments to the frame can be made. For example, the distribution of holes for LED lighting can be optimized. A brief FEA analysis was conducted to create the distribution. Yet, extra holes can be introduced to emit more light while remaining above the desired FOS. A more comprehensive analysis should be executed to determine the optimal distribution.

In low-resource settings, medical devices are sterilized by chemical immersion. So, heat resistance for autoclaves is not required. However, the materials should be resistant to cleaning chemicals. The prototype had an aluminum 6060 T66 frame, PLA housing, and polyolefin sealing. The first can withstand most chemical immersion liquids [72], but resistance to strong alkali is insufficient. The other two materials have poor chemical resistance[1]. The chemical resistances were not tested, but manufacturer specifications were assumed.

Alternative materials should be used for future prototypes. Nylon is suitable for the housing, and chemical-resistant heat shrinks are commercially available. stainless steel BioDur 108 provides excellent chemical resistance for the frame [72]. Ultimately, the chemical resistance to common compounds (hydrogen peroxide, ethylene oxide, and peracetic acid) should be verified.

Waterproofness level IP67 requires the device to be submerged for 30 minutes, $150\,\mathrm{mm}$ below the surface. Visual inspection, however, confirmed the device is not waterproof due to large gaps in the housing. The sealing around the frame's loop appears to be waterproof when properly installed. However, waterproofness level IP67 could not be verified.

The lifting device's design aimed to be biocompatible according to ISO 10993-1 2018 standards. It is an externally communicating medical device in contact with tissue for a limited duration (< 24h). Hence, the device should be biologically tested on cytotoxicity, sensitization, irritation or intracutaneous reactivity, material-mediated pyrogenicity, and acute systematic toxicity.

Stainless steel BioDur 108 and PLA/Nylon are expected to be biocompatible. On the other hand, the polyolefin heat shrink is not medical grade, but those are commercially available. Nevertheless, biocompatibility tests are extremely expensive and should only be executed for a semi-finished product.

To conclude, the prototype is neither sterilizable nor waterproof, and biocompatibility is unknown. Design requirements $R1$ and $R2$ and aim $P3_A$ are unsatisfied.

Furthermore, the prototype's endcap and RAIS joint were 3D printed from PLA. In the final design, however, these should be machined from stainless steel. The prototype weights $170\,\mathrm{g}$, whereas the final design is estimated at $300\,\mathrm{g}$; both are well below the maximum of $500\,\mathrm{g}$, satisfying requirement $U2$.

Lastly, the 3D-printed RAIS joint fits decently in the retractor arm, although the connection is somewhat loose due to the shrinking of PLA. A machined part with accurate dimensions will result in a slightly better fit. Nevertheless, the connection is sufficient when tightened, and requirement $U1$ is satisfied.

[1] www.markforged.com

Imaging system

Design requirements $P2, U3, C2, R3$ and aims $V4_A$, and $R4_A$ regard the imaging system. The wide-angle camera provides an excellent overview of the abdominopelvic cavity, and most areas can be observed. However, orienting the device in the desired position was challenging, and changing the orientation would be impossible during operations. Therefore, a movable camera will be necessary for many laparoscopic procedures.

The camera's distance to the target tissue is fixed, unlike laparoscopes. Consequently, digital zoom is essential for close-up inspection of tissue. This is impossible with the default Windows camera app, but it can be achieved with imaging software like Resolume Avenue. While the software improves imaging quality, it is expensive and not beginner-friendly.

Dr. Gnanaraj confirmed that the image quality is superior to that of laparoscopes in low-resource settings and non-inferior to those used in HICs. However, that was observed in the user test with an external camera module. The prototype does not have a functional camera sensor. Yet, design aim $V4_A$ is satisfied.

The lifting device's LED strip surpasses laparoscopes' lighting, offering light from all directions rather than a single point. This minimizes shadows and removes the need for repositioning to achieve a clear, shadow-free view.

Nevertheless, the LED strip generates excessive heat. The surface temperature test of Section 12.2 predicts that the lifting device will exceed the $41°$ maximum temperature from design requirement $P2$, despite using less powerful LEDs.

The selected concept included a water-cooling system, which was ignored in the final design as it would be too demanding and expensive to manufacture. It was deemed out of the project's scope. A more straightforward solution would be a custom LED circuit.

An LED circuit with only one resistor could be created, shown in Figure 14.3. The resistor - generating the bulk of heat - could be placed in the housing outside the abdomen, reducing the surface temperature in contact with human tissue. Such a circuit is more susceptible to manufacturing differences between LEDs, more difficult to create, and more expensive. Nevertheless, it should be considered to reduce the product surface temperature for future development.

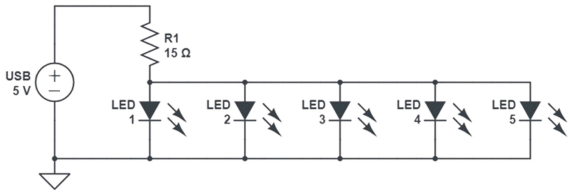

Figure 14.3: A custom LED circuit with one resistor.

The only supply required for the lifting device functionality is electricity, provided by two USB-A cables. One cable also transfers camera data. This complies with the set requirement. However, a much longer single USB-A cable is preferred, simplifying cleaning and minimizing cables in the operating room, which are difficult to manage. Large commercial available components or a custom circuit are required for this. Despite that, design requirements $C2$ and $U3$ are satisfied.

Lastly, the durability of the device is unknown. This can only be tested with a semi-finished product by doing multiple reprocessing cycles. The lifetime of the electronics is the expected bottleneck, but these can be easily replaced. Thus, design requirement $R3$ is satisfied, yet design aim $R4_A$ remains unknown.

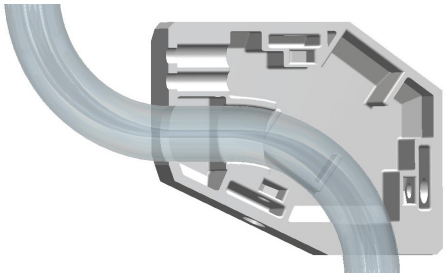

Figure 14.4: The housing's shape fits around the bent frame, making it vulnerable to bending inaccuracies.

Production & Assembly

The last two design requirements, $C1$ and $C3$, regard the production and assembly process. Additionally, the outcome of requirement $V2$ was affected by the process, as the imaging system is defective. The process was described in depth in Section 11.2. This section discusses the important findings.

The large $60\,\mathrm{mm}$ radius bends for the loop were successful; the required forces were acceptable, resulting in an accurate bend with limited surface imperfections and negligible flattening. In contrast, the 3D-printed die is merely strong enough, and the machined handle tool created friction with the tube.

In contrast, the small $30\,\mathrm{mm}$ radius bends resulted in severe tube flattening despite annealing and filling it with quartz sand. Hence, the prototype has larger $43\,\mathrm{mm}$ bends made by a regular pipe bender. It is expected that the flattening occurred because the quartz sand was not sufficiently compressed. The filler material can be pressurized by making a bend that will eventually be cut off, but this method has to be verified.

Nevertheless, the user test indicated that no bend is desirable; the connection should be perpendicular as in Figure 13.4. This implies a different manufacturing approach is necessary.

Furthermore, the RAIS connector joint does not have to be in the center of the loop, unlike the RAIS lifting device. This simplifies the upright to a straight section without bends, resulting in a simpler housing. Currently, it has a shape fit around the bent frame (Figure 14.4), making it vulnerable to manufacturing inaccuracies. With a straight upright section, the housing can be less complex, removing the gaps. Nonetheless, the housing must be sealed. Furthermore, a stronger connection with the frame is necessary since the housing will be used to operate the lifting device.

Moreover, heat shrink is an insufficient sealing technique for this application. It wrinkled, making it susceptible to HBM built up. The inside was scratched by the holes for LED lighting, decreasing the transparency. Lastly, the shrinking temperature (70–$100\,^{\circ}\mathrm{C}$) surpasses the camera's allowable operating temperature of $70\,^{\circ}\mathrm{C}$.

Imaging system assembly

The imaging system consists of two parts: a modified LED strip and a camera module in a holder with a magnet, shown in Figure 14.5. Independently, both parts can move through the entire frame. The camera assembly can be rotated from the outside with a second magnet.

The camera assembly dimensions were at the limit of what could fit through a bent $12\mathrm{x}1\,\mathrm{mm}$ tube. Hence, the LED strip and camera assembly together got stuck. When the imaging system was extracted from the frame, the camera module's flat flex cable was partly torn, making the system defective. Consequently, the final prototype is not fully functional.

(a) Render of the magnet holder.

(b) Picture of the imaging system assembly.

Figure 14.5: The imaging system. (1) is the 3D-printed holder, (2) the magnet, (3) the camera module. (4) the LED strip, and (5) the wires.

During the user test, again, the camera's flat flex cable was found to be fragile, requiring precautionary measures like reinforcing the cable-sensor connection and minimizing applied forces. However, these do not solve the assembly issue. Solutions include increasing the tube size (violating design requirement $P1$), using a smaller camera module, or the simplest option: reducing the magnet and holder size and using thinner LED strip wires.

The prototype was manufactured using simple production techniques that are affordable and available around the globe. The material costs of the prototype were € 43, and those of the final design were estimated at € 63. Assuming the lifting device will be manufactured locally in LMICs, the total production costs of a stainless steel lifting device will be approximately € 150. Therefore, despite failing to create a fully functional prototype, design requirements $C1$ and $C3$ were satisfied.

14.2. Limitations

The lifting device's most important limitation is that its lack of full functionality. Due to an improper assembling technique, the imaging system became defective.

The camera position was a core focus of the project. An extensive box trainer experiment was executed before selecting a concept. However, experimental results were limited by the participants' inexperience. Additionally, the tasks and environment were not realistic. No unambiguous distinction between the camera positions could be made due to these limitations.

Moreover, the fixed camera positions were not quantitatively compared to laparoscopes, which can be moved around target tissue. This was addressed with a user test. However, no indisputable conclusion can be drawn from that test.

The quality of the electronic components was not validated in this project since it had already been done in a previous study. Nevertheless, the combination of the LED light and camera has not yet been verified. Moreover, the failure of the electronics was also not inspected. The LED strip is not insulated, making it susceptible to current leakage. LED burnout and an overheated camera sensor are also potential hazards.

Furthermore, the lifting device's shape and size are incorrect. Limitations in the production technique resulted in tube flattening for $30\,\mathrm{mm}$ radius bends. Hence, the prototype's dimensions differ from the final design.

More local-end users should be consulted in the design process. This was initially addressed by surveying to establish the design requirements. However, in later stages, the design was discussed with only two local-end users.

These discussions were conducted online for logistic reasons, and CAD drawings were used as there was no prototype yet. This complicated the conversations, resulting in misunderstandings and missing feedback. For example, Dr. Gnanaraj noticed that the loop shape was clockwise during the user test. Addressing such crucial aspects earlier could have eliminated the need for significant redesigns.

Moreover, the user test was executed with only one surgeon. Although he was a GILLS expert and led advancements in underserved areas, user tests with several surgeons is crucial for a complete validation.

The production process was created for an aluminum frame. Theoretically, annealed stainless steel could be bent with the custom tools (when reinforced). However, this would require excessive force. Instead, rotary draw bending machines, which can achieve higher forces and precision than manual compression bending, should be used. The effects of work hardening on stainless steel 17-4 PH were not evaluated.

A considerable limitation of the design is the sealing of the holes. The heat shrink cannot be used in clinical practice. A transparent resin and a disposable seal were considered. However, these were rejected because the electronics would become irreplaceable or an undesired supply would be introduced.

Several design requirements and aims were not experimentally verified. The product surface temperature was not measured but assumed to exceed $41\,^{\circ}\mathrm{C}$ due to findings from previous research. The waterproofness was not assessed with a sufficient test. The manufacturers' specified chemical resistance and biocompatibility of the materials were assumed. Lastly, the durability and lifetime of the lifting device have not been investigated.

14.3. Recommendations

This lifting device distinguishes itself from existing products by integrating an imaging system. It aimed to enable laparoscopic surgery in low-resource settings without expensive laparoscopes and the need for assistants to operate these scopes. Ultimately, this should increase the adoption of GILLS in LMICs.

Nevertheless, several improvements should be made. Three focus points were identified. The first is the shape of the frame. The loop should be smaller, have a smaller tube diameter, and be counterclockwise. The upright section should be simplified to a straight section with a perpendicular connection to the loop section, i.e., without a bend.

The second focus point regards the imaging system. The camera should be adjustable to make small changes during operations. It should be positioned closer to the incision point, and digital zoom is crucial. The assembly of the module should be thoughtfully considered. The LED lighting should be customized with one resistor to generate the bulk of heat outside the human body. Lastly, only one longer USB-A cable should be used.

Thirdly, the sealing technique should be improved. Clear infill resin or disposable sealing are potential solutions, but they have significant drawbacks. It is recommended that different sealing methods be explored. Figure 14.6 shows an example solution to these points. However, manufacturability should not be overlooked.

(a) An example solution **(b)** Current design **(c)** RAIS lifting device

Figure 14.6: An example solution that satisfies many recommendations (left). The current design and RAIS device are presented for comparison.

For future development, local-end users should be involved throughout the entire design process. It is recommended that quick and simple prototypes be created early to make discussions easier and more effective.

Furthermore, the high-quality and inexpensive camera module was the key technology of the device. However, it resulted in various design constraints. For future development, other camera modules should be considered, although these have to be validated. Moreover, fundamentally different design and production techniques should be explored to incorporate all improvements.

15

Conclusion

This study aimed to improve the implementation of laparoscopic surgery in low-resource settings by designing, building, and validating an abdominal wall lift device with an integrated imaging system for GILLS and SILS. The device's two core functions - lifting the abdominal wall and creating vision inside the abdominopelvic cavity - eliminate the need for carbon dioxide gas, general anesthetics, and expensive laparoscopes.

The design was context-driven by surgeon visibility, patient safety, user-friendliness, manufacturability, cost-effectiveness, and robustness based on literature and feedback from rural surgeons and biomedical engineers. The lifting device comprises a stainless steel tubular hook with an internal imaging system made from inexpensive, readily available products. It can be inserted in the abdomen through a small incision, lifts the abdominal wall, and creates a clear view of target tissue.

An aluminum prototype was created to validate the concept. The device was evaluated using six verification tests and a user test by GILLS expert Dr. Gnanaraj. The prototype demonstrates the potential of the technology; however, a core functionality was not satisfied due to a defective camera module. Surgeon visibility was a prime focus of this study, but no unambiguous best camera position was identified. Sufficient operational space can be created, supported by a dimensional analysis and a structural strength test.

Design improvements should focus on three aspects: the frame's shape, the imaging system, and the sealing technique. The current design and production principle has strict dimensional constraints. A fundamentally new design approach should be considered. Local-end users should be involved throughout the entire design process.

An improved and functional device will give an excellent overview of the abdominopelvic cavity. Digital zoom facilitates common laparoscopic procedures without requiring expensive laparoscopes and assisting staff to operate those, although it is argued a movable camera is necessary. If laparoscopes are available, the device can contribute by providing a view of the overall structure, including the target and the surrounding dissection.

To conclude, this study illustrated the potential of integrating an abdominal wall lift device and imaging system despite the substantial constraints of the current tubular design. The cost-effective alternative eliminates the reliance on carbon dioxide gas, expensive laparoscopes, general anesthesia, and untrained assisting staff. Therefore, development should continue to improve access to laparoscopic surgery worldwide.

References

[1] Andre M Naude, Chris F Heyns, and Surena F Matin. “Laparoscopic urology training in South Africa”. In: *Journal of endourology* 19.10 (2005), pp. 1180–1184.

[2] Nakul P Raykar et al. “The How Project: understanding contextual challenges to global surgical care provision in low-resource settings”. In: *BMJ Global Health* 1.4 (Dec. 2016), e000075. ISSN: 2059-7908. DOI: 10.1136/bmjgh-2016-000075.

[3] J Raiga et al. “Introduction of gynecologic endoscopic surgery in an African setting”. In: *International Journal of Gynecology & Obstetrics* 46.3 (1994), pp. 261–264.

[4] Enver Okan Hamamci et al. “Use of laparoscopic splenectomy in developing countries: analysis of cost and strategies for reducing cost”. In: *Journal of Laparoendoscopic & Advanced Surgical Techniques* 12.4 (2002), pp. 253–258.

[5] Anand G Nande et al. “Modified technique of gasless laparoscopic cholecystectomy in a developing country: a 5-year experience”. In: *Digestive Surgery* 19.5 (2002), pp. 366–372.

[6] Ian Choy et al. “Barriers to the uptake of laparoscopic surgery in a lower-middle-income country”. In: *Surgical Endoscopy* 27.11 (May 2013), pp. 4009–4015. ISSN: 1432-2218. DOI: 10.1007/s00464-013-3019-z.

[7] Guy-Bernard Cadiére, Jacques Himpens, and J Bruyns. “Laparoscopic surgery and the third world”. In: *Surgical endoscopy* 10.10 (1996), pp. 957–958.

[8] Rebekka Troller et al. “First experience in laparoscopic surgery in low and middle income countries: A systematic review”. In: *World Journal of Gastrointestinal Surgery* 16.2 (Feb. 2024), pp. 546–553. ISSN: 1948-9366. DOI: 10.4240/wjgs.v16.i2.546.

[9] M. Marriott Webb et al. “The RAIS Device for Global Surgery: Using a Participatory Design Approach to Navigate the Translational Pathway to Clinical Use”. In: *IEEE Journal of Translational Engineering in Health and Medicine* 10 (2022), pp. 1–12. ISSN: 2168-2372. DOI: 10.1109/jtehm.2022.3177313.

[10] John G Meara et al. “Global Surgery 2030: evidence and solutions for achieving health, welfare, and economic development”. In: *The Lancet* 386.9993 (Aug. 2015), pp. 569–624. ISSN: 0140-6736. DOI: 10.1016/s0140-6736(15)60160-x.

[11] W S Bolton et al. “Disseminating technology in global surgery”. In: *British Journal of Surgery* 106.2 (Jan. 2019), e34–e43. ISSN: 1365-2168. DOI: 10.1002/bjs.11036.

[12] Sheng-Hua Li et al. “Impact of gasless laparoscopy on circulation, respiration, stress response, and other complications in gynecological geriatrics”. In: *International Journal of Clinical and Experimental Medicine* 7.9 (2014), p. 2877.

[13] S Akira et al. “Gasless laparoscopically assisted myomectomy using a wound retraction system”. In: *Asian Journal of Endoscopic Surgery* 4.3 (2011), pp. 133–137.

[14] Alfredo Damiani et al. “Laparoscopic myomectomy for very large myomas using an isobaric (gasless) technique”. In: *JSLS: Journal of the Society of Laparoendoscopic Surgeons* 9.4 (2005), p. 434.

[15] Stefano Palomba et al. “New tool (Laparotenser) for gasless laparoscopic myomectomy: a multicenter-controlled study”. In: *Fertility and sterility* 94.3 (2010), pp. 1090–1096.

[16] C. N. Gutt et al. “Instruments for gasless laparoscopic surgery”. In: *Minimally Invasive Therapy & Allied Technologies* 5.3 (Jan. 1996), pp. 307–312. ISSN: 1365-2931. DOI: 10.3109/13645709609153312.

[17] V. Paolucci et al. “Gasless laparoscopy in abdominal surgery”. In: *Surgical Endoscopy* 9.5 (May 1995), pp. 497–500. ISSN: 1432-2218. DOI: 10.1007/bf00206834.

[18] J. Gnanaraj and M. Rhodes. “Laparoscopic surgery in middle- and low-income countries: gasless lift laparoscopic surgery”. In: *Surgical Endoscopy* 30.5 (Aug. 2015), pp. 2151–2154. ISSN: 1432-2218. DOI: 10.1007/s00464-015-4433-1.

[19] Anurag Mishra et al. “Evaluation of Gasless Laparoscopy as a Tool for Minimal Access Surgery in Low-to Middle-Income Countries: A Phase II Noninferiority Randomized Controlled Study”. In: *Journal of the American College of Surgeons* 231.5 (Nov. 2020), pp. 511–519. ISSN: 1072-7515. DOI: 10.1016/j.jamcollsurg.2020.07.783.

[20] Mi Kyoung Kim et al. “Gasless Total Laparoscopic Hysterectomy with New Abdominal-Wall Retraction System”. In: *JSLS: Journal of the Society of Laparoscopic & Robotic Surgeons* 24.1 (2020), e2019.00061. ISSN: 1938-3797. DOI: 10.4293/jsls.2019.00061.

[21] Ellen Wilkinson et al. “Barriers and facilitators of laparoscopic surgical training in rural north-east India: a qualitative study”. In: *IJS Global Health* 3.6 (2020), e29.

[22] Norma E. Farrow et al. “Laparoscopic experience and attitudes toward a low-cost laparoscopic system among surgeons in East, Central, and Southern Africa: a survey study”. In: *Surgical Endoscopy* 35.12 (Nov. 2020), pp. 6539–6548. ISSN: 1432-2218. DOI: 10.1007/s00464-020-08151-w.

[23] Maryam Alfa-Wali and Samuel Osaghae. “Practice, training and safety of laparoscopic surgery in low and middle-income countries”. In: *World Journal of Gastrointestinal Surgery* 9.1 (2017), p. 13. ISSN: 1948-9366. DOI: 10.4240/wjgs.v9.i1.13.

[24] N. Aruparayil et al. “Clinical effectiveness of gasless laparoscopic surgery for abdominal conditions: systematic review and meta-analysis”. In: *Surgical Endoscopy* 35.12 (Aug. 2021), pp. 6427–6437. ISSN: 1432-2218. DOI: 10.1007/s00464-021-08677-7.

[25] Martin Nyundo et al. “Assessment of resource capacity and barriers to effective practice of laparoscopic surgery in training hospitals affiliated with the College of Surgeons of East, Central and Southern Africa (COSECSA)”. In: *Surgical Endoscopy* 37.7 (Mar. 2023), pp. 5121–5128. ISSN: 1432-2218. DOI: 10.1007/s00464-023-09985-w.

[26] Tiffany E. Chao et al. “Systematic review of laparoscopic surgery in low- and middle-income countries: benefits, challenges, and strategies”. In: *Surgical Endoscopy* 30.1 (Apr. 2015), pp. 1–10. ISSN: 1432-2218. DOI: 10.1007/s00464-015-4201-2.

[27] Patrizia Berto et al. “Cost of laparoscopy and laparotomy in the surgical treatment of colorectal cancer”. In: *Surgical Endoscopy* 26.5 (Dec. 2011), pp. 1444–1453. ISSN: 1432-2218. DOI: 10.1007/s00464-011-2053-y.

[28] R.M. Oosting et al. “Roadmap for Design of Surgical Equipment for Safe Surgery Worldwide”. In: *2018 IEEE Global Humanitarian Technology Conference (GHTC)*. 2018, pp. 1–8. DOI: 10.1109/GHTC.2018.8601913.

[29] R.M. Oosting and J. Dankelman. *BME for Global Health - About*. Delft University of Technology. URL: https://www.bmeforglobalhealth.com/about.

[30] Robbert den Butter. “Improving access to laparoscopic bilateral tubal ligation in lmics: A novel lifting device with an integrated imaging system”. MA thesis. Delft University of Technology, Jan. 2024. URL: http://resolver.tudelft.nl/uuid:05113292-4aaa-4600-9fc6-09fe556fbdc8.

[31] *NCI Dictionary of Cancer Terms*. National Cancer Institute. URL: https://www.cancer.gov/publications/dictionaries/cancer-terms/def/minimally-invasive-surgery.

[32] Vijayashree Thimmaiah and VasanthaKumar Janardhana. “A Prospective, randomized, single-blind, comparative study of dexmedetomidine and propofol infusion for intraoperative hemodynamics and recovery characteristics in laparoscopic surgeries”. In: *Anesthesia: Essays and Researches* 13.3 (2019), p. 492. ISSN: 0259-1162. DOI: 10.4103/aer.aer_8_19.

[33] Kamran Mohiuddin and Scott J. Swanson. “Maximizing the benefit of minimally invasive surgery”. In: *Journal of Surgical Oncology* 108.5 (Aug. 2013), pp. 315–319. ISSN: 1096-9098. DOI: 10.1002/jso.23398.

[34] “Minimally Invasive Surgery”. In: *Endoscopy* 36.1 (Jan. 2004), pp. 48–51. ISSN: 1438-8812. DOI: 10.1055/s-2004-814113.

[35] Giorgio Gandaglia et al. “Effect of Minimally Invasive Surgery on the Risk for Surgical Site Infections: Results From the National Surgical Quality Improvement Program (NSQIP) Database”. In: *JAMA Surgery* 149.10 (Oct. 2014), p. 1039. ISSN: 2168-6254. DOI: 10.1001/jamasurg.2014.292.

[36] HJ Asbun et al. “Successfully establishing laparoscopic surgery programs in developing countries: clinical results and lessons learned”. In: *Surgical endoscopy* 10 (1996), pp. 1000–1003.

[37] BV MacFadyen et al. “Bile duct injury after laparoscopic cholecystectomy: the United States experience”. In: *Surgical endoscopy* 12 (1998), pp. 315–321.

[38] David C Wherry et al. “An external audit of laparoscopic cholecystectomy performed in medical treatment facilities of the Department of Defense”. In: *Annals of surgery* 220.5 (1994), pp. 626–634.

[39] Mee Joo Kang et al. “Establishing a Sustainable Training Program for Laparoscopy in Resource-Limited Settings: Experience in Ghana”. In: *Annals of Global Health* 86.1 (2020). ISSN: 2214-9996. DOI: 10.5334/aogh.2957.

[40] RJ Baigrie and Douglas Stupart. “Introduction of laparoscopic colorectal cancer surgery in developing nations”. In: *Journal of British Surgery* 97.5 (2010), pp. 625–627.

[41] Allan Okrainec, Lloyd Smith, and Georges Azzie. “Surgical simulation in Africa: the feasibility and impact of a 3-day fundamentals of laparoscopic surgery course”. In: *Surgical Endoscopy* 23.11 (Apr. 2009), pp. 2493–2498. ISSN: 1432-2218. DOI: 10.1007/s00464-009-0424-4.

[42] Marja-T. Mäkinen and Arvi Yli-Hankala. “The effect of laparoscopic cholecystectomy on respiratory compliance as determined by continuous spirometry”. In: *Journal of Clinical Anesthesia* 8.2 (Mar. 1996), pp. 119–122. ISSN: 0952-8180. DOI: 10.1016/0952-8180(95)00195-6.

[43] P. PELOSI et al. “Effects of carbon dioxide insufflation for laparoscopic cholecystectomy on the respiratory system”. In: *Anaesthesia* 51.8 (Aug. 1996), pp. 744–749. ISSN: 1365-2044. DOI: 10.1111/j.1365-2044.1996.tb07888.x.

[44] J. G. McLaughlin et al. “The adverse hemodynamic effects of laparoscopic cholecystectomy”. In: *Surgical Endoscopy* 9.2 (Feb. 1995), pp. 121–124. ISSN: 1432-2218. DOI: 10.1007/bf00191950.

[45] Patrick F. Leahy. “A Novel Isobaric (Gas-Less) Laparoscopic Surgery Device”. In: *Surgical Innovation* 30.6 (Sept. 2023), pp. 758–761. ISSN: 1553-3514. DOI: 10.1177/15533506231206039.

[46] Rodrigo Donalisio da Silva et al. “Significance of Surgical Plume Obstruction During Laparoscopy”. In: *JSLS: Journal of the Society of Laparoendoscopic Surgeons* 18.3 (2014), e2014.00269. ISSN: 1938-3797. DOI: 10.4293/jsls.2014.00269.

[47] Nicholas E. Power et al. “Environmental Impact of Minimally Invasive Surgery in the United States: An Estimate of the Carbon Dioxide Footprint”. In: *Journal of Endourology* 26.12 (Dec. 2012), pp. 1639–1644. ISSN: 1557-900X. DOI: 10.1089/end.2012.0298.

[48] Haitham Shoman et al. “Safety and efficiency of gasless laparoscopy: a systematic review protocol”. In: *Systematic Reviews* 9.1 (Apr. 2020). ISSN: 2046-4053. DOI: 10.1186/s13643-020-01365-y.

[49] Daniel Kruschinski. *Atlas of Lift-Laparoscopy*. May 2007. DOI: 10.3109/9780203308370.

[50] Aryaman Gupta et al. “KeyLoop: Mechanical Retraction of the Abdominal Wall for Gasless Laparoscopy”. In: *Surgical Innovation* 29.1 (July 2021), pp. 88–97. ISSN: 1553-3514. DOI: 10.1177/15533506211031084.

[51] Lovenish Bains et al. “Gasless Laparoscopic Surgery-A Technique Requiring Multidisciplinary Collaboration to Improve Equitable Access to Surgery Worldwide”. In: *Surgical Innovation* 30.1 (Dec. 2022), pp. 131–133. ISSN: 1553-3514. DOI: 10.1177/15533506221145305.

[52] Medscape. *Body fat is a better measure of obesity in midlife than BMI*. May 2024. URL: https://www.medscape.com/viewarticle/body-fat-better-measure-obesity-midlife-than-bmi-2024a10009d8.

[53] Nathaniel J. Soper, L. Michael Brunt, and Kurt Kerbl. “Laparoscopic General Surgery”. In: *New England Journal of Medicine* 330.6 (Feb. 1994), pp. 409–419. ISSN: 1533-4406. DOI: 10.1056/nejm199402103300608.

[54] Aksu Tarik and Coskun Fehmi. “Complications of gynaecological laparoscopy–a retrospective analysis of 3572 cases from a single institute”. In: *Journal of Obstetrics and Gynaecology* 24.7 (Jan. 2004), pp. 813–816. ISSN: 1364-6893. DOI: 10.1080/01443610400014857.

[55] Caroline GL Cao et al. “Hierarchical decomposition of laparoscopic procedures”. In: *Medicine meets virtual reality*. IOS Press. 1999, pp. 83–89.

[56] R Vecchio, BV MacFayden, and F Palazzo. “History of laparoscopic surgery”. In: *Panminerva medica* 42.1 (2000), pp. 87–90. ISSN: 0031-0808. URL: http://europepmc.org/abstract/MED/11019611.

[57] Kathleen Mitchell, Matthew Burrows, and Kendra Staley. *Design Drivers*. 2020. URL: https://pressbooks.pub/universityreading/chapter/reading-3-design-drivers/#footnote-82-1.

[58] Corrado Poli and C Poli. “Design for manufacturing: a structured approach”. In: Butterworth-Heinemann, 2001, pp. 1–2.

[59] Sagar Jawale, Gnanaraj Jesudian, and Prakash Agarwal. “Rigid video laparoscope: a low-cost alternative to traditional diagnostic laparoscopy and laparoscopic surgery”. In: *Mini-invasive Surgery* 2019 (June 2019). ISSN: 2574-1225. DOI: 10.20517/2574-1225.2019.12.

[60] Annemiek G.C. van Boeijen, Jaap Daalhuizen, and Jelle Zijlstra. *Delft Design Guide: Perspectives, models, approaches, methods*. English. 2nd. BIS Publishers, 2020. ISBN: 978-90-6369-540-8.

[61] W. Flynn and P. Vickerton. *Anatomy, Abdomen and Pelvis: Abdominal Wall*. StatPearls. 2023. URL: https://www.ncbi.nlm.nih.gov/books/NBK551649/.

[62] Kyleigh Kriener et al. “Mechanical Characterization of the Human Abdominal Wall Using Uniaxial Tensile Testing”. In: *Bioengineering* 10.10 (Oct. 2023), p. 1213. ISSN: 2306-5354. DOI: 10.3390/bioengineering10101213.

[63] Arati Srivastava and Ashutosh Niranjan. “Secrets of safe laparoscopic surgery: Anaesthetic and surgical considerations”. In: *Journal of Minimal Access Surgery* 6.4 (2010), p. 91. ISSN: 0972-9941. DOI: 10.4103/0972-9941.72593.

[64] Octavio Hypolito et al. “Effects of elevated artificial pneumoperitoneum pressure on invasive blood pressure and levels of blood gases”. In: *Brazilian Journal of Anesthesiology (English Edition)* 64.2 (Mar. 2014), pp. 98–104. ISSN: 0104-0014. DOI: 10.1016/j.bjane.2013.03.020.

[65] R. Stephen Smith. “Gasless Laparoscopy and Conventional Instruments: The Next Phase of Minimally Invasive Surgery”. In: *Archives of Surgery* 128.10 (Oct. 1993), p. 1102. ISSN: 0004-0010. DOI: 10.1001/archsurg.1993.01420220022003.

[66] Albert K Chin et al. “Gasless laparoscopy using a planar lifting technique.” In: *Journal of the American College of Surgeons* 178.4 (1994), pp. 401–403.

[67] H Tintara et al. “Simplified abdominal wall-lifting device for gasless laparoscopy”. In: *International Journal of Gynecology & Obstetrics* 61.2 (May 1998), pp. 165–170. ISSN: 0020-7292. DOI: 10.1016/s0020-7292(98)00023-x.

[68] William S. Bolton et al. “Gasless Laparoscopic Surgery for Minimally Invasive Surgery in Low-Resource Settings: Methods for Evaluating Surgical Field of View and Abdominal Wall Lift Force”. In: *Surgical Innovation* 28.4 (Oct. 2020), pp. 513–515. ISSN: 1553-3514. DOI: 10.1177/1553350620964331.

[69] Dassault Systèmes. *SOLIDWORKS Simulation*. Version 2023. Computer software. 2023. URL: https://www.solidworks.com/product/solidworks-simulation.

[70] R. C. Hibbeler. *Mechanics of Materials*. 10th. Pearson, 201, pp. 311–313.

[71] Oliver A Bauchau and James I Craig. “Euler-Bernoulli beam theory”. In: *Structural analysis*. Springer, 2009, pp. 173–221.

[72] Ansys Inc. *Ansys Granta EduPack*. Version 2023. Computer software. 2023. URL: https://www.grantadesign.com/education/.

[73] Alessandro U. Rebora and Gianluca Vernassa. “Transverse Circular Holes in Cylindrical Tubes Loaded in Traction and in Flexion: A New Analytical Approximation of the Stress Concentration Factor”. In: *Materials* 13.6 (Mar. 2020), p. 1331. ISSN: 1996-1944. DOI: 10.3390/ma13061331.

[74] ForceSense. *The Lapron Box Trainer*. https://lapron.net/.

[75] Tim Horeman. *Force-based assessment of tissue handling skills*. Apr. 2014, pp. 4–8. ISBN: 978-94-6186-268-6.

[76] RK Mishra. “Principle of Laparoscopic Port Position”. In: *Textbook of Practical Laparoscopic Surgery*. Jaypee Brothers Medical Publishers (P) Ltd., 2013, pp. 95–95. ISBN: 9789350259412. DOI: 10.5005/jp/books/11753_7.

[77] Zacharias Zachariou. “Ergonomics in Minimally Invasive Surgery”. In: *ESPES Manual of Pediatric Minimally Invasive Surgery*. Springer International Publishing, 2019, pp. 17–25. ISBN: 9783030009649. DOI: 10.1007/978-3-030-00964-9_2.

[78] R Tejas, Pavan Macherla, and N Shylashree. “Image sensor—CCD and CMOS”. In: *Microelectronics, Communication Systems, Machine Learning and Internet of Things: Select Proceedings of MCMI 2020*. Springer, 2022, pp. 455–484.

[79] William N Ross et al. “Imaging with organic indicators and high-speed charge-coupled device cameras in neurons: some applications where these classic techniques have advantages”. In: *Neurophotonics* 2.2 (2015), pp. 021005–021005.

[80] Robert J Gove. “CMOS image sensor technology advances for mobile devices”. In: *High Performance Silicon Imaging*. Elsevier, 2020, pp. 185–240.

[81] R.K. Mishra. *An ideal high definition endoscopic camera system*. URL: https://www.laparoscopyhospital.com/HD-Endoscopic-Camera.html.

[82] Y. Izumi, T. Kawano, and T. Iwai. “Development and clinical application of semi-loop-shaped retractor for gasless laparoscopic surgery”. In: *Surgical Endoscopy* 17.9 (Sept. 2003), pp. 1488–1493. ISSN: 1432-2218. DOI: 10.1007/s00464-002-8768-z.

[83] Ruben Bayu Kristiawan et al. “A review on the fused deposition modeling (FDM) 3D printing: Filament processing, materials, and printing parameters”. In: *Open Engineering* 11.1 (Jan. 2021), pp. 639–649. ISSN: 2391-5439. DOI: 10.1515/eng-2021-0063.

[84] Sabit Hasçelik, Ömer T. Öztürk, and Sezer Özerinç. “Mechanical Properties of Nylon Parts Produced by Fused Deposition Modeling”. In: *International Journal of Modern Manufacturing Technologies* 13.2 (Dec. 2021), pp. 34–38. ISSN: 2067-3604. DOI: 10.54684/ijmmt.2021.13.2.34.

[85] Saji Gomez et al. “Impact of Maturity Stages, Shrink-Wrap Packaging and Storage Temperature on Shelf Life and Quality of Pineapple (Ananas comosus (L.) Merr.) Fruit ‘Mauritius’”. In: *Journal of Horticultural Research* 31.1 (Jan. 2023), pp. 35–46. ISSN: 2353-3978. DOI: 10.2478/johr-2023-0021.

[86] Noam Eliaz. “Corrosion of Metallic Biomaterials: A Review”. In: *Materials* 12.3 (Jan. 2019), p. 407. ISSN: 1996-1944. DOI: 10.3390/ma12030407.

[87] Lokeswar Patnaik, Saikat Ranjan Maity, and Sunil Kumar. “Status of nickel free stainless steel in biomedical field: A review of last 10 years and what else can be done”. In: *Materials Today: Proceedings* 26 (2020), pp. 638–643. ISSN: 2214-7853. DOI: 10.1016/j.matpr.2019.12.205.

[88] A. Bardelcik. “The Effect of Element Formulation on the Prediction of Boost Effects in Numerical Tube Bending”. In: *AIP Conference Proceedings*. Vol. 778. AIP, 2005, pp. 774–780. DOI: 10.1063/1.2011316.

[89] M. Strano. “Automatic tooling design for rotary draw bending of tubes”. In: *The International Journal of Advanced Manufacturing Technology* 26.7–8 (Oct. 2005), pp. 733–740. ISSN: 1433-3015. DOI: 10.1007/s00170-003-2055-6.

[90] Ryohei Miyazaki and Sumio Hoka. “What is the predictor of the intraoperative body temperature in abdominal surgery?” In: *Journal of Anesthesia* 33.1 (Nov. 2018), pp. 67–73. ISSN: 1438-8359. DOI: 10.1007/s00540-018-2585-6.

[91] Caris E. Grimes et al. “Systematic Review of Barriers to Surgical Care in Low□Income and Middle□Income Countries”. In: *World Journal of Surgery* 35.5 (Mar. 2011), pp. 941–950. ISSN: 1432-2323. DOI: 10.1007/s00268-011-1010-1.

[92] Theodore R. Breton. “Evidence that capital formation is overestimated in low- and middle-income countries in ICP 2011”. In: *Applied Economics Letters* 23.13 (Dec. 2015), pp. 903–907. ISSN: 1466-4291. DOI: 10.1080/13504851.2015.1119784.

[93] Dilay Hacıdursunoğlu Erbaş, Hatice Azizoğlu, and Fatma Eti Aslan. “Problems Related to Cables and Connections in the Operating Room: Systematic Review and Meta-Analysis”. In: (2023).

[94] Grzegorz S. Litynski. “Mouret, Dubois, and Perissat: The Laparoscopic Breakthrough in Europe (1987-1988)”. In: *JSLS.* 3.2 (1999), pp. 163–167.

[95] Jeffrey V. Rosenfeld. “MINIMALLY INVASIVE NEUROSURGERY”. In: *Australian and New Zealand Journal of Surgery* 66.8 (Aug. 1996), pp. 553–559. ISSN: 0004-8682. DOI: 10.1111/j.1445-2197.1996.tb00808.x.

[96] Trishul Kapoor et al. “Cost Analysis and Supply Utilization of Laparoscopic Cholecystectomy”. In: *Minimally Invasive Surgery* 2018 (Dec. 2018), pp. 1–5. ISSN: 2090-1453. DOI: 10.1155/2018/7838103.

[97] Max K. H. Wong, Alva K. Y. Sit, and Timmy W. K. Au. “Minimally invasive thoracic surgery: beyond surgical access”. In: *Journal of Thoracic Disease* 10.S16 (June 2018), S1884–S1891. ISSN: 2077-6624. DOI: 10.21037/jtd.2018.05.196.

[98] Kasey Leigh Wood et al. “Access to common laparoscopic general surgical procedures: do racial disparities exist?” In: *Surgical Endoscopy* 34.3 (June 2019), pp. 1376–1386. ISSN: 1432-2218. DOI: 10.1007/s00464-019-06912-w.

[99] Jacek A. Śmigielski, Łukasz Piskorz, and Włodzimierz Koptas. “Comparison of treatment costs of laparoscopic and open surgery”. In: *Videosurgery and Other Miniinvasive Techniques* 3 (2015), pp. 437–441. ISSN: 1895-4588. DOI: 10.5114/wiitm.2015.54055.

[100] Adewale Adisa et al. “A Prospective, Observational Cost Comparison of Laparoscopic and Open Appendicectomy in Three Tertiary Hospitals in Nigeria”. In: *World Journal of Surgery* 47.12 (Oct. 2023), pp. 3042–3050. ISSN: 1432-2323. DOI: 10.1007/s00268-023-07148-5.

[101] Giselle G. Hamad and Myriam Curet. “Minimally invasive surgery”. In: *The American Journal of Surgery* 199.2 (Feb. 2010), pp. 263–265. ISSN: 0002-9610. DOI: 10.1016/j.amjsurg.2009.05.008.

[102] Ninh T. Nguyen et al. “Laparoscopic Versus Open Gastric Bypass: A Randomized Study of Outcomes, Quality of Life, and Costs”. In: *Annals of Surgery* 234.3 (Sept. 2001), pp. 279–291. ISSN: 0003-4932. DOI: 10.1097/00000658-200109000-00002.

[103] Stefan Sauerland, Thomas Jaschinski, and Edmund AM Neugebauer. “Laparoscopic versus open surgery for suspected appendicitis”. In: *Cochrane Database of Systematic Reviews* (Oct. 2010). ISSN: 1465-1858. DOI: 10.1002/14651858.cd001546.pub3.

[104] C. M. Poon et al. “Two-port versus four-port laparoscopic cholecystectomy”. In: *Surgical Endoscopy* 17.10 (Oct. 2003), pp. 1624–1627. ISSN: 1432-2218. DOI: 10.1007/s00464-002-8718-9.

[105] Gokulakkrishna Subhas et al. “Laparoscopic three-port distal pancreatectomy”. In: *HPB* 13.5 (May 2011), pp. 361–363. ISSN: 1365-182X. DOI: 10.1111/j.1477-2574.2011.00297.x.

[106] Rafael Antoniazzi Abaid, Ivan CECCONELLO, and Bruno ZILBERSTEIN. “Simplified laparoscopic cholecystectomy with two incisions”. In: *ABCD. Arquivos Brasileiros de Cirurgia Digestiva (São Paulo)* 27.2 (June 2014), pp. 154–156. ISSN: 0102-6720. DOI: 10.1590/s0102-67202014000200014.

[107] C Clay Cothren et al. “Can we afford to do laparoscopic appendectomy in an academic hospital?” In: *The American journal of surgery* 190.6 (2005), pp. 973–977.

[108] Society of American Gastrointestinal Endoscopic Surgeons (SAGES). *Guidelines for Diagnostic Laparoscopy*. Jan. 2021. URL: https://www.sages.org/publications/guidelines/guidelines-for-diagnostic-laparoscopy/.

[109] Hirotomo Nishii et al. “Laparoscopic surgery by abdominal wall lifting using original lifting bars”. In: *Surgical Laparoscopy Endoscopy & Percutaneous Techniques* 7.2 (1997), pp. 124–128.

[110] Daijo Hashimoto et al. “Laparoscopic cholecystectomy: an approach without pneumoperitoneum”. In: *Surgical Endoscopy* 7.1 (1993), pp. 54–56. ISSN: 1432-2218. DOI: 10.1007/bf00591239.

[111] Naoya Ikeda et al. “Simple technique for gasless transumbilical single-incisional laparoscopic-assisted appendectomy”. In: *Langenbeck’s Archives of Surgery* 399.3 (Jan. 2014), pp. 359–366. ISSN: 1435-2451. DOI: 10.1007/s00423-014-1164-z.

[112] L. Angelini et al. “Combination of subcutaneous abdominal wall retraction and optical trocar to minimize pneumoperitoneum-related effects and needle and trocar injuries in laparoscopic surgery”. In: *Surgical Endoscopy* 11.10 (Oct. 1997), pp. 1006–1009. ISSN: 1432-2218. DOI: 10.1007/s004649900512.

[113] Shigeo Akira et al. “Gasless laparoscopic surgery using a new intra-abdominal fan retractor system: an experience of 500 cases”. In: *Journal of Nippon Medical School* 72.4 (2005), pp. 213–216.

[114] Dong-Bo Wu et al. “Preliminary study on the application of an umbrella-like abdominal wall-lifting device in gasless laparoscopic surgery”. In: *Journal of Laparoendoscopic & Advanced Surgical Techniques* 23.3 (2013), pp. 246–249.

[115] MARCO P VIANI et al. “Gasless laparoscopic gastrostomy”. In: *Journal of Laparoendoscopic Surgery* 5.4 (1995), pp. 245–249.

[116] H. Nakamura et al. “Fishing-rod-type abdominal wall lifter for gasless laparoscopic surgery”. In: *Surgical Endoscopy* 10.9 (Sept. 1996), pp. 944–946. ISSN: 1432-2218. DOI: 10.1007/bf00188492.

[117] T. E. Udwadia et al. “Vacuum-assisted abdominal wall lift for minimal-access surgery: a porcine model study”. In: *Surgical Endoscopy* 19.8 (July 2005), pp. 1113–1119. ISSN: 1432-2218. DOI: 10.1007/s00464-004-2131-5.

[118] Tanveer Anjum Chaudhry et al. “Gender differences and delay in presentation of childhood squint”. In: *Journal of the Pakistan Medical Association* 59.4 (2009), p. 229.

[119] Furqan B. Irfan, Bismah B. Irfan, and David A. Spiegel. “Barriers to Accessing Surgical Care in Pakistan: Healthcare Barrier Model and Quantitative Systematic Review”. In: *Journal of Surgical Research* 176.1 (July 2012), pp. 84–94. ISSN: 0022-4804. DOI: 10.1016/j.jss.2011.07.046.

[120] Annie Bronsard et al. “Why are children brought late for cataract surgery? Qualitative findings from Tanzania”. In: *Ophthalmic epidemiology* 15.6 (2008), pp. 383–388.

[121] Paul A Athanasiov et al. “Cataract surgical coverage and self-reported barriers to cataract surgery in a rural Myanmar population”. In: *Clinical & experimental ophthalmology* 36.6 (2008), pp. 521–525.

[122] TS Chandrashekhar et al. “Coverage, utilization and barriers to cataract surgical services in rural South India: results from a population-based study”. In: *Public health* 121.2 (2007), pp. 130–136.

[123] Fahim Ullah, Mohammad Tahir, Muhammad Aslam, et al. “Mammalian bite injuries to the head and neck region.” In: *Journal of the College of Physicians and Surgeons–pakistan: JCPSP* 15.8 (2005), pp. 485–488.

[124] R Geneau et al. “The social and family dynamics behind the uptake of cataract surgery: findings from Kilimanjaro region, Tanzania”. In: *British journal of ophthalmology* 89.11 (2005), pp. 1399–1402.

[125] Muhammad Shahzad Shamim et al. “Pituitary adenomas: presentations and outcomes in a South Asian country”. In: *Canadian journal of neurological sciences* 35.2 (2008), pp. 198–203.

[126] Raza M Khan et al. “Vesicovaginal fistula: an experience of 30 cases at Ayub Teaching Hospital Abbottabad”. In: *Journal of Ayub Medical College Abbottabad* 17.3 (2005).

[127] George Schieber et al. “Financing health systems”. In: *Dis Cont Prior Develop Count* 3 (2006), p. 225.

[128] Mushtaq Ahmed et al. “Survey of surgical emergencies in a rural population in the Northern Areas of Pakistan”. In: *Tropical medicine & international health* 4.12 (1999), pp. 846–857.

[129] Marga Kowalewski, Phare Mujinja, and Albrecht Jahn. “Can mothers afford maternal health care costs? User costs of maternity services in rural Tanzania”. In: *African journal of reproductive health* (2002), pp. 65–73.

[130] Marquise Kouo-Ngamby et al. “A cross-sectional survey of emergency and essential surgical care capacity among hospitals with high trauma burden in a Central African country”. In: *BMC Health Services Research* 15.1 (June 2015). ISSN: 1472-6963. DOI: 10.1186/s12913-015-1147-y.

[131] T Peter Kingham et al. “Quantifying surgical capacity in Sierra Leone: a guide for improving surgical care”. In: *Archives of surgery* 144.2 (2009), pp. 122–127.

[132] Natalie Elkheir et al. “A cross-sectional survey of essential surgical capacity in Somalia”. In: *BMJ Open* 4.5 (May 2014), e004360. ISSN: 2044-6055. DOI: 10.1136/bmjopen-2013-004360.

[133] Tiffany E. Chao et al. “Survey of Surgery and Anesthesia Infrastructure in Ethiopia”. In: *World Journal of Surgery* 36.11 (Aug. 2012), pp. 2545–2553. ISSN: 1432-2323. DOI: 10.1007/s00268-012-1729-3.

[134] Sanaullah Memon et al. “Pattern of obstructed labour at a public sector university hospital of Sindh, Pakistan”. In: *Journal of the Liaquat University of Medical and Health Sciences* 8 (Jan. 2009), pp. 60–64.

[135] Jaymie Ang Henry et al. “Surgical and anaesthetic capacity of hospitals in Malawi: key insights”. In: *Health Policy and Planning* 30.8 (Sept. 2014), pp. 985–994. ISSN: 1460-2237. DOI: 10.1093/heapol/czu102.

[136] Rele Ologunde et al. “Surgical care in low and middle-income countries: Burden and barriers”. In: *International Journal of Surgery* 12.8 (Aug. 2014), pp. 858–863. ISSN: 1743-9191. DOI: 10.1016/j.ijsu.2014.07.009.

[137] Bernd Rechel et al. “Organization and financing of public health services in Europe: country reports”. In: (2018).

[138] Laura K. Muldoon, William E. Hogg, and Miriam Levitt. “Primary Care (PC) and Primary Health Care (PHC): What is the Difference?” In: *Canadian Journal of Public Health* 97.5 (Sept. 2006), pp. 409–411. ISSN: 1920-7476. DOI: 10.1007/bf03405354.

[139] NHS England. *The healthcare ecosystem*. URL: https://digital.nhs.uk/developer/guides-and-documentation/introduction-to-healthcare-technology/the-healthcare-ecosystem.

[140] AbdulrahmanS Al-Mulhim and TarekT Amin. “Outcome of laparoscopic cholecystectomy at a secondary level of care in Saudi Arabia”. In: *Saudi Journal of Gastroenterology* 17.1 (2011), p. 47. ISSN: 1319-3767. DOI: 10.4103/1319-3767.74484.

[141] Chandrakant Lahariya. “Health & Wellness Centers to Strengthen Primary Health Care in India: Concept, Progress and Ways Forward”. In: *The Indian Journal of Pediatrics* 87.11 (July 2020), pp. 916–929. ISSN: 0973-7693. DOI: 10.1007/s12098-020-03359-z.

[142] Satish Rudrappa, Deepak Venkatesh Agarkhed, and Sushrut S. Vaidya. “Healthcare Systems: India”. In: *Quality Spine Care*. Springer International Publishing, Oct. 2018, pp. 211–224. ISBN: 9783319979908. DOI: 10.1007/978-3-319-97990-8_13.

[143] Herbert B. Peterson. “Sterilization”. In: *Obstetrics & Gynecology* 111.1 (Jan. 2008), pp. 189–203. ISSN: 0029-7844. DOI: 10.1097/01.aog.0000298621.98372.62.

[144] L. Silvia Munoz-Price et al. “Infection prevention in the operating room anesthesia work area”. In: *Infection Control & Hospital Epidemiology* 40.1 (Dec. 2018), pp. 1–17. ISSN: 1559-6834. DOI: 10.1017/ice.2018.303.

[145] Alexander Cuncannon, Aliyah Dosani, and Olive Fast. “Sterile processing in low- and middle-income countries: an integrative review”. In: *Journal of Infection Prevention* 22.1 (Aug. 2020), pp. 28–38. ISSN: 1757-1782. DOI: 10.1177/1757177420947468.

[146] Olive Fast et al. “Limited sterile processing capabilities for safe surgery in low-income and middle-income countries: experience in the Republic of Congo, Madagascar and Benin”. In: *BMJ Global Health* 2.Suppl 4 (Sept. 2017), e000428. ISSN: 2059-7908. DOI: 10.1136/bmjgh-2017-000428.

[147] “Report on the burden of endemic health care-associated infection worldwide”. In: *Secondary report on the burden of endemic health care-associated infection worldwide* (2011). URL: https://apps.who.int/iris/bitstream/handle/10665/80135/9789241501507_eng.pdf;jsessionid=3EF49BB2FE66B25701CB266FAE049A3B?sequence=1.

[148] Daniel Robertson et al. “Assessment of laparoscopic instrument reprocessing in rural India: a mixed methods study”. In: *Antimicrobial Resistance & Infection Control* 10.1 (July 2021). ISSN: 2047-2994. DOI: 10.1186/s13756-021-00976-x.

[149] Gopal Panta et al. “Compliance of primary and secondary care public hospitals with standard practices for reprocessing and steam sterilization of reusable medical devices in Nepal: findings from nation-wide multicenter clustered audits”. In: *BMC Health Services Research* 20.1 (Oct. 2020). ISSN: 1472-6963. DOI: 10.1186/s12913-020-05788-0.

[150] Rose Seavey. “The need for educated staff in sterile processing—patient safety depends on it”. In: *Perioperative Nursing Clinics* 4.2 (2009), pp. 181–192.

[151] Olive Fast et al. “Mixed methods evaluation of the impact of a short term training program on sterile processing knowledge, practice, and attitude in three hospitals in Benin”. In: *Antimicrobial Resistance & Infection Control* 7.1 (Feb. 2018). ISSN: 2047-2994. DOI: 10.1186/s13756-018-0312-6.

[152] Valentina Nino et al. “An Enhanced Kaizen Event in a Sterile Processing Department of a Rural Hospital: A Case Study”. In: *International Journal of Environmental Research and Public Health* 17.23 (Nov. 2020), p. 8748. ISSN: 1660-4601. DOI: 10.3390/ijerph17238748.

[153] James T Walker. *Decontamination in hospitals and healthcare*. Woodhead Publishing, 2019.

[154] R. Malkin. *Medical Instrumentation in the Developing World*. Engineering World Health, 2006. ISBN: 9780978556907. URL: https://books.google.nl/books?id=ezgOnwEACAAJ.

[155] Beverly D. Bradley et al. “A retrospective analysis of oxygen concentrator maintenance needs and costs in a low-resource setting: experience from The Gambia”. In: *Health and Technology* 4.4 (Feb. 2015), pp. 319–328. ISSN: 2190-7196. DOI: 10.1007/s12553-015-0094-2.

[156] RM Oosting et al. “Equipment for essential surgical care in 9 countries across Africa: availability, barriers and need for novel design”. In: *Health and Technology* 9 (2019), pp. 269–275.

[157] Robert A. Malkin. “Design of Health Care Technologies for the Developing World”. In: *Annual Review of Biomedical Engineering* 9.1 (Aug. 2007), pp. 567–587. ISSN: 1545-4274. DOI: 10.1146/annurev.bioeng.9.060906.151913.

[158] M Ogembo-Kachieng’a and WO Ogara. “Strategic management of technology in public health sector in Kenya and South Africa”. In: *East African Medical Journal* 81.6 (Oct. 2004). ISSN: 0012-835X. DOI: 10.4314/eamj.v81i6.9176.

[159] Michelle R. Notrica et al. “Rwandan Surgical and Anesthesia Infrastructure: A Survey of District Hospitals”. In: *World Journal of Surgery* 35.8 (May 2011), pp. 1770–1780. ISSN: 1432-2323. DOI: 10.1007/s00268-011-1125-4.

[160] David A. Spiegel et al. “Quantifying Surgical and Anesthetic Availability at Primary Health Facilities in Mongolia”. In: *World Journal of Surgery* 35.2 (Dec. 2010), pp. 272–279. ISSN: 1432-2323. DOI: 10.1007/s00268-010-0904-7.

[161] Reinou S. Groen et al. “A Tool and Index to Assess Surgical Capacity in Low Income Countries: An Initial Implementation in Sierra Leone”. In: *World Journal of Surgery* 36.8 (Apr. 2012), pp. 1970–1977. ISSN: 1432-2323. DOI: 10.1007/s00268-012-1591-3.

[162] Jaymie A. Henry et al. “A Survey of Surgical Capacity in Rural Southern Nigeria: Opportunities for Change”. In: *World Journal of Surgery* 36.12 (Sept. 2012), pp. 2811–2818. ISSN: 1432-2323. DOI: 10.1007/s00268-012-1764-0.

[163] Staffan Bergström et al. “Workforce Innovations to Expand the Capacity for Surgical Services”. In: *Disease Control Priorities, Third Edition (Volume 1): Essential Surgery*. The World Bank, Mar. 2015, pp. 307–316. DOI: 10.1596/978-1-4648-0346-8_ch17.

[164] Mekam T. Okoye et al. “A Pilot Survey of Pediatric Surgical Capacity in West Africa”. In: *World Journal of Surgery* 39.3 (Dec. 2014), pp. 669–676. ISSN: 1432-2323. DOI: 10.1007/s00268-014-2868-5.

[165] Dane Emmerling, Alexander Dahinten, and Robert A. Malkin. “Problems with systems of medical equipment provision: an evaluation in Honduras, Rwanda and Cambodia identifies opportunities to strengthen healthcare systems”. In: *Health and Technology* 8.1–2 (Nov. 2017), pp. 129–135. ISSN: 2190-7196. DOI: 10.1007/s12553-017-0210-6.

[166] R. Neighbour and R. Eltringham. “The design of medical equipment for low income countries: dual standards or common sense”. In: *7th International Conference on Appropriate Healthcare Technologies for Developing Countries*. Institution of Engineering and Technology, 2012. DOI: 10.1049/cp.2012.1462.

[167] Robert Malkin and Kim von Oldenburg Beer. “Diffusion of Novel Healthcare Technologies to Resource Poor Settings”. In: *Annals of Biomedical Engineering* 41.9 (Feb. 2013), pp. 1841–1850. ISSN: 1573-9686. DOI: 10.1007/s10439-013-0750-5.

[168] Adam L. Kushner. “Addressing the Millennium Development Goals From a Surgical Perspective: Essential Surgery and Anesthesia in 8 Low- and Middle-Income Countries”. In: *Archives of Surgery* 145.2 (Feb. 2010), p. 154. ISSN: 0004-0010. DOI: 10.1001/archsurg.2009.263.

[169] Breedveld Wentink. “Eye-hand coordination in laparoscopy - an overview of experiments and supporting aids”. In: *Minimally Invasive Therapy & Allied Technologies* 10.3 (Jan. 2001), pp. 155–162. ISSN: 1365-2931. DOI: 10.1080/136457001753192277.

[170] Paul Breedveld, Ton van Lunteren, and Henk G. Stassen. “Improvement of Depth Perception and Eye-Hand Coordination in Laparoscopic Surgery 1”. In: *IFAC Proceedings Volumes* 31.26 (Sept. 1998), pp. 449–454. ISSN: 1474-6670. DOI: 10.1016/s1474-6670(17)40134-0.

[171] Susumu Miura et al. “Optimal monitor positioning and camera rotation angle for mirror image: overcoming reverse alignment during laparoscopic colorectal surgery”. In: *Scientific Reports* 9.1 (June 2019). ISSN: 2045-2322. DOI: 10.1038/s41598-019-44939-0.

[172] William CS Meng et al. “Optimal position of working ports in laparoscopic surgery: an in vitro study”. In: *Surgical Laparoscopy Endoscopy & Percutaneous Techniques* 6.4 (1996), pp. 278–281.

[173] Marelyn Medina. “Image rotation and reversal-major obstacles in learning intracorporeal suturing and knot-tying”. In: *JSLS: Journal of the Society of Laparoendoscopic Surgeons* 1.4 (1997), p. 331.

[174] George B Hanna, Sami M Shimi, and Alfred Cuschieri. “Task performance in endoscopic surgery is influenced by location of the image display”. In: *Annals of surgery* 227.4 (1998), pp. 481–484.

[175] Liam A. Haveran et al. “Optimizing laparoscopic task efficiency: the role of camera and monitor positions”. In: *Surgical Endoscopy* 21.6 (Apr. 2007), pp. 980–984. ISSN: 1432-2218. DOI: 10.1007/s00464-007-9360-3.

[176] Paul Breedveld et al. “Manipulation in Laparoscopic Surgery: Overview of Impeding Effects and Supporting Aids”. In: *Journal of Laparoendoscopic & Advanced Surgical Techniques* 9.6 (Dec. 1999), pp. 469–480. ISSN: 1557-9034. DOI: 10.1089/lap.1999.9.469.

[177] R. Berguer et al. “A comparison of surgeons’ posture during laparoscopic and open surgical procedures”. In: *Surgical Endoscopy* 11.2 (Feb. 1997), pp. 139–142. ISSN: 1432-2218. DOI: 10.1007/s004649900316.

[178] MR Treat et al. “A surgeon’s perspective on the difficulties of laparoscopic surgery”. In: *Computer Integrated Surgery: Technology and Clinical Applications* 42 (1996), pp. 559–560.

[179] F Tendick et al. “Perception and manipulation problems in endoscopic surgery”. In: *Computer-integrated surgery: technology and clinical applications. MIT Press, Cambridge, Massachusetts* (1996), pp. 567–576.

[180] J. Danis. “Theoretical basis for camera control in teleoperating”. In: *Surgical Endoscopy* 10.8 (Aug. 1996), pp. 804–808. ISSN: 1432-2218. DOI: 10.1007/bf00189538.

[181] J. K. Champion et al. “Teaching basic video skills as an aid in laparoscopic suturing”. In: *Surgical Endoscopy* 10.1 (Jan. 1996), pp. 23–25. ISSN: 1432-2218. DOI: 10.1007/s004649910004.

[182] Jiabin Zheng, Junjiang Wang, and Yong Li. “I am your eyes—the reflection of being a camera-holder in laparoscopic gastrointestinal surgery”. In: *Annals of Laparoscopic and Endoscopic Surgery* 2 (Apr. 2017), pp. 62–62. ISSN: 2518-6973. DOI: 10.21037/ales.2017.02.23.

[183] M. O. Schurr et al. “Human sense of vision: A guide to future endoscopic imaging systems”. In: *Minimally Invasive Therapy & Allied Technologies* 5.5 (Jan. 1996), pp. 410–418. ISSN: 1365-2931. DOI: 10.3109/13645709609153702.

[184] E Schippers and V Schumpelick. “Requirements and possibilities of computer-assisted endoscope surgery”. In: *Computer Integrated Surgery: Technology and Clinical Applications* 42 (1996), pp. 561–566.

[185] A. Cuschieri. “Visual display technology for endoscopic surgery”. In: *Minimally Invasive Therapy & Allied Technologies* 5.5 (Jan. 1996), pp. 427–434. ISSN: 1365-2931. DOI: 10.3109/13645709609153704.

[186] T.B. Sheridan. “Human factors in telesurgery”. In: *Computer-Integrated Surgery* (1996), pp. 223–230.

[187] PAUL BREEDVELD et al. “Observation in Laparoscopic Surgery: Overview of Impeding Effects and Supporting Aids”. In: *Journal of Laparoendoscopic & Advanced Surgical Techniques* 10.5 (Oct. 2000), pp. 231–241. ISSN: 1557-9034. DOI: 10.1089/lap.2000.10.231.

[188] James J. Gibson. *The Ecological Approach to Visual Perception: Classic Edition*. Psychology Press, Nov. 2014. ISBN: 9781315740218. DOI: 10.4324/9781315740218.

[189] David Regan, Kenneth Beverley, and Max Cynader. “The Visual Perception of Motion in Depth”. In: *Scientific American* 241.1 (July 1979), pp. 136–151. ISSN: 0036-8733. DOI: 10.1038/scientificamerican0779-136.

[190] Fred Anton Voorhorst. “Affording action: Implementing perception-action coupling for endoscopy. [PhD thesis: ISBN 90-9011715-6]”. In: *Delft University of Technology, Faculty of Design, Engineering and Production.* (1998).

[191] Continiummechanics.org. *Beam Bending*. 2017. URL: https://www.continuummechanics.org/beambending.html.

[192] Xiang Yun, Zhongxing Wang, and Leroy Gardner. “Full-range stress–strain curves for aluminum alloys”. In: *Journal of Structural Engineering* 147.6 (2021), p. 04021060.

A

Laparoscopic Surgery

This appendix describes laparoscopic surgery starting with conventional laparosopy with CO_2 pneumoperitoneum. The following section describes abdominal wall lift devices.

A.1. Conventional Laparoscopy

Minimally invasive surgery (MIS) is done using small incisions and few stitches [31], which offers several advantages over open surgical procedures, such as decreased postoperative pain, faster recovery times, fewer operative and postoperative major complications, less scarring, a shorter hospital stay, and less stress on the immune system [33, 34, 35]. Since its first performance in 1987 [94], MIS has fundamentally reformed surgical practices in numerous medical fields, such as neurosurgery, laparoscopic surgery, gynecological surgery, orthopedic surgery, and thoracic surgery [95, 96, 97].

Laparoscopy is a form of MIS that is performed in the abdomen or pelvis regions with the use of small incisions of around $5\text{-}15\,\mathrm{mm}$ [32]. It is quickly becoming the standard of care for many routine operations in the abdominopelvic cavity [98]. Open surgery, however, is slightly quicker, cheaper, and requires less skill of the surgeon [99, 100]. Moreover, laparoscopic surgery leads to a prolonged learning curve for most surgeons as it is a more challenging technique than open surgery [101]. Unlike the $200\,\mathrm{mm}$ midline incision required for open laparotomy [102, 103], four or fewer small keyhole incisions of $10\,\mathrm{mm}$ are sufficient for laparoscopic procedures [104, 105, 106], as shown in Figure A.1.

Figure A.1: A conventional laparoscopic procedure with four keyhole incisions. The abdomen is inflated, and three laparoscopic instruments and a laparoscope are inserted through the abdominal wall.

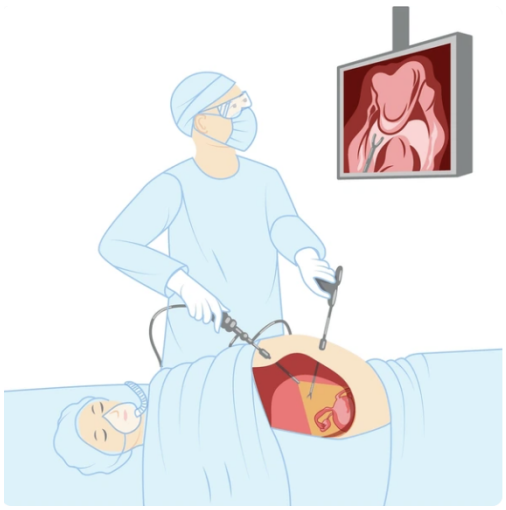

Figure A.2: Illustration of a surgical procedure where the surgeon operates both the laparoscope and instrument.

The preparation of conventional laparoscopic surgery follows the same four steps for all types of procedures. Figure A.2 shows a typical surgeon's position after preparation.

1. Patients are positioned on the surgical table in the Trendelenburg position, lying supine with their head lowered below their feet at a slight angle. They are then placed under general anesthesia and are intubated.
2. A Veress needle, with a typical $2\,\mathrm{mm}$ diameter, is then inserted through the abdominal wall. Carbon dioxide gas is introduced via the needle to inflate the abdominopelvic cavity to approcimately $15\,\mathrm{mmHg}$. Operational volume is created by pushing the abdominall wall away from the organs. The so called pneumoperitoneum is the surgeon's working space.
3. The surgeon makes two to four small incisions, starting with the primary incision or supraumbilical port near the umbilicus. Gas-tight trocars with inner diameters between $5\,\mathrm{mm}$ to $10\,\mathrm{mm}$ are placed in the incisions.
4. The laparoscope, featuring a camera and light source at the tip of a $10\,\mathrm{mm}$ tube, is inserted through the primary incision. High-quality images are displayed on a monitor, enabling the surgeon to place other ports and insert laparoscopic instruments for the procedure under vision of the laparoscope.

Laparoscopic instruments like graspers, scissors, staplers, suction-irrigation devices and electrocautery devices have long 5-$10\,\mathrm{mm}$ shafts and miniaturized tips to fit the trocar. The instruments are specifically designed for laparoscopic surgery and their complexity makes them expensive even by HIC's standards [107].

The surgeon operates these instruments through the trocars while viewing the magnified laparoscope images on the monitor. Once the procedure is complete, any excised tissue or organs can be extracted through the trocars. The instruments are ejected, the carbon dioxide is released, and the trocars are removed. Adhesive strips, clips or sutures are used to close the incisions.

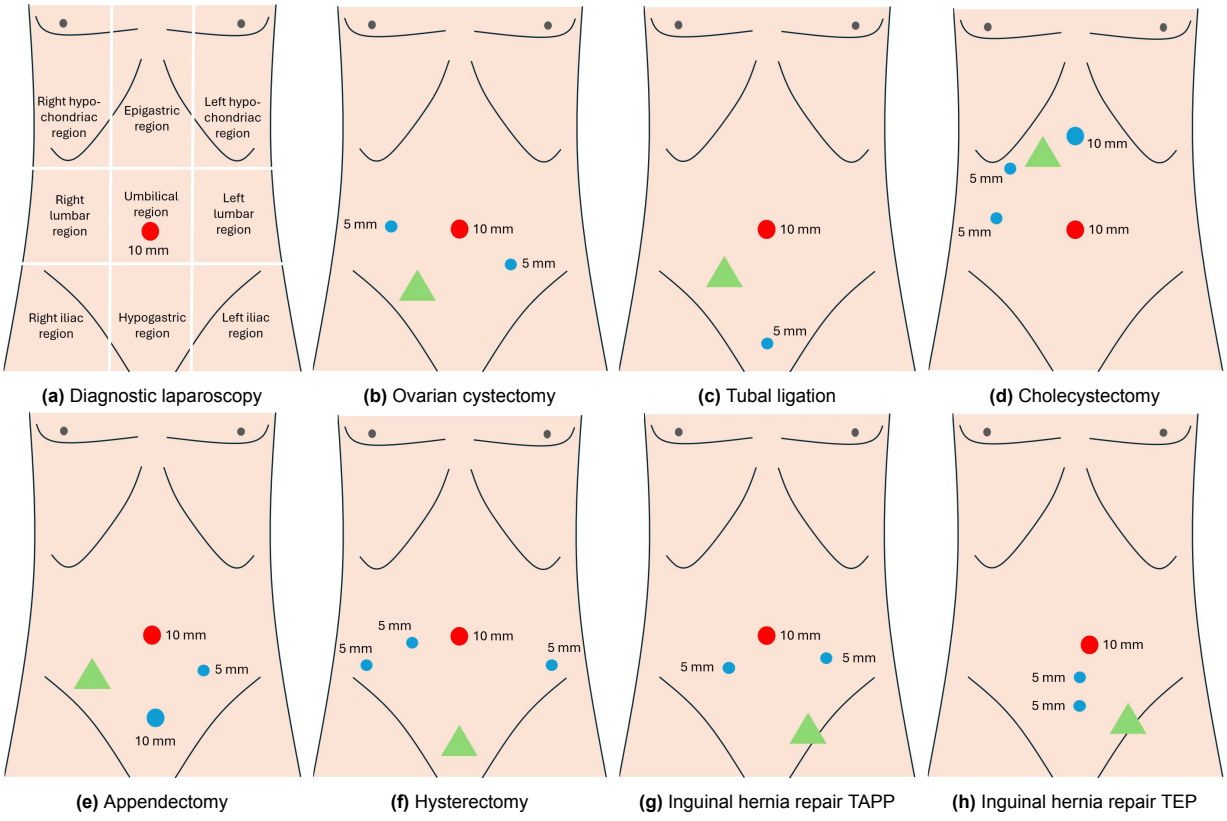

Figure A.3: Typical port placement for the most common laparoscopic procedures. The abdominal regions are depicted in sub-figure a. The red dot is the port for the laparoscope, the blue dots are ports for instruments, and the green triangle is the target location.

Common laparoscopic procedures are diagnostic laparoscopy, ovarian cystectomy, tubal ligation, cholecystectomy, appendectomy, hysterectomy, and inguinal hernia repair [53, 54, 55, 56]. The placement of the trocars highly depends on the type of procedure, the patient's anatomy, and the surgeon's preference. Figure A.3 shows typical port placements for the most common laparoscopic procedures. In diagnostic laparoscopy, only one port is placed; usually, an umbilical port is recommended for optimal visualization of the entire abdominal cavity [108]. The umbilical port is used for the laparoscope in most procedures.

In ovarian cystectomy (ovarian cyst removal), two additional $5\,\mathrm{mm}$ ports for instruments are placed in the left or right lumbar region and the opposite iliac region, depending on the ovary. Only one $5\,\mathrm{mm}$ instrument port in the hypogastric region is used for tubal ligation (tying of fallopian tubes). For cholecystectomy (gall bladder removal), a $10\,\mathrm{mm}$ port is placed in the epigastric region, and two $5\,\mathrm{mm}$ ports are placed in the right lumbar region. Appendectomy (appendix removal) makes use of a $10\,\mathrm{mm}$ port in the hypogastric region and a $5\,\mathrm{mm}$ port in the left iliac region. Two $5\,\mathrm{mm}$ ports are placed in the right lumbar region and one in the left lumbar region for hysterectomy (uturus removal). Laparoscopic inguinal hernia repair can be performed using two main techniques: the Transabdominal Preperitoneal (TAPP) approach and the Totally Extraperitoneal (TEP) approach. TAPP makes use of two $5\,\mathrm{mm}$ ports in the left and right lumbar regions and TEP of two $5\,\mathrm{mm}$ ports in the hypogastric region.

A.2. Abdominal-Wall Lift Devices

In Gas Insufflation-Less Laparoscopic Surgery (GILLS), an abdominal-wall lift (AWL) device raises the abdominal wall to create operative space [9]. This method offers several benefits over conventional laparoscopy [12, 13]. The preparation of GILLS generally follows the same steps as conventional laparoscopy, but there is no need for general anesthesia, carbon dioxide gas, and gas-tight trocars. Since research began in 1991 [48], numerous AWL device iterations have been developed and tested, described in four categories in this section.

Loop-Shaped AWL Devices

Loop-shaped AWL devices are the current state-of-the-art (Figure A.4). These devices require a single incision, have no moving parts, and are easily mounted on retractor arms. Since the Abdo-Lift, "tenting" - where lifting is localized near the device, restricting visibility and causing high tissue tension - has been significantly reduced [49]. These devices were optimized for low-resource settings, and recent designs like the Keyloop [50], RAIS [9], and STAAN [51] were successfully tested in LMICs.

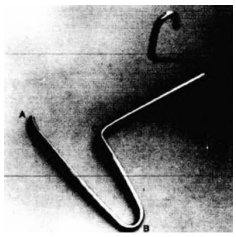

(a) Nishii et al. (2007) [109]

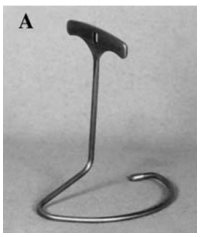

(b) Izumi et al. (2003) [82]

(c) Kruschinski et al. (2007) [49]

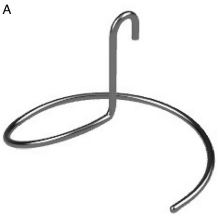

(d) Gupta et al. (2022) [50]

(e) Webb et al. (2022) [9]

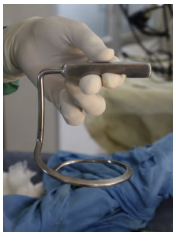

(f) Bains et al. (2022) [51]

Figure A.4: Loop-shaped AWL devices

Wire-Based AWL Devices

Wire-based AWL devices, first developed in Japan in 1993, lift the abdominal wall through wires inserted via abdominal incisions (Figure A.5a). These early designs faced challenges such as interference with the surgeon's workspace and setup complexity [110]. Later designs, including single-wire and multi-wire systems, emerged in 2014 but shared limitations like tenting (Figure A.5b) [111].

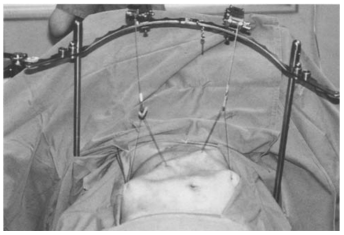

(a) Hashimoto et al. (1993) [110]

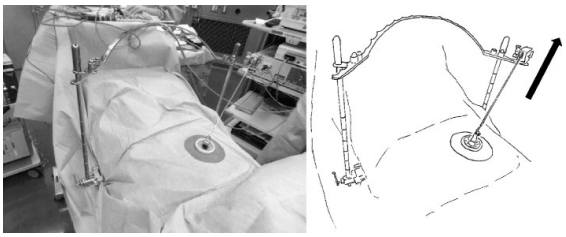

(b) Ikeda et al. (2014) [111]

Figure A.5: Wire based AWL devices

Mechanical AWL Devices

Introduced shortly after wire-based devices, mechanical AWL devices use expandable legs to hook and lift the abdominal wall. Early designs involved 2–3 legs expanding inside the abdomen (Figure A.6a and 2.5b) [112, 113]. In 2013, more sophisticated devices were introduced with up to 8 legs, enhancing usability but at a higher cost and reduced comfort (Figure A.6c) [114].

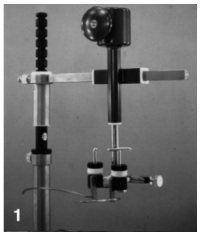

(a) Angelini et al. (1997) [112]

(b) Akira et al. (2005) [113]

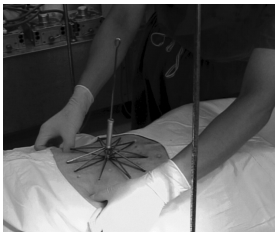

(c) Wu et al. (2013) [114]

Figure A.6: Mechanical based AWL devices

Alternative AWL Devices

Alternative designs include inflatable balloons that lift the wall from the inside but suffer from tenting (Figure A.7a) [115]. A device with side-lifting rods provides dome-shaped spaces (Figure A.7b) [116]. However, the setup is complex, and extra incisions are required. Lastly, a device with external suction lifts the abdomen without incisions in the abdominal wall (Figure A.7c), but was never tested on human patients [117].

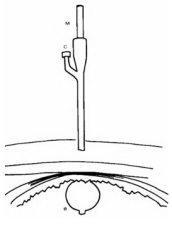

(a) Viani et al. (1995) [115]

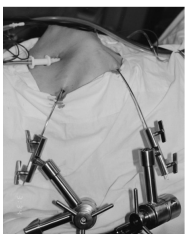

(b) Nakamura et al. (1996) [116]

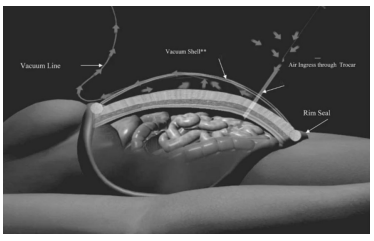

(c) Uswadia et al. (2005) [117]

Figure A.7: Alternative AWL devices

B

Context in LMICs

Functioning surgical equipment requires a good understanding of the context [28]. Surgical barriers, the structure of the health care system, and aspects of safe surgery should be researched. Nine contextual factors were identified: (A) hospital and surgery types, (B) availability of equipment, (C) procurement, (D) infrastructure (water, electricity, etc.), (E) team composition and training, (F) maintenance, (G) sterilization, (H) storage, and (I) daily usage.

Barriers to surgical care access

Cultural barriers

Patients in LMICs face barriers such as poor disease awareness, socioeconomic status, societal norms, and illiteracy, leading to delayed or incomplete treatment [91, 118, 119]. Fear of disease, surgery, anesthesia, and fatalistic or religious beliefs worsen these delays [120, 121, 122]. Social stigma, lack of support, and reliance on alternative medicine further deter care-seeking [123, 124, 125]. Socioeconomic and class disparities also impact access [91, 126]. (*Contextual factor A*)

Financial barriers

Financial constraints are a major obstacle, encompassing direct costs (fees, drugs, tests) and indirect costs (lost income, transport) [91, 120]. Most patients in LMICs pay out-of-pocket, often delaying care until funds are raised or opting for local healers [127, 128, 129]. Time costs frequently exceed direct expenses [129]. (*Contextual factor C*)

Structural barriers

Structural issues include limited infrastructure, staff, and supplies, particularly at district hospitals [130, 131, 132]. Patients often travel long distances for care, hindered by poor referral systems and inadequate hospital distribution [133, 134]. Shortages of specialists and equipment result in long waiting times and delays, with poor communication across healthcare levels worsening outcomes [135, 136]. (*Contextual factor D*)

Healthcare system structure

Healthcare is generally divided into primary, secondary, and tertiary levels. Primary care covers basic services like chronic condition management and referrals, while secondary care includes specialized consultations and surgeries. Tertiary care offers advanced procedures like organ transplants and intensive care [137, 138, 139].

Laparoscopic surgeries may be secondary or tertiary, depending on complexity [140]. Healthcare systems differ by country: in Cameroon, hospitals range from district (primary) to general (tertiary) [130]. In Malawi, central hospitals form the tertiary level, with mission hospitals filling gaps [135]. India's public system focuses on rural primary healthcare centers, while the private sector dominates urban secondary and tertiary care [141, 142]. Design of surgical equipment must consider varying hospital types and resource availability worldwide [28]. (*Contextual factor A*)

Aspects of Safe Surgery

Safe surgery requires complex processes (anesthesia, sterilization, maintenance), experienced teams, equipment, and infrastructure [28]. These aspects are outlined and compared to LMIC conditions.

Operating Theatre Processes

Safe surgery depends on processes beyond the procedure itself. Anesthesia must be administered, and a sterile processing department (SPD) ensures sterile equipment. Reliable supply chains, regular maintenance, and proper storage are essential [28, 143, 144]. (*Contextual factor H*)

Sterile processing practices vary worldwide [145]. LMICs face higher surgical site infection rates (1.2%-70%) than HICs (1.2%-5.2%) [146, 147]. Poor compliance with WHO sterile processing guidelines in LMICs is common, with inadequate equipment, quality monitoring, and workflow [145, 146, 148, 149]. Low education levels among SP staff worsen these issues [149]. Training is critical [150]. Inexpensive measures, like proper detergents, workflows separating dirty and clean areas, and the three-bucket system, improve outcomes [151, 152]. Adhering to guidelines ensures quality device reprocessing [153]. (*Contextual factor E & G*)

Planned maintenance (e.g., replacing filters, calibrations) and repairs are essential [154]. Maintenance options include service contracts or in-house technicians (BMETs) [155]. In nine African countries, 68% of facilities had in-house maintenance, 36% had service contracts, and 10% lacked maintenance access [156]. Main barriers include spare parts availability and technical expertise [157, 158]. (*Contextual factor F*)

Anesthesia complications are major causes of surgical deaths in Rwandan district hospitals [159]. Limited anesthesia services and machine availability hinder safety [135, 160]. Many machines remain unused due to insufficient training and repairs [159]. Staff shortages further increase this challenge. (*Contextual factor B*)

Team

Surgical teams include surgeons, anesthesiologists, nurses, and sometimes gynecologists [133, 161]. The primary limitation in LMICs is workforce shortages [162, 132]. Sub-Saharan Africa has less than 1% of U.S. surgeons for a population three times larger [163]. Training programs have increased physician numbers but often lack incentives for surgeons and anesthesiologists [133]. Rapidly increasing numbers of medical students strain educational quality. LMICs often rely on general doctors or non-physician staff for surgery and anesthesia, limiting procedure safety and complexity [164, 130, 160]. (*Contextual factor E*)

Surgical Equipment

Basic surgical tools are essential, while specialized equipment varies by procedure. Equipment is acquired through donations, purchases, or leasing [165]. Donations often overlook maintenance costs and remain underutilized [28]. Leasing ensures better equipment functionality [165]. WHO guidelines provide a framework for device safety but often ignore LMIC-specific challenges like tropical climates and low resources [166, 167]. (*Contextual factor B & I*)

Many LMIC facilities report supply shortages, including basic tools and advanced equipment like monitors and oxygen sources [164, 160]. Supply issues force hospitals to limit procedures, compromising patient safety [135]. (*Contextual factor C*)

Infrastructure

Electricity and clean water are critical for safe surgery. Many LMIC hospitals face intermittent electricity and water shortages, compromising sterilization and equipment use [133, 162, 160]. Backup generators are common, but not universal [135]. High temperatures and humidity in LMICs can damage equipment [166]. Infrastructure is often better in private missionary hospitals than in district hospitals, which frequently lack basic amenities [168, 130]. Delivery challenges in remote regions further stress the need for durable equipment [166]. (*Contextual factor D*)

C

Camera Postion Analysis

C.1. Impaired eye-hand coordination

During laparoscopic surgery, the surgeon processes a monitor's camera feed to guide hand movements. The visual and motor cortices process spatial information to control the instruments, but the indirect visualization introduces challenges in coordination [169].

Key issues include camera misalignment and instrument misorientation. Unlike open surgery, where surgeons observe their hands and instruments directly, laparoscopic surgeons rely solely on the monitor, losing simultaneous hand and operative field visibility. A rotated laparoscopic camera view worsens the misorientation, requiring surgeons to adjust hand movements mentally to compensate for it. Extensive training is necessary to overcome the effects [170].

Optimal setups place the monitor in front of the surgeon and align the camera with their line of sight, enabling smoother coordination [171, 172, 173, 174, 175]. The optimal range is within L$60°$ to R$60°$ (Figure C.1).

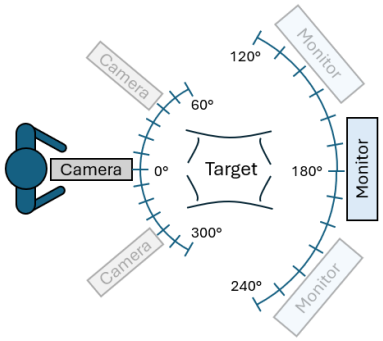

Figure C.1: Monitor and camera angle compared to surgeon's line of sight 0° [175].

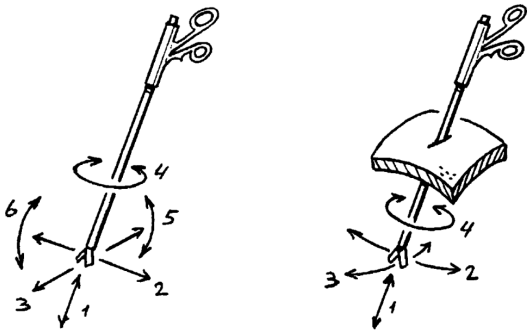

Figure C.2: Degrees of freedom of instruments when freely movable vs. inserted through the abdominal wall [176].

Effects of the Incision Point

The incision point restricts instrument tip movements and reduces degrees of freedom (DOF) from six to four (Figure C.2), forcing awkward hand positions and increasing fatigue [177]. This limitation complicates observing structures from multiple sides and mirrors hand movements as the tip moves oppositely to the hand. Forces are also scaled and mirrored, complicating tactile feedback [178, 179].

Friction between instrument shafts and airtight trocars further hinders movement. In GILLS, friction is reduced by simpler valveless trocars, improving ease of longitudinal motion [16].

Impeding Observation Effects

During laparoscopic surgery, surgeons often depend on camera assistants to adjust the laparoscope [180]. This indirect adjustment can cause communication issues, unstable images, and visual fatigue [181, 182]. Magnified views enhance detail but limit the field of view, making it harder to identify structures and increasing the risk of unseen injuries from off-screen instruments [183]. Typically, camera operators opt for a clear visual to gain a deeper understanding of the entire structure, encompassing the target and the surrounding dissection [182].

Camera and monitor quality (resolution, contrast, illumination) significantly affect task performance [184, 185, 186]. Dirt or vapor on the lens often interrupts procedures. However, preheating the laparoscope can reduce vapor buildup [187].

Depth Perception Challenges

One major challenge in determining spatial information during laparoscopic surgery is perceiving distances and movements perpendicular to the image on the retina [187]. Depth perception relies on three key sources: pictorial information, parallax, and visuomotor cues [188, 189, 185].

Pictorial information includes visual cues in the image that suggest spatial relationships, such as overlapping objects indicating relative distance or an object touching its shadow on a surface [186].

Parallax involves changes in the relative positions of objects when the observer's viewpoint shifts. It includes two types: stereovision, where images from the left and right eyes differ due to their separation, and movement parallax, where shifts occur when the observer's head moves. In laparoscopic surgery, motion parallax can also result from camera movement but is limited by the constrained movement of the laparoscope [185].

Visuomotor cues involve eye and lens adjustments, including convergence (eyes turning inward to focus on an object) and accommodation (lens adjustments to sharpen focus). However, these cues are ineffective in laparoscopic surgery because the surgeon's eyes focus on the flat monitor screen rather than the actual operative field [187].

Conventional laparoscopes further hinder depth perception; the lens's surrounding light source eliminates shadows, and monocular imaging prevents stereovision. While motion parallax is partially present during camera adjustments, it provides limited spatial information due to restricted laparoscope mobility. Techniques like adding shadows via specialized lighting or using stereo-laparoscopes have been explored, but results are inconsistent. Advanced systems incorporating head-coupled movement parallax offer potential improvements but are often costly and complex [183, 187, 190].

C.2. Box-trainer Experiment: Protocol

Protocol for participant C

1. The informed consent document is presented to the participant. (2 min)
2. Briefing of the experiment. (5 min)
3. The participant gets familiar with the environment. (9 min)
4. The Zig-zag loop task will be performed. (changing camera positions: 3 min)
   (a) Camera Position B (3 min)
   (b) Camera Position C (3 min)
   (c) Camera Position A (3 min)
5. The participant gets familiar with the second task. (5 min)
6. The Wire chaser task will be performed. (changing camera positions: 3 min)
   (a) Camera Position C (3 min)
   (b) Camera Position A (3 min)
   (c) Camera Position B (3 min)
7. A brief interview (5 min)

D

Production & Assembly

This appendix describes the production techniques utilized to manufacture the lifting device. Section D.1 outlines the bending of the tubular frame, including the required forces and tools. Other production techniques will be explained in Section D.2, and the production steps are listed in Section D.3.

D.1. Tube bending

The frame design consists of a round tube in a loop shape. Various production methods were considered to achieve this form, including bending, milling, hydroforming, metal 3D printing, stretch forming, casting, and welding. The STAAN lifting device currently uses casting and welding. Casting enables intricate details but requires expensive molds. Hydroforming and stretch forming involve advanced machinery with high setup costs. Milling and metal 3D printing are better for small quantities, but milling is unsuitable for hollow structures, and 3D printing requires significant post-processing, adding time and expense. Bending was identified as the most viable method for this design.

Bending offers excellent design flexibility, crucial for creating the loop shape, and preserves the material's structural integrity [88], unlike welding, casting, or 3D printing. It also produces a smooth surface finish, reducing post-processing needs. These advantages lower material use, labor, and tool costs, making bending the most economical method for producing the looped structure.

The tube-bending process requires precise management of key variables [89]. A straight section at least 2.5 times the tube diameter is needed for clamping and to minimize slip and kinking at the inner radius. The minimum bend radius is 2.5 times the tube diameter. Smaller radii risk imperfections like flattening or collapse, which can be mitigated by filling the tube with a mandrel, sand, or frozen water to distribute pressure. Elastic recovery after force release (spring back) can cause dimensional inaccuracies. To counter this, the die's bend radius should be designed 3% smaller than the desired tube radius, and the bend angle increased by $1°$ to $2°$ for aluminum and $2°$ to $3°$ for stainless steel.

Smaller bend radii require higher bending forces, which can be achieved manually with a lever or reduced by annealing. Annealing increases ductility by heating the material above its recrystallization temperature, making it easier to bend. However, uncontrolled annealing risks excessive grain growth, reducing mechanical properties like strength and hardness, as well as corrosion resistance. Additionally, hot bending offers less precision than cold bending.

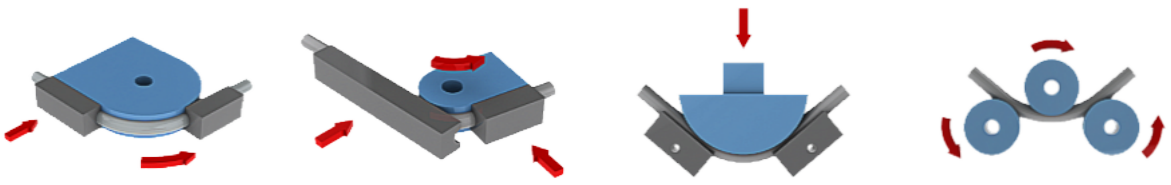

(a) Compression bending **(b)** Rotary draw bending **(c)** Ram bending **(d)** Roll bending

Figure D.1: The four most common bending techniques. The bend dies are blue, the clamps and pressure dies are gray, and the forces and movements are red.

The four main bending techniques are compression bending, rotary draw bending, ram bending, and roll bending, shown in Figure D.1. Ram and roll bending are unsuitable for the frame as they are limited to large radii and lack precision and repeatability.

Compression bending involves deforming the tube around a fixed bend die using a wiper die. This cost-effective technique is common in manual tube benders but struggles with small radii bends and precision compared to rotary draw bending.

Rotary draw bending, also known as mandrel bending when a mandrel is used, secures the tube with a clamp die and bends it by rotating the bend die. A pressure die holds the tube in place during rotation. This technique provides higher precision and force capability than manual methods.

TU Delft has two rotary draw bending machines (CBC UNI 42) capable of bending $12\,\mathrm{mm}$ diameter tubes but lacking standard dies for the required $60\,\mathrm{mm}$ and $30\,\mathrm{mm}$ radii. Custom aluminum dies, estimated at € 400 each, exceed the project's budget.

Therefore, compression bending was used for prototypes. However, future iterations should consider rotary draw bending for its higher precision. The following sections detail the bending forces and manufacturing tools used.

Required bending moment

Plastically deforming a material requires a bending moment that creates internal stresses above the material's yield stress. In this subsection, the required force to create the circular loop shape will be calculated. The material for the prototype frame is aluminum EN AW-6060 T66 quality with mechanical properties according to EN 755-2, as shown in Appendix E.

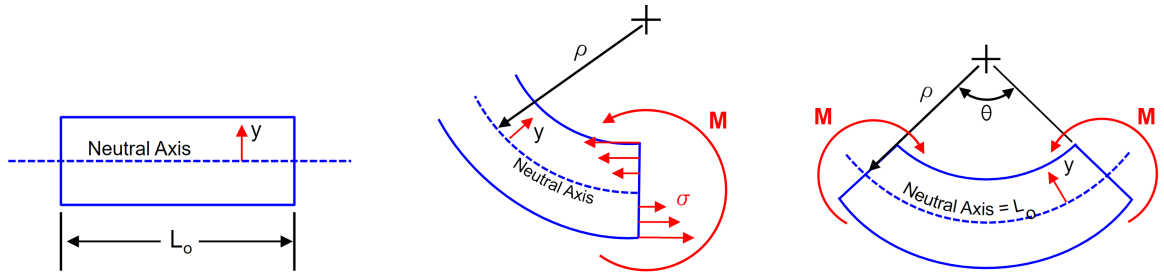

(a) A straight beam **(b)** Stress in a beam **(c)** Arc of a beam

Figure D.2: General visualization of bending strain and stress in beams [191]. L_0 is the initial length, y the distance from the neutral axis, ρ the radius of curvature, θ the arc angle, M the bending moment, and σ the stress.

Before bending, the frame is a straight round tube with length L_0, as shown in Figure D.2a. When a bending moment, M, is applied (Figure D.2b), the material at the inner radius of the bent is under compression, and the material at the outer radius is under tension. The shape of the material deforms accordingly, as depicted in Figure D.2c. The neutral axis' radius of curvature, ρ, is small for sharp curves and infinite for straight paths. The length of an arc is equal to the radius of curvature times the arc angle θ. Hence, the relation on the neutral axis is defined as in Equation D.1. The arc length at any distance from the neutral axis, y, is described by Equation D.2.

$$L_0 = \rho\theta \tag{D.1}$$

$$L = (\rho - y)\theta \tag{D.2}$$

Now the strain, ε_x, can be expressed as Equation D.3, which can be simplified to Equation D.4.

$$\varepsilon = \frac{L - L_0}{L_0} = \frac{(\rho - y)\theta - \rho\theta}{\rho\theta} \tag{D.3}$$

$$\varepsilon = -\frac{y}{\rho} \tag{D.4}$$

For a round tube, the neutral axis is exactly in the center, and the highest strain occurs at the outermost radius. The strain is largest for small bending radii. Therefore, ρ is equal to the bending radius of $30\,\mathrm{mm}$, and y is equal to negative half the diameter of the tube, $y = -6\,\mathrm{mm}$. Thus, the maximum strain in the material is $\varepsilon_m = 0.02$.

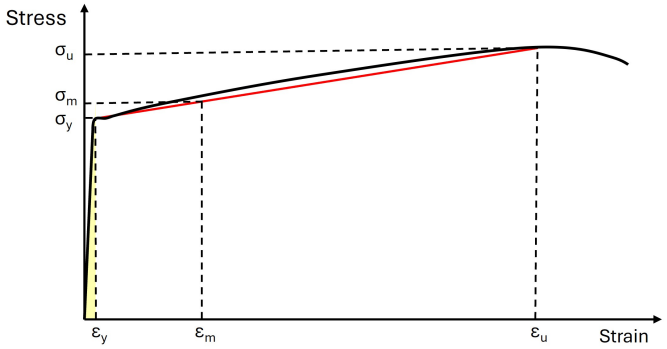

Figure D.3: Typical stress-strain curve for aluminum alloys. The red line is a linear simplification from the yield stress point to the ultimate tensile strength.

Suppose this strain is within the elastic limit (colored yellow in Figure D.3) with an elastic modulus, E, of $70\,\mathrm{GPa}$. Then, the stress in the material would be equal to $\sigma = E\varepsilon_m = 1.4\,\mathrm{GPa}$, which is well above the material yield stress, σ_y, of $160\,\mathrm{MPa}$ and not in the elastic region. Thus, bending a $12\,\mathrm{mm}$ aluminum tube with a radius of $30\,\mathrm{mm}$ deforms the material plastically.

The strain in the material corresponds to a stress between the yield stress and the ultimate tensile strength, σ_u, of $215\,\mathrm{MPa}$. The strain at the yield stress point is approximately $\varepsilon_y = \sigma_y/E = 0.0023$, and at the ultimate tensile strength, it can be predicted by Equation D.5 [192].

$$\varepsilon_u = 0.1(1 - \frac{\sigma_y}{\sigma_u}) + 0.06 = 0.086 \tag{D.5}$$

According to the data sheet (Appendix E), the material could fracture at an 0.08 elongation. So, the actual strain at the ultimate tensile strength must be lower than the predicted, and for the following extrapolation, a strain of $\varepsilon_u = 0.08$ is used.

The stress-strain curve in the plastic region is simplified to a linear slope from the yield stress point to the ultimate tensile strength. The slope coefficient equals the increase in stress over the increase in strain. Equation D.6 is used to extrapolate the stress in the material for the maximum strain, ε_m, during bending.

$$\sigma_m = \sigma_y + \frac{\sigma_u - \sigma_y}{\varepsilon_u - \varepsilon_y}(\varepsilon_m - \varepsilon_y) = 173\,\mathrm{MPa} \tag{D.6}$$

A stress of $173\,\mathrm{MPa}$ is needed to deform the material in the desired shape. As explained before, a bending moment is required to achieve the stress in the material. The section modulus, W, of a tube can be used to calculate the required moment. The formula is given in Equation D.7, where D and d are the outer and inner diameters of the tube, respectively. Equation D.8 shows the required bending moment.

$$W = \frac{\pi}{32D}(D^4 - d^4) = 88\,\mathrm{mm}^3 \tag{D.7}$$

$$M = \sigma_m W = 15\,\mathrm{Nm} \tag{D.8}$$

So, a bending moment of $15\,\mathrm{Nm}$ is required to bend the $12\mathrm{x}1\,\mathrm{mm}$ tube with a radius of $30\,\mathrm{mm}$. In comparison, the pedals and the cassette on a road bike are secured manually with a tool by applying $10\,\mathrm{Nm}$ and $40\,\mathrm{Nm}$, respectively. Thus, the required bending moment can easily be achieved by hand using a proper lever tool.

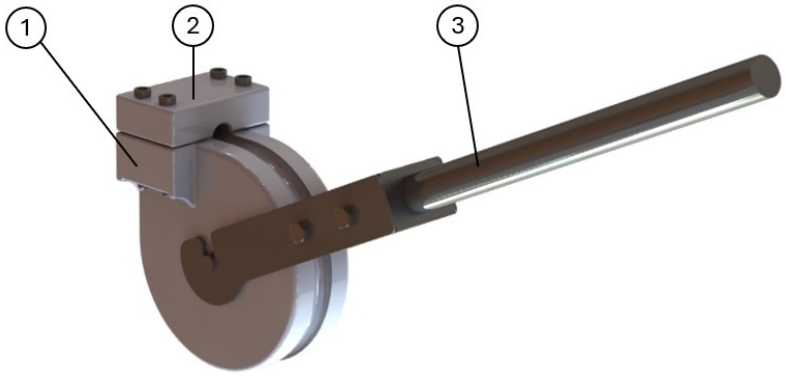

Figure D.4: The bending tool assembly. (1) is the bending die, (2) is the clamp, and (3) is the handle.

Bending tools

Thus, a proper tool was needed to bend the frame in the desired shape. It is presented in Figure D.4. The bending tool consists of three components: a die, a clamp, and a handle. The tube is locked in place between the die and the clamp. The handle rotates around the center axis of the die to bend the tube.

The die and clamp form fit around the tube's outer diameter. They are tightened by four M6 bolts and are fixed in a vice. Both were 3D-printed from PLA. The die guides the tube along the radius of the bend, and the form-fit ensures the tube's wall retains its circular shape – i.e., no flattening occurs. The die has a 3% smaller radius than the desired $60\,\mathrm{mm}$ loop radius to account for elastic recovery. It has a stainless steel axis in the center to which the handle is connected.

The handle bends the tube around the bending die. The largest forces appear on this component and the stainless steel axis. Hence, the handle is a machined component. It consists of three parts as indicated in Figure D.5. The main part is milled from aluminum and – similar to the die – has $12\,\mathrm{mm}$ form fit around the tube. Two laser-cutted steelplates are attached to the main part by four M6 bolts. These are connected to the die's axis. At the opposite side of the main part, a turned stainless steel lever is attached to decrease the required muscle force.

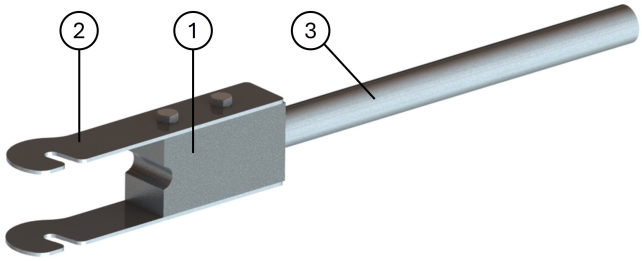

Figure D.5: The bending handle. (1) is the main aluminum milled part, (2) are the laser-cut steel plates, and (3) is the stainless steel lever.

Figure D.6: Flattening of the tube after bending with a $30\,\mathrm{mm}$ radius.

The tool works fine for the $60\,\mathrm{mm}$ radius bends. Negligible flattening and surface imperfections occur. A similar tool was made for the smaller $30\,\mathrm{mm}$ bends. Unfortunately, the tube was severely flattened after bending (Figure D.6). Even when the tube was annealed and filled with quartz sand, the wall did not retain its circular shape. This was odd and unexpected since, in prior experience, the technique worked well for this exact bending radius.

Consequently, the prototype design had to be altered. A regular pipe bender with a $43\,\mathrm{mm}$ bending radius was used. The radius is larger than designed at first. Hence, the upright section's shape is different than shown in Figure 9.2.

D.2. Other production techniques

Drilling serves as the second production method, responsible for creating all 22 holes in the tubular frame. Precision in the location and orientation of these holes is crucial for optimal device performance. The hole for the camera should be in the middle of the loop, and the rotation angle should be $60°$. The holes for LED lighting should be uniformly distributed over $180°$.

Furthermore, the holes should be drilled exactly at the center line of the tube. Otherwise, the drill bit will slip, resulting in inaccurate holes. Additionally, the tube should be secured adequately to provide stability. Two custom 3D-printed jigs were made to ensure drilling precision. These are displayed in Figure D.7.

Figure D.7: The drill jigs for creating the camera hole (left) and the twenty holes for lighting (right).

The RAIS joint and the endcap were designed to be both machined with a lathe and a milling machine. Despite their high cost, such machines are widely available in machining facilities and accessible to biomedical engineers LMICs.

In Figure D.8, the technical drawings of the RAIS joint are presented. It comprises two parts: a pole and a connector, which are welded together. Starting with a $10\,\mathrm{mm}$ diameter, $55\,\mathrm{mm}$ long rod, the pole is lathe-turned to $7.9\,\mathrm{mm}$ for the first $35\,\mathrm{mm}$, and the last $20\,\mathrm{mm}$ is reduced to $9.9\,\mathrm{mm}$. This allows a tight connection at both the tubular frame and connector joint.

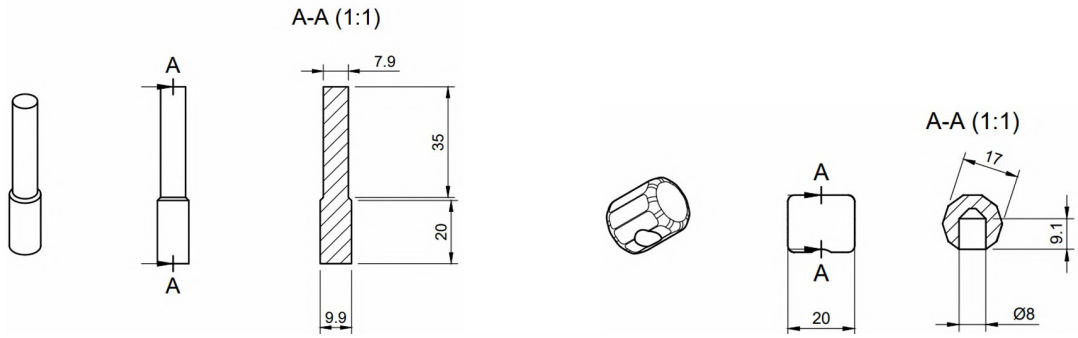

Figure D.8: The technical drawings of the two RAIS joint parts. Left is the pole and right is the connector.

The connector is a decagon (ten-sided polygon) with a hole to attach to the pole. An $18\,\mathrm{mm}$ diameter, $40\,\mathrm{mm}$ long rod is milled into a decagon by rotating every $36°$ and removing $0.5\,\mathrm{mm}$ per cut, resulting in $17\,\mathrm{mm}$ distance between opposite sides. The workpiece is then moved to a lathe, where the edges are rounded and it is trimmed to a $20\,\mathrm{mm}$ length. Finally, a $8\,\mathrm{mm}$ diameter hole is drilled in the center of a decagon side.

Figure D.9 shows the technical drawing of the endcap. Starting with a $12\,\mathrm{mm}$ diameter, $20\,\mathrm{mm}$ long rod, the endcap's first $5\,\mathrm{mm}$ is turned down to a $10\,\mathrm{mm}$ diameter. The spade tip is shaped on a milling machine and a $2\,\mathrm{mm}$ diameter hole is drilled for the connection with the frame. All machined parts are surface-finished by hand sanding.

For the final prototype, the RAIS joint and endcap were not machined from metal. They were 3D-printed with identical dimensions. Three more parts were 3D-printed for the prototype: two parts for the housing of electronics and a magnet holder.

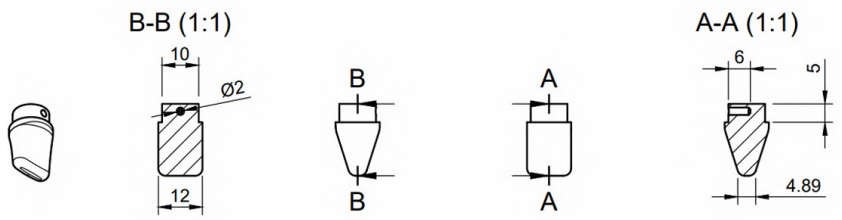

Figure D.9: Technical drawing of the endcap.

The electronics' housing parts snugly fit around the bent frame. The camera module's PCB can be placed in the right part, as shown in Figure 9.4, and three M3 nuts are inserted for the connection with the left part. Limited post-processing was required.

The magnet holder is a 3D printed part that fits around the camera sensor (Figure D.10a). A magnet is placed in the holder, which can be used to rotate the camera sensor in the tube. This is necessary to orient the camera sensor in the designated hole. The camera holder is placed in between the two sections of the LED strip, as shown in Figure D.10b – the production steps will be explained in detail in Section D.3.

(a) Render of the magnet holder.

(b) Picture of the imaging system assembly.

Figure D.10: The imaging system. (1) is the 3D-printed holder, (2) the magnet, (3) the camera module. (4) the LED strip, and (5) the wires.

D.3. Production steps

The prototype was manufactured using the described production techniques. This section gives a comprehensive overview of all production steps. First, a flowchart of the steps is presented in Figure 10.9. Then the definitions of the five bends will be given. Lastly, detailed descriptions of the steps are listed with the required tools, materials, and approximate time.

The desired shape of the tubular frame was created by five bends, indicated in Figure D.11. The $60\,\mathrm{mm}$ radius bends for the loop shape are named L_1 and L_2. The $43\,\mathrm{mm}$ radius bends for the upright section are defined as B_1, B_2, and B_3.

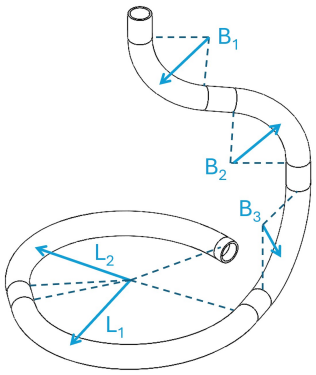

Figure D.11: The five bends of the tubular frame.

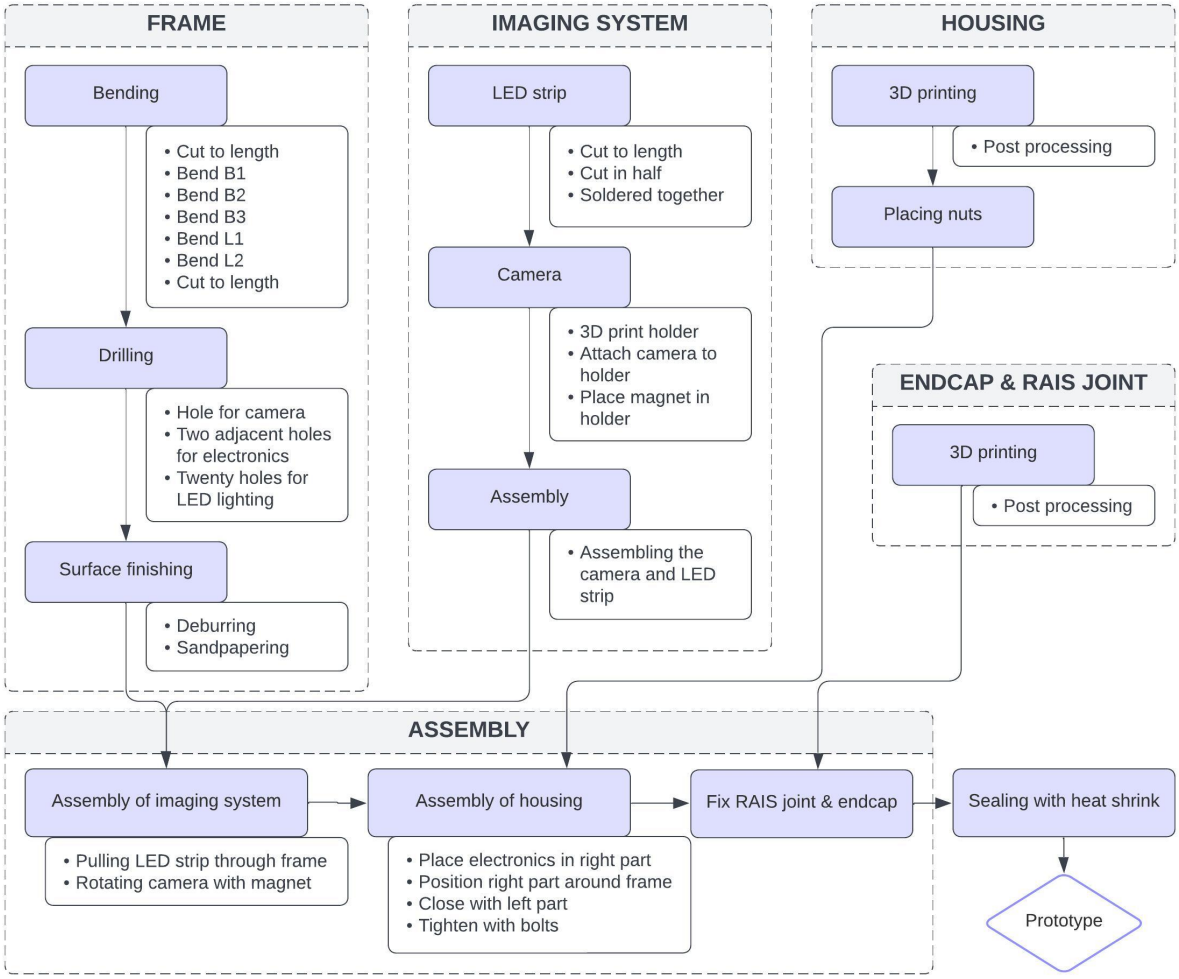

Figure D.12: Flowchart of the prototype's production process.

The production steps are listed below. The steps follow the overview of Figure D.12. Before the production of the lifting device could start, the custom tools had to be made. That took approximately three days. The complete production of a prototype takes approximately two days. However, some processes can be done simultaneously – for example, 3D-printing.

1. **Bending**: The bending of the consists of seven steps in a specific order.
   - 1.1 The tube is cut to a length of $700\,\mathrm{mm}$.
   - 1.2 Bend B_1 is made. The standard pipe bender is placed around the tube's endpoint, and the tube is bent $77°$.
   - 1.3 Bend B_2 is made. The standard pipe bender is placed around the tube $100\,\mathrm{mm}$ from the previous bend with a rotation angle of $180°$. The tube is bent $77°$.
   - 1.4 Bend B_3 is made. The standard pipe bender is placed around the tube $110\,\mathrm{mm}$ from the previous bend with the rotation angle of $52°$ counterclockwise. The tube is bent $90°$.
   - 1.5 Bend L_1 is made. The custom bending tool is placed around the tube $227\,\mathrm{mm}$ from the previous bend with a rotation angle of $95°$ counterclockwise. The tube is bent $140°$.
   - 1.6 Bend L_2 is made. The custom bending tool is placed around the tube $227\,\mathrm{mm}$ from the previous bend with a rotation angle of $5°$ counterclockwise. The tube is bent $140°$.
   - 1.7 The endpoints are cut to a length of $5\,\mathrm{mm}$.

   Required materials and tools: a 12x$1\,\mathrm{mm}$ tube, a hacksaw, a pipe bender, the custom bending tool, and a vice.

   Estimated time: 3 hours.

2. **Drilling**: The drilling of the 22 holes consists of three independent steps.
   2.1 The $7\,\mathrm{mm}$ diameter hole for the camera is made. The small drill jig is placed between bend L_1 and L_2 with a rotation angle of $30°$.
   2.2 The two adjacent $9\,\mathrm{mm}$ diameter holes for the electronics are made. The tube is fixed around bend B_2. The holes are $10\,\mathrm{mm}$ apart and the material between the holes is removed with a cutting plier.
   2.3 The twenty $5.5\,\mathrm{mm}$ diameter holes for lighting are made. The large drill jig is placed around bend L_1 and L_2 consecutively.

   Required materials and tools: a drilling machine and a cutting plier.

   Estimated time: 2 hours.

3. **Surface finishing**: Sharp edges are removed from the holes and cuts with a deburring tool and a file. Imperfections of the frame are removed with fine-grit sandpaper.

   Required materials and tools: a deburring tool, a file, and fine-grit sandpaper.

   Estimated time: 45 minutes.

4. **LED strip**: The LED strip is cut into two pieces of $100\,\mathrm{mm}$. Two $25\,\mathrm{mm}$ wires are soldered between these strips.

   Required materials and tools: the LED strip, soldering equipment and a scissor.

   Estimated time: 45 minutes.

5. **Camera assembly**: The magnet holder is 3D-printed. The camera is attached to the holder, and the magnet is placed in there. These parts are placed between the two soldered LED strips.

   Required materials and tools: the camera module, a magnet, and filament.

   Estimated time: 15 minutes.

6. **3D-printing**: The housing, endcap, and RAIS joint are 3D-printed and limited post-processing is necessary. Three M3 nuts are placed in the housing's right part.

   Required materials and tools: filament, pliers and three M3 nuts.

   Estimated time: 15 minutes.

7. **Assembly of the imaging system**: A thin wire is attached to the endpoint of the LED strip. The imaging system is pulled through the frame. The camera sensor can be rotated with a magnet to orient it in the designated hole.

   Required materials and tools: a thin wire and a magnet.

   Estimated time: 30 minutes.

8. **Assembly of the housing**: The camera module's PCB and the cables are placed in the housing's right part. The right part is positioned around bend B_2 of the frame. The left part is placed on top of the right part and these are tightened with three M3 bolts.

   Required materials and tools: three M3 bolts and an allen key.

   Estimated time: 15 minutes.

9. **Assembly of the RAIS joint and endcap**: The RAIS joint and endcap are glued to the endpoints of the frame. The RAIS connector should be parallel to the camera.

   Required materials and tools: glue.

   Estimated time: 15 minutes.

10. **Sealing**: The holes in the frame are sealed with a heat shrink, and a copolyester lens covers the camera sensor.

    Required materials and tools: a $12.7\,\mathrm{mm}$ heat shrink and a copolyester lens.

    Estimated time: 30 minutes.

Following these steps leads to the final prototype. The production process of that prototype will be discussed in Chapter 11.

Data Sheet Aluminum EN AW-6060

EN AW-6060 | DATA SHEET

ALUMERO
ALIVE WITH ALUMINIUM

The alloy EN AW-6060 is a widely used extrusion alloy, suitable for applications where no special strength properties are required. Parts can be produced with a very good surface quality, suitable for many coating operations. Typical application fields are furniture, finishing materials, windows and doors, carbody finishing, façade construction, lighting columns and flagpoles, architecture, and food industry.

Chemical composition according to EN573-3 (weight %, remainder Al)

Si	Fe	Cu	Mn	Mg	Cr	Zn	Ti	remarks	others	
0.30 – 0.60	0.10 – 0.30	max. 0.10	max. 0.10	0.35 – 0.60	max. 0.05	max. 0.15	max. 0.10		each max. 0.05	total max. 0.15

Mechanical properties according to EN755-2

Temper*	Wall thickness	Yield stress	Tensile strength	Elongation		Hardness**
	e***	$Rp_{0.2}$ [MPa]	Rm [MPa]	A [%]	A_{50mm} [%]	HB
T4	e ≤ 25	60	120	16	14	45
T5	e ≤ 5	120	160	8	6	55
	5 < e ≤ 25	100	140	8	6	50
T6	e ≤ 5	150	190	8	6	65
	5 < e ≤ 25	140	170	8	6	60
T66	e ≤ 5	160	215	8	6	70
	5 < e ≤ 25	150	195	8	6	65

* Temper designation according to EN515: T4-Naturally aged to a stable condition, T5-cooled from an elevated temperature forming operation and artificially aged, T6-Solution heat treated, quenched and artificially aged, T66-cooled from an elevated temperature forming operation and artificially aged to a condition with higher mechanical properties through special control of manufacturing processes. T6 and T66 properties can be achieved by press quenching)
** Hardness values are for indication only *** For different wall thicknesses within one profile, the lowest specified properties shall be considered as valid for the whole profile cross section

Physical properties (approximate values, 20 °C)

Density [kg/m³]	Melting range [°C]	Electrical conductivity [MS/m]	Thermal conductivity [W/m.K]	Co-efficient of thermal expansion 10^{-6}/K (20-100 °C)	Modulus of elasticity [GPa]
2700	585 – 650	28 – 34	200 – 220	23.4	~ 70

Weldability*
Gas: 3 TIG: 2 MIG: 2
Typical filler materials (EN ISO18273): AlMg5Cr(A) or AlSi5, and AlMg3 when the product has to be anodised. Due to the heat input during welding the mechanical properties will be reduced by approximately 50% (ref. EN1999 -1).

Machining characteristics*
T4 temper: 3 T5 and T6 temper: 2

Coating properties*
Hard/protective anodising: 1 Decorative/bright/colour anodising: 1

Corrosion resistance*
General: 1 Marine: 2

Values are copies from the material data sheets of Aluminium Verlag and ÖNORM EN755-2.
Ranking from 1 (very good) to 6 (unsuitable).

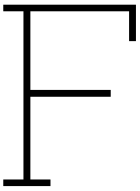

Survey questionnaire

Survey: Gasless Laparoscopic Surgery

Start of Block: Introduction

Welcome!

TU Delft Biomedical Engineering for Global Health Lab is developing an Abdominal-Wall Lift (AWL) device with an integrated imaging system for Gas Insufflation-Less Laparoscopic Surgery (GILLS) in low-resource settings.

This survey will take about 5 minutes, and the results will be used to modify the design requirements of the new AWL device. The survey is anonymous, but in the last section, you have the option to leave your contact details voluntarily. By filling in this survey, you give informed consent to contributing to this research, which will be published online as a master's thesis and perhaps in the future as an academic paper.

If you have any questions, comments, or suggestions, please email us at m.bakkum@student.tudelft.nl with any information you want to share.

Thank you in advance for taking this survey - your feedback is truly appreciated!

- ○ Yes, I give consent (1)
- ○ No, I do not give consent (2)

Respondent Information
First, biographical data of the respondents is gathered. As the survey is anonymous, no personal details will be requested. A brief introduction to the topic is given below.

Laparoscopic surgery is a form of minimally invasive surgery that is performed in the abdomen or pelvis regions with the use of small incisions of around 5-15 millimeters. This offers several advantages over open surgical procedures, such as decreased postoperative pain, faster recovery times, fewer operative and postoperative major complications, less scarring, and a shorter hospital stay.

In Gas Insufflation-Less Laparoscopic Surgery (GILLS) the abdominal wall is physically raised by an abdominal-wall lift (AWL) device to create operative space. This technique has been reported to have various advantages over conventional laparoscopy, such as shorter hospital stays, less shoulder pain, less influence on cardiopulmonary function, and less postoperative nausea and vomiting.

Q1 In which country do you currently reside?

▼ Afghanistan (1) ... Zimbabwe (1357)

Q2 What is your main profession?

_____

Q3 Do you have knowledge about laparoscopic surgery?

	1 (1)	2 (2)	3 (3)	
No knowledge	○	○	○	Expert

Q4 Do you have experience in performing laparoscopic surgery?

	1 (1)	2 (2)	3 (3)	
No experience	○	○	○	Regularly

Q5 Do you have knowledge about Gas Insufflation-Less Laparoscopic Surgery?

	1 (1)	2 (2)	3 (3)	
No knowledge	○	○	○	Expert

Q6 Do you have experience in performing Gas Insufflation-Less Laparoscopic Surgery?

	1 (1)	2 (2)	3 (3)	
No experience	○	○	○	Regularly

End of Block: Introduction

Start of Block: Experience in performing gasless laparoscopy

Q7 Current Abdominal Wall Lift (AWL) devices
You stated that you have experience performing Gas Insufflation-Less Laparoscopic Surgery (GILLS). The following questions will be about the AWL device you have used.

Q8 What AWL device have you used?

- ☐ Abdolift (1)
- ☐ Keyloop (2)
- ☐ RAIS (3)
- ☐ Other device (4) _____
- ☐ STAAN (5)
- ☐ Hashimoto's device (6)
- ☐ Shrikande's device (7)

Q9 Please check the procedures you have performed with this AWL device(s).

- [ ] Appendectomy (1)
- [ ] Gastrostomy or Jejunostomy tube (2)
- [ ] Inguinal hernia (3)
- [ ] Cholecystectomy (4)
- [ ] Ventral hernia (5)
- [ ] Small bowel resection (6)
- [ ] Gastric wedge resection (7)
- [ ] Colectomy with primary anastomosis (8)
- [ ] Hartmann's procedure (9)
- [ ] Splenectomy (10)
- [ ] Roux-en-Y Gastric Bypass (11)
- [ ] Hepatic wedge resection (12)
- [ ] Distal Pancreatectomy (13)
- [ ] Whipple (14)
- [ ] Other procedures (15) _____

Q10 How strongly do you agree or disagree with the statements about the [**device**]?
*[**device**] = device chosen in Q8*

	Agree (1)	Neither agree nor disagree (2)	Disagree (3)
The device is easy to insert (1)	○	○	○
The device is easy to adjust (2)	○	○	○
The device is easy to remove (3)	○	○	○
The device is easy to connect to a retractor arm (4)	○	○	○
It is easy to position the laparoscope while using the AWL device (5)	○	○	○
During blind entry of the device, patient tissue is damaged sometimes (6)	○	○	○
Frames or wires interfere movement of surgical instruments (7)	○	○	○
The operational volume* is large enough (i.e. no tenting occurs and there is enough space to operate) (8)	○	○	○
More fogging occurs when using this device compared to standard gas laparoscopy (disagree if less fogging occurs) (9)	○	○	○
The device can be used on patients of all sizes (10)	○	○	○

*operational volume is the space created inside the abdomen. In conventional laparoscopy, this is created by a carbon dioxide pneumoperitoneum.

Q11 Did you encounter problems other than those stated before?

Please elaborate on the problem and how often it occurred

_____

_____

_____

_____

_____

End of Block: Experience in performing gasless laparoscopy

Start of Block: Everyone

A new Abdominal-Wall Lift (AWL) device TU Delft Biomedical Engineering for Global Health Lab is developing an Abdominal-Wall Lift (AWL) device with an integrated imaging system for Gas Insufflation-Less Laparoscopic Surgery (GILLS) in low-resource settings. This eliminates the need for an expensive laparoscope, general anesthesia, and carbon dioxide, which are often not available in low-resource settings. GILLS could help the adoption of laparoscopic surgery in low- and middle-income countries (LMIC).

Q12 **You will purchase and use the new AWL device.**

Please rank the features you consider most important (1) to least important (5)
**operational space is the volume created inside the abdomen. In conventional laparoscopy, this is created by a carbon dioxide pneumoperitoneum.*

_____ **Surgeon visibility**: encompasses the operational space* created by the AWL device and the quality of the imaging system. (1)
_____ **Costs**: consists of upfront costs, running costs, and maintenance costs (e.g., costs to the hospital). (2)
_____ **Robustness**: the durability, reliability, and sturdiness of the AWL device. (3)
_____ **User-friendliness**: how easy it is to use other instrumentation with the lift device and how easily the user interface can be operated. (4)
_____ **Patient outcomes:** the results from treatments patients have received whilst in hospital. (5)

Q13 Are there other important features for the new AWL device?

Please elaborate the feature

_____

_____

_____

Q14 What laparoscopic surgeries should an AWL device with an integrated imaging system be able to perform, in your opinion?

If you have no knowledge about the surgeries, please skip this question.

- [ ] Appendectomy (1)
- [ ] Gastrostomy or Jejunostomy tube (2)
- [ ] Inguinal hernia (3)
- [ ] Cholecystectomy (4)
- [ ] Ventral hernia (5)
- [ ] Small bowel resection (6)
- [ ] Gastric wedge resection (7)
- [ ] Colectomy with primary anastomosis (8)
- [ ] Hartmann's procedure (9)
- [ ] Splenectomy (10)
- [ ] Roux-en-Y Gastric Bypass (11)
- [ ] Hepatic wedge resection (12)
- [ ] Distal Pancreatectomy (13)
- [ ] Whipple (14)
- [ ] Other procedures (15) _____

End of Block: Everyone

Start of Block: Contact information

As stated before, this questionnaire can be submitted anonymously. However, if you do not mind, please fill in your contact details. The author will use this to clarify the answers you gave or to get in contact for further questions about the topic. This will be truly appreciated.

Q15 Please fill in your full name.

Do not answer if you want to submit the questionnaire anonymously.

_____

Q16 Please fill in your email address.

Do not answer if you want to submit the questionnaire anonymously.

_____

Q17 May the author ask you to clarify some of your answers?

- ○ Yes, the author may ask me to clarify my answers (1)
- ○ No, the author may not ask me to clarify my answers (2)

Q18 May the author get in contact with you for further questions about the topic?

- ○ Yes, the author may get in contact with me for further questions (1)
- ○ No, the author may not get in contact with me for further questions (2)

End of Block: Contact information

End of Survey